Manufacturing and characterization of polymer-derived ceramic matrix composites for high-temperature aerospace applications

by

Bailey Walke

B.S., Kansas State University, 2025

A REPORT

submitted in partial fulfillment of the requirements for the degree

MASTER OF SCIENCE

Department of Mechanical & Nuclear Engineering
Carl R. Ice College of Engineering

KANSAS STATE UNIVERSITY
Manhattan, Kansas

2026

Approved by:

Co-Major Professor
Dr. Mingjun Wei

Approved by:

Co-Major Professor
Dr. Gurpreet Singh

Copyright

ABSTRACT

Ceramic matrix composites (CMCs) are engineered materials designed for operation in extreme environments, where their low density, high temperature capability, oxidation resistance, and damage tolerance make them attractive for aerospace and energy applications such as rocket nozzles, thermal protection systems, and turbine components. Polymer-derived ceramic matrix composites produced through polymer infiltration and pyrolysis (PIP) provide a relatively low-cost and scalable fabrication method compared to other ceramic composite manufacturing techniques. However, traditional PIP processing requires multiple infiltration and high-temperature pyrolysis cycles to build sufficient ceramic matrix content, resulting in long processing times and limited manufacturing scalability.

This research investigates carbon fiber reinforced ceramic matrix composites produced using polysilazane and boron-modified polysilazane preceramic precursors to form SiCN and SiBCN ceramic matrices. Two processing methods were studied and compared. The first method used the traditional multi-cycle PIP process, which includes repeated polymer infiltration, crosslinking at elevated temperature in an inert environment, and pyrolysis at high temperature, repeated for multiple cycles. The second method used a modified multi-cycle process in which multiple infiltration and crosslinking cycles were performed prior to a single pyrolysis cycle, with the goal of reducing processing time and improving manufacturing scalability.

Samples produced using both processing methods were evaluated using weight analysis, ceramic yield calculations, oxidation testing, scanning electron microscopy (SEM), X-ray fluorescence (XRF), Fourier transform infrared spectroscopy (FTIR), and mechanical testing. SEM was used to evaluate ceramic coating formation and fiber surface coverage, while FTIR and XRF were used to

confirm polymer-to-ceramic conversion and ceramic phase formation. Oxidation resistance was evaluated by exposing samples to elevated temperature in air and measuring weight retention. Mechanical testing was conducted to compare stiffness, strength, and toughness of ceramic-coated fiber bundles to uncoated carbon fiber bundles.

Results showed that increasing infiltration cycles increased ceramic matrix formation and improved oxidation resistance for both SiCN and SiBCN ceramic matrix composites. The modified multi-infiltration single-pyrolysis process produced composites with comparable ceramic matrix formation, oxidation resistance, microstructure, and mechanical behavior while significantly reducing the number of high-temperature pyrolysis cycles required. This reduction in furnace processing time represents a significant advantage for manufacturing scalability and production efficiency.

Overall, this research demonstrates that multi-cycle infiltration followed by a single pyrolysis cycle is a viable alternative to traditional multi-cycle PIP processing and offers a more scalable manufacturing method for polymer-derived ceramic matrix composites for high-temperature structural applications.

TABLE OF CONTENTS

LIST OF FIGURES

LIST OF EQUATIONS

LIST OF TABLES

ACKNOWLEDGEMENTS

I would like to express my gratitude to my research advisor, **Dr. Gurpreet Singh,** for the opportunity to work on this project for the last three years. His mentorship, guidance and trust has been instrumental in shaping my development as a researcher. Dr. Singh consistently challenges me to think critically and independently while providing the support needed to navigate the complexities of this work.

I would also like to thank the other members of my advisory committee, **Dr. Mingjun Wei** and **Dr. Melanie Derby,** for their guidance, and encouragement, and valuable feedback throughout this process. Their support and perspectives have significantly strengthened this work.

I would like to thank **Arijit Roy** for assistance with XRF data collection and visualization.

Paul Snider has been an incredible mentor to me as the faculty advisor for my other passion project, CubeSat. He has had the strongest influence on my growth as an engineer and has had significant impact on the trajectory of my career. Dream big, and serious fun!

Dr. Frank Tracz is the reason I attended Kansas State. My time in the marching band under his leadership brought me so much joy and growth in many ways. Thank you for teaching me to leave it better than I found it and the value of showing up and giving my all. Happy Trails, DT!

Dr. Alex Wimmer has had the greatest impact on my leadership than anyone I have ever known. He is shining example of leading by example and intentionality, and despite his incredibly long list of responsibilities, always makes me feel heard and valued. Thank you for everything, DW.

To my second family: **Delayne Johnson** and **Julie Rietz:** thank you for your presence and love for most of my life. Delayne, my chosen aunt, your friendship and care has meant so much to my family and I, and Julie, from baton coach to second mom, your guidance and belief in me helped shape me into who I am today.

Finally, I would like to thank my closest friends, **Shreya Gaddi, Sheridan Bredehoeft, Sierra Creek, Katie Harris, Makayla More, Christy Reiter,** and **Evie Rodenbaugh**. Thank you for making me happy. I think one of the main reasons I was successful at K-State was because I was genuinely happy, thank you all for keeping me grounded and pushing me to be my best self.

This research is based on work supported by the National Science Foundation, under grant no. 1743701 to G. Singh.

DEDICATION

I dedicate this work to my parents, **Michelle Walke** and the Honorable **Jason Walke**.

Although I did not inherit the STEM gene directly from my parents, they each instilled in me unique qualities that have shaped me into a strong engineer.

My mom is a Mensa-member genius, a self-taught architect, a creative talent, and a true research expert in any discipline she pursues. From designing my twirling costumes for 18 years to designing a house with no training in architecture or construction science, she has always demonstrated an astonishing ability to not only become proficient, but often exceptional, in skills she has never formally studied. She is resilient, insightful, resourceful, and highly organized, with an impeccable attention to detail that is unmatched by anyone I've ever met. These are qualities that she has taught me that have been invaluable in my development as an engineer and researcher.

My dad, recently inducted as a District Judge for Iowa's 5th Judicial District, built one of the most successful legal careers as an attorney in the state. While he is incredibly intelligent in his own right, it is his competitive spirit and care for those around him that has most profoundly influenced me. Although trial law is an inherently competitive field, my dad was constantly in competition with himself to be the best version of himself for his clients. He worked countless extra hours and went above and beyond to be fully prepared every milestone, never settling for mediocrity. Unlike many peers in his profession, he developed friendships with many of his clients that lasted beyond the gavel hit in their favor, which is a true testament to his character and genuine care for others. And even under immense pressure, he always makes time for the people around him, especially my mom and I, and never misses the opportunity to lighten the mood with his sense of humor.

Together, my parents have spent the last 23 years pouring everything into me. I have never questioned their support and love for me, and they have always believed in my dream of being a rocket scientist. I owe everything I have, and everything that I will become, to them.

Mom and dad, I am lucky to make you proud, because I am so proud to call you both my parents.

And though she be but little, she is fierce.

INTRODUCTION

Ceramic matrix composites (CMCs) are advanced structural materials designed for high-temperature and extreme environment applications where traditional metals and polymer matrix composites cannot perform adequately [1]. These materials consist of high-strength ceramic or carbon fibers embedded within a ceramic matrix, combining the high-temperature capability and oxidation resistance of ceramics with the toughness and damage tolerance provided by fiber reinforcement. Because of these properties, CMCs are increasingly used in aerospace propulsion systems, hypersonic vehicles, gas turbines, and energy systems where materials must operate at temperatures exceeding the limits of conventional alloys [5],[14].

One of the major challenges in the widespread adoption of ceramic matrix composites is manufacturing complexity and cost. Several fabrication methods exist for producing CMCs, including chemical vapor infiltration (CVI), melt infiltration (MI), and polymer infiltration and pyrolysis (PIP). Among these methods, the polymer infiltration and pyrolysis process is attractive due to its relatively low processing temperature, ability to produce complex shapes, and compatibility with a wide range of polymer-derived ceramic precursors. In the PIP process, a liquid polymer precursor infiltrates a fiber preform, is crosslinked into a solid network, and then pyrolyzed at high temperature to convert the polymer into a ceramic matrix [5]. However, the ceramic yield from a single infiltration and pyrolysis cycle is typically low, requiring multiple cycles to achieve sufficient matrix density. These repeated cycles significantly increase processing time, energy consumption, and manufacturing cost, which limits the scalability of the process for large-scale production of CMC components.

Polymer-derived ceramics such as silicon carbonitride (SiCN) and silicon boron carbonitride (SiBCN) are of particular interest for high-temperature applications due to their thermal stability, oxidation resistance, and amorphous nanocomposite structure that resists crystallization at elevated temperatures [6]. When combined with carbon fiber reinforcement, these materials can produce lightweight composites with good mechanical properties and improved oxidation resistance compared to unprotected carbon fibers. However, the relationship between processing method, ceramic yield, microstructure development, and final composite properties must be better understood in order to optimize manufacturing methods and improve scalability.

The purpose of this research is to investigate and compare two polymer infiltration and pyrolysis processing approaches for producing carbon fiber reinforced SiCN and SiBCN ceramic matrix composites. The first method utilizes a traditional multi-cycle PIP process consisting of repeated infiltration, crosslinking, and pyrolysis cycles. The second method modifies this process by performing multiple infiltration and crosslinking steps followed by a single final pyrolysis cycle, with the goal of reducing processing time while maintaining adequate ceramic matrix formation and composite performance. The two methods are compared using weight and ceramic yield analysis, oxidation testing, scanning electron microscopy, X-ray fluorescence, and tensile testing to evaluate differences in ceramic conversion, microstructure, oxidation resistance, and mechanical properties.

The overall goal of this work is to evaluate whether reducing the number of pyrolysis cycles can significantly decrease manufacturing time while still producing ceramic matrix composites with acceptable material properties. Improving the efficiency and scalability of polymer-derived ceramic matrix composite manufacturing could help enable broader use of these materials in aerospace, energy, and high-temperature structural applications.

This report is organized as follows. Chapter 1 provides background information on ceramic matrix composites, polymer-derived ceramics, common manufacturing methods, and engineering applications. Chapter 2 presents the traditional multi-cycle polymer infiltration and pyrolysis method and associated characterization results. Chapter 3 presents the modified multi-infiltration single-pyrolysis method and associated testing results. Chapter 4 compares the two processing methods in terms of ceramic yield, oxidation resistance, microstructure, phase composition, mechanical properties, and manufacturing scalability. Finally, conclusions and recommendations for future work are presented in Chapter 5.

CHAPTER 1: REVIEW OF LITERATURE

1.1 Ceramic Matrix Composites

Ceramic matrix composites (CMCs) are a class of advanced high-temperature structural materials consisting of ceramic reinforcing fibers embedded within a ceramic matrix. These materials were developed to overcome the inherent brittleness and low fracture toughness of monolithic ceramics while maintaining their excellent high-temperature capability, oxidation resistance, and low density [1]. By combining ceramic fibers with a ceramic matrix, CMCs provide improved damage tolerance, thermal stability, and structural reliability in extreme environments where conventional metallic alloys and polymer matrix composites cannot operate [2]. As a result, CMCs have become increasingly important for aerospace propulsion systems, thermal protection systems, energy generation systems, and other high-temperature engineering applications [14].

1.1.1 Structure and Components of Ceramic Matrix Composites

CMCs consist of three primary structural components: reinforcement fibers, a ceramic matrix, and a fiber-matrix interface. Each component contributes to the overall thermal stability and mechanical behavior of the composite. The interaction between these determines the strength, toughness, and thermal capability of the material. A visualization of CMC components and structure is shown in Figure 1-1.

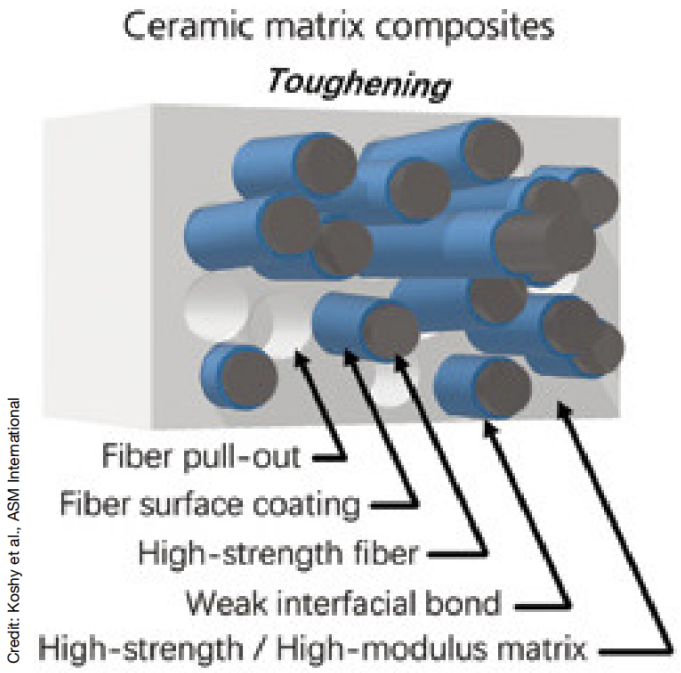

Figure 1-1: Ceramic Matrix Composite Components and Structure [14]

1.1.1.1 Reinforcing Fibers

The reinforcement fibers are the primary load-bearing component in CMCs. They are largely responsible for the strength and damage tolerance of the composite. Monolithic ceramics fail catastrophically due to brittle fracture, whereas CMCs rely on high-strength fibers to carry the load after matrix cracking occurs. Once the matrix begins to fracture, the load transfers to the fibers via shear stresses at the fiber-matrix interface, allowing the composite to carry load with non-brittle failure behavior [1], [2].

Silicon carbide fibers are most selected as reinforcement in advanced ceramic composites due to their high-temperature mechanical properties and oxidation resistance. Carbon fibers and oxide ceramic fibers are also used depending on the environment and temperature requirements.

The architecture of the reinforcement fibers heavily influences composite performance. Fibers can be arranged in woven fabrics, braided structures, and unidirectional plies depending on the desired

properties. Woven or braided architecture provides improved multi-directional strength and resistance to delamination, which makes them suitable for complex structures. Unidirectional fibers provide maximum strength and stiffness in a single direction.

1.1.1.2 Ceramic Matrix

The ceramic matrix in CMCs surrounds the reinforcement fibers and is significant to the function of the composite. It transfers load between fibers, protects fibers from degradation, and contributes to stiffness and thermal stability of the composite. The most common matrix materials used in CMCs are silicon carbide (SiC), alumina (Al_2O_3), silicon nitride (Si_3N_4) and carbon. These materials are selected based on environmental conditions and mechanical requirements [1]. Among these materials, silicon carbide matrices are particularly common for high-temperature CMCs due to their excellent oxidation resistance and mechanical stability.

The matrix is typically brittle and exhibits linear elastic behavior prior to fracture. Cracking in the matrix occurs at relatively low strains, around 0.1%, which is significantly lower than that of the reinforcement fibers. Once the matrix cracks, load is transferred to the fibers through shear stresses at the fiber-matrix interface. These loads can be managed through pullout mechanisms and fiber bridging by introducing an interface layer.

Matrix properties strongly influence mechanical and thermal properties of the composite, including elastic modulus, fracture toughness, thermal conductivity, and oxidation resistance. Thermal mismatch between the reinforcement and matrix can create residual stresses during processing, which can either degrade or improve the composite performance depending on the direction and magnitude of the mismatch [3].

The matrix can be introduced into the fiber preform using several processing methods, such as polymer infiltration and pyrolysis (PIP), chemical vapor infiltration (CVI), or melt infiltration (MI), which will be discussed later. These manufacturing methods influence density, porosity, and mechanical structure.

1.1.1.3 Fiber-Matrix Interface

A key component of CMCs is the fiber-matrix (FM) interface, which is a thin coating applied to the surface of reinforcement fibers prior to matrix infiltration. A significant difference between CMCs and polymer or metal composites is that CMCs are classified as inverse composites, meaning that under a mechanical load, the brittle matrix fails first at relatively low strains, typically around 0.1% [1]. Because of this, matrix cracks are deflected at the fiber-matrix interface to avoid early failure of the composite. This is accomplished by introducing a weak FM bond by introducing a thin layer of weak material [1].

If the fiber and matrix are bonded too strongly, cracks created under load propagating through the matrix would damage fibers, resulting in brittle failure similar to monolithic ceramics. Instead, the interface material is designed to allow cracks to propagate along the fiber surface rather than cutting through the fiber. Crack deflection increases the energy required for crack propagation and is the primary toughness mechanism in CMCs. In addition to crack deflection, fibers bridge crack surfaces and carry load across the crack to further increase toughness and prevent catastrophic sudden failure [2]. The crack deflection mechanism between the interface and reinforcement materials is shown in Figure 1-2.

Common interface materials are boron nitride (BN) and pyrolytic carbon (PyC). These coatings usually have a thickness of 100–1000 nm and enable fiber pullout and crack bridging during

pullout [2]. In high-temperature and oxidative environments, multilayer interfaces such as BN/SiC are used to maintain mechanical behavior while also improving oxidation resistance. The thickness, microstructure, and composition of the interface strongly influence the performance of the composite.

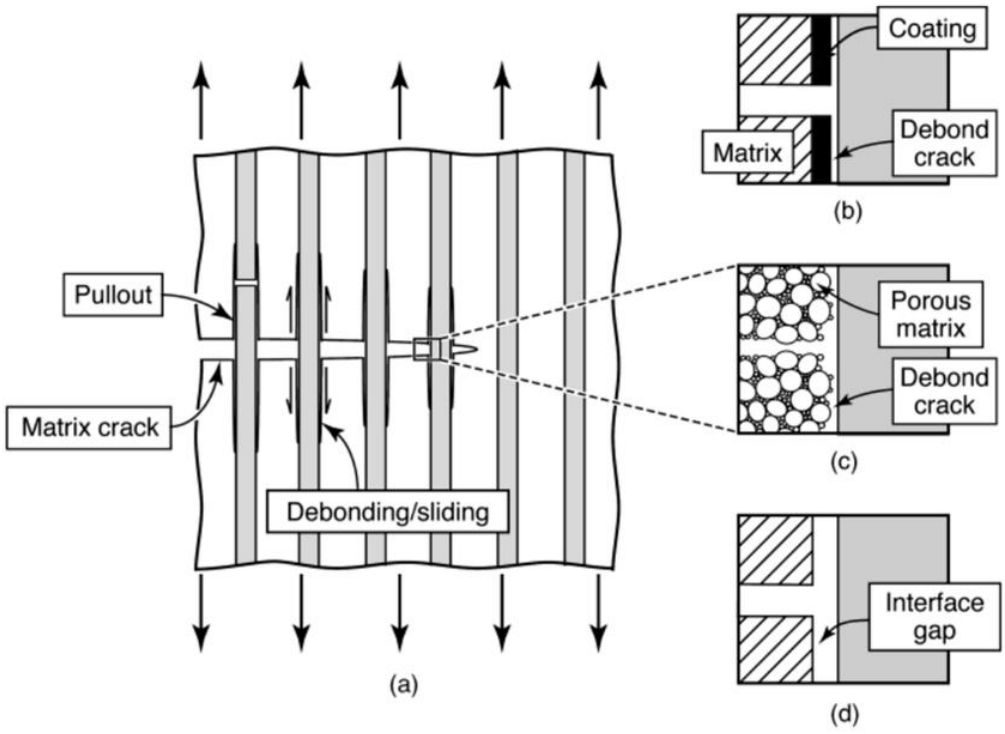

Figure 1-2: Reinforcement Mechanisms for Continuous-Fiber Ceramic Composites [26]

1.1.2 Types of Ceramic Matrix Composites

CMCs are commonly categorized based on the chemical composition of the reinforcing fibers and matrix materials. The two primary categories are oxide CMCs and non-oxide CMCs. The distinction between these two classes is important because it largely determines the operating temperature range, environmental resistance, and mechanical performance of the composite.

Oxide CMCs are composed entirely of oxide materials, typically alumina or aluminosilicate fibers embedded in oxide matrices such as alumina or mullite. Because these materials are already in an

oxidized state, oxide CMCs exhibit excellent environmental stability and oxidation resistance at elevated temperatures. However, oxide ceramics generally have lower thermal conductivity and lower maximum operating temperatures than non-oxide systems, which typically limits oxide CMCs to service temperatures below approximately 1200–1300 °C. Oxide CMCs are commonly used in industrial high-temperature environments such as furnace components, heat exchangers, and thermal insulation structures where oxidation resistance is more important than maximum temperature capability.

Non-oxide CMCs include materials based on carbides, nitrides, and carbon, such as carbon–carbon (C/C), carbon–silicon carbide (C/SiC), and silicon carbide–silicon carbide (SiC/SiC) composites. Among these materials, SiC/SiC composites are widely used in aerospace propulsion and turbine engine applications due to their high-temperature strength, oxidation resistance, and thermal conductivity. Non-oxide CMCs can typically operate at higher temperatures than oxide CMCs but may require environmental barrier coatings to prevent oxidation and environmental degradation. The choice between oxide and non-oxide CMCs therefore depends primarily on operating environment, temperature requirements, and mechanical performance needs.

1.1.3 Mechanical Behavior of Ceramic Matrix Composites

The mechanical behavior of monolithic CMCs is fundamentally different from that of monolithic ceramics due to the presence of reinforcement fibers and interface layers. Monolithic ceramics demonstrate linear elastic behavior followed by sudden brittle facture once critical stress is reached. In contrast, CMCs exhibit nonlinear stress-strain behavior due to their progressive damage mechanisms. Figure 1-3 illustrates the difference in failure behavior between monolithic ceramics and ceramic matrix composites, highlighting the brittle failure under low strain of the

monolithic ceramic, and the increased load bearing capability at higher strains of the ceramic matrix composite by adding reinforcement and interface materials.

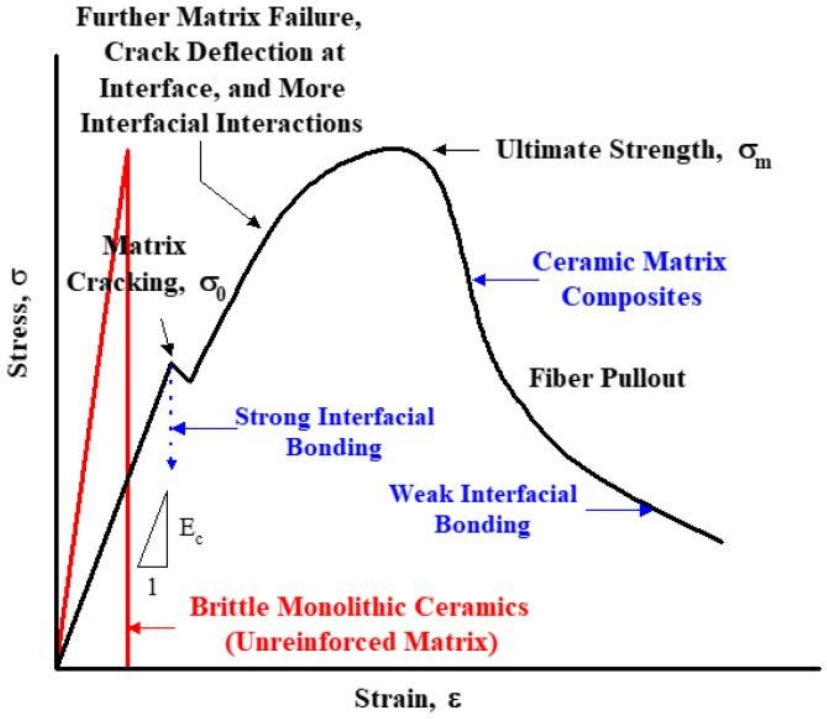

Figure 1-3: Stress-Strain Behavior of CMCs vs. Traditional Ceramics [27]

The stress–strain behavior of CMCs typically consists of multiple stages. In the initial stage, the composite behaves elastically as both the matrix and fibers carry load. As the load increases, matrix cracking begins to occur due to the low strain-to-failure of the ceramic matrix. During this stage, the load is transferred to the reinforcing fibers through shear stresses at the fiber–matrix interface. Multiple matrix cracks may form while the composite continues to carry increasing load. In the final stage, fiber debonding, sliding, and fiber pullout occur, resulting in gradual failure of the composite rather than sudden fracture. This behavior is often referred to as pseudo-ductile behavior and is one of the primary advantages of CMCs over monolithic ceramics [1], [5].

Fracture toughness in CMCs is significantly higher than in monolithic ceramics due to toughening mechanisms such as crack deflection, fiber bridging, and fiber pullout. These mechanisms absorb energy during crack propagation and improve damage tolerance. The fracture behavior of CMCs depends strongly on fiber strength, interface shear strength, fiber volume fraction, and fiber architecture. The interface properties are particularly important because they control fiber debonding and pullout behavior, which are the primary mechanisms responsible for toughness in CMCs [6].

CMCs also exhibit excellent high-temperature mechanical properties compared to metals and polymer matrix composites. CMCs retain strength and stiffness at elevated temperatures where metals may creep or lose strength and polymers would degrade. Silicon carbide-based CMCs, in particular, demonstrate excellent creep resistance and high-temperature strength, making them suitable for turbine engines, rocket propulsion components, and thermal protection systems. However, mechanical properties at high temperature are influenced by oxidation, creep, fiber degradation, and interface stability, which must be considered in high-temperature applications [5].

1.2 Polymer Derived Ceramics

Polymer-derived ceramics (PDCs) are a class of advanced ceramics produced through the thermal conversion of preceramic polymers into inorganic ceramic materials. Unlike conventional ceramic processing, which relies on powder consolidation and sintering, PDCs are formed through chemical transformation of an organosilicon polymer into a ceramic network via crosslinking and pyrolysis. This processing route allows the composition and microstructure of the ceramic to be

controlled through the molecular design of the precursor polymer, providing a high degree of flexibility in tailoring material properties [8]–[10].

Common PDCs include silicon carbide (SiC), silicon carbonitride (SiCN), silicon oxycarbide (SiOC), silicon nitride (Si_3N_4), and silicon boron carbonitride (SiBCN). These materials are known for their high-temperature stability, oxidation resistance, creep resistance, and thermal shock resistance, making them attractive for high-temperature structural applications, coatings, fibers, and CMCs matrices [8], [9]. In particular, PDCs are widely used in CMCs because the liquid polymer precursor can be infiltrated into fiber preforms prior to ceramic conversion.

The PDC synthesis process generally involves three main stages: precursor synthesis and processing, polymer-to-ceramic conversion through pyrolysis, and microstructural evolution during high-temperature exposure. The following sections describe these stages in more detail, including preceramic polymer precursors, polymer-to-ceramic conversion mechanisms, and the resulting ceramic microstructures and structure–property relationships [8]–[10].

1.2.1 Preceramic-Polymer Precursor

PDCs are synthesized from preceramic polymer precursors that undergo crosslinking and pyrolysis to form ceramic materials such as silicon carbide, silicon nitride, silicon carbonitride, silicon oxycarbide, and silicon boron carbonitride. Unlike conventional ceramic processing, where composition is determined by ceramic powders and sintering conditions, PDCs obtain their composition, structure, and microstructure directly from the molecular chemistry of the precursor polymer. As a result, precursor chemistry plays a critical role in determining ceramic composition, microstructure, ceramic yield, shrinkage behavior, and final mechanical and thermal properties [8], [13].

Preceramic polymers used in PDC processing are typically organosilicon polymers containing silicon atoms bonded to carbon, nitrogen, oxygen, or boron. The most common precursor families include polycarbosilanes, polysilazanes, polysiloxanes, and polyborosilazanes, which produce SiC, SiCN or Si_3N_4, SiOC, and SiBCN ceramics, respectively. Preceramic organosilicon polymers families are shown in Figure 1-4. These polymers are attractive because they can be processed using conventional polymer processing methods such as casting, extrusion, injection molding, fiber spinning, coating, and infiltration into fiber preforms before conversion into ceramics, enabling fabrication of complex shapes, coatings, fibers, and matrix materials for CMCs [8]–[10], [12].

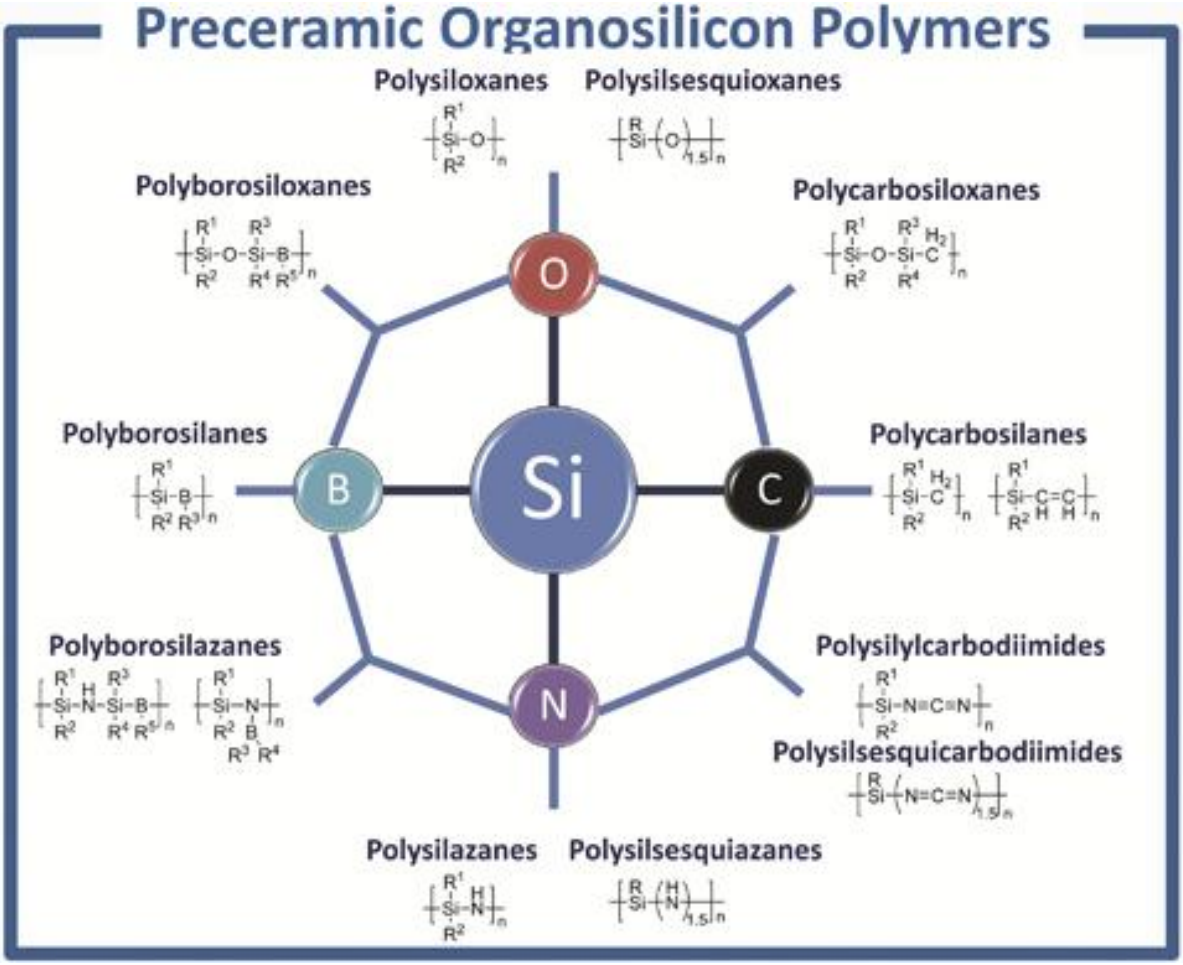

Figure 1-4: Families of Preceramic Organosilicon Polymers [6]

The molecular structure of the precursor polymer determines the composition of the final ceramic after pyrolysis. For example, polycarbosilanes contain Si–C bonds and typically yield silicon carbide ceramics, while polysilazanes contain Si–N bonds and produce silicon carbonitride or silicon nitride ceramics. Polysiloxanes produce silicon oxycarbide ceramics due to the presence of Si–O bonds, and polyborosilazanes introduce boron into the ceramic network, forming SiBCN ceramics with improved high-temperature stability and oxidation resistance. Because the ceramic composition is controlled by precursor chemistry, the structure and properties of the final ceramic can be tailored through molecular design of the precursor polymer [8]–[11].

One of the most significant advantages of PDCs processing is the ability to tailor ceramic composition through molecular design of the precursor polymer. Additional elements such as boron, aluminum, titanium, zirconium, hafnium, or oxygen can be incorporated into the polymer backbone or side groups, allowing thermal stability, oxidation resistance, creep resistance, and mechanical behavior of the resulting ceramic to be customized. This tunability is a major advantage of the PDC route compared to traditional ceramic processing methods [8]–[10], [11].

1.2.1.1 System Type

PDCs are often classified based on the number of elements present in the ceramic network, typically referred to as ternary, quaternary, and quinary systems. Increasing the number of elements in the ceramic network increases structural disorder and reduces atomic diffusion, which suppresses crystallization and improves high-temperature stability and creep resistance. This concept is particularly important for SiCN and SiBCN systems, where multicomponent compositions can remain amorphous to significantly higher temperatures than binary ceramics such as SiC or Si_3N_4 [9], [10], [15].

1.2.1.1.1 Ternary Systems

Ternary PDCs contain three primary elements, typically silicon combined with carbon, nitrogen, or oxygen. Common ternary systems include Si–C–O (SiOC), Si–C–N (SiCN), and Si–B–N (SiBN). These materials typically form amorphous ceramic networks consisting of silicon-centered tetrahedral units bonded to carbon, nitrogen, or oxygen atoms. Ternary systems are relatively easy to synthesize and are commonly used in coatings, fibers, and matrix materials; however, they tend to crystallize at lower temperatures compared to higher-order systems, typically in the range of 1400–1500 °C depending on composition and processing conditions [9], [10], [16].

1.2.1.1.2 Quaternary Systems

Quaternary PDCs contain four elements, such as Si–B–C–N, Si–Al–C–N, or Si–C–N–O. The addition of a fourth element, particularly boron or aluminum, significantly improves high-temperature stability and creep resistance. For example, boron-containing systems such as SiBCN ceramics exhibit delayed crystallization and improved oxidation resistance due to the formation of boron-containing phases that inhibit grain growth and phase separation at high temperature. These materials often maintain amorphous or nanocomposite structures at higher temperatures than ternary systems, which contributes to improved creep resistance and structural stability [9], [10], [15], [17].

1.2.1.1.3 Quinary Systems

Quinary systems contain five elements, such as Si–B–C–N–O or Si–Al–B–C–N. These systems represent some of the most thermally stable PDCs because the increased chemical complexity suppresses crystallization and maintains an amorphous nanocomposite structure to very high

temperatures. As a result, quinary PDCs can remain amorphous at temperatures exceeding 1700 °C, making them attractive for ultra-high-temperature applications such as thermal protection systems and CMCs matrices [9], [10], [15].

1.2.1.1.4 Modified Polysilazane Precursors

The incorporation of additional elements into polysilazane precursors allows the formation of quaternary and quinary PDCs such as SiBCN, SiAlCN, SiZrCN, and SiHfCN. These elements modify crystallization behavior, oxidation resistance, creep resistance, and high-temperature stability by forming secondary phases or inhibiting grain growth and phase separation. A summary of common modified polysilazane precursors and their property improvements is given in Table 1-1. Elemental additions are commonly used to improve oxidation resistance, high-temperature strength, and creep resistance in PDC systems [10],[15].

Table 1-1: Effect of Elemental Additions in Modified Polysilazane Precursors on Composition and High-Temperature Material Properties [8],[11]

Added Element	Typical Ceramic System	Primary Effect	Property Improvements
Boron (B)	Si–B–C–N	Inhibits crystallization	Improves high-temperature stability and creep resistance
Aluminum (Al)	Si–Al–C–N	Forms oxide barriers	Improves oxidation resistance and creep resistance
Oxygen (O)	Si–C–N–O	Forms SiOC phase	Improves oxidation resistance and thermal stability
Zirconium (Zr)	Si–Zr–C–N	Forms ZrC/ZrO_2 phases	Improves high-temperature strength and oxidation resistance
Hafnium (Hf)	Si–Hf–C–N	Forms HfC/HfO_2	Improves ultra-high-temperature stability
Titanium (Ti)	Si–Ti–C–N	Forms TiC/TiN	Improves hardness and wear resistance
Yttrium (Y)	Si–Y–C–N	Stabilizes oxide phases	Improves oxidation resistance and creep resistance
Molybdenum (Mo)	Si–Mo–C–N	Forms Mo_2C	Improves high-temperature strength
Tungsten (W)	Si–W–C–N	Forms WC	Improves high-temperature strength and hardness

Increasing the number of alloying elements increases structural disorder and reduces atomic diffusion, which delays crystallization and grain growth. Therefore, quaternary and quinary PDCs typically exhibit improved high-temperature stability and creep resistance compared to ternary systems. This approach has been widely used in the development of ultra-high-temperature PDCs for aerospace and thermal protection applications [9], [10], [17].

1.2.1.2 Processing Behavior and Ceramic Yield

Another important factor in precursor selection is ceramic yield, defined as the fraction of mass remaining after pyrolysis. Preceramic polymers can be processed using conventional polymer processing techniques such as casting, extrusion, injection molding, coating, and infiltration into fiber preforms. After shaping, the polymer is crosslinked and pyrolyzed to form the ceramic. During pyrolysis, organic groups are removed as gaseous species, resulting in mass loss, shrinkage, and potential porosity formation. Low ceramic yield results in significant shrinkage and potential cracking during polymer-to-ceramic conversion; therefore, precursor polymers with higher crosslink density and fewer volatile side groups are preferred [8], [11], [12].

Precursor chemistry must be carefully designed to balance processability, ceramic yield, shrinkage, and final ceramic properties. The ability to design precursor polymers with tailored composition and properties makes PDCs highly versatile materials for high-temperature structural applications, coatings, fibers, and CMCs [8]–[10].

1.2.2 Polymer-to-Ceramic Conversion

The polymer-to-ceramic conversion process is the defining step in the PDC route, during which a preceramic polymer is transformed into an inorganic ceramic through crosslinking, thermal decomposition, gas evolution, and pyrolysis. This process involves significant chemical and

microstructural changes and ultimately results in amorphous or nanocrystalline ceramic material. The final ceramic composition, ceramic yield, porosity, and microstructure are strongly dependent on precursor chemistry, curing behavior, pyrolysis temperature, heating rate, and atmosphere [8],[13]. Unlike conventional ceramic processing, where ceramics are formed through powder sintering and grain growth, PDCs form through chemical decomposition and atomic rearrangement of the polymer network.

During processing, the preceramic polymer must first be crosslinked or cured to form an infusible solid. Crosslinking prevents melting or deformation during heating and allows the material to retain its shape during pyrolysis. Crosslinking can occur through thermal curing, oxidation curing, electron beam irradiation, or chemical reactions such as hydrosilylation and dehydrocoupling reactions. The degree of crosslinking significantly influences ceramic yield and dimensional stability, since insufficient crosslinking can result in excessive mass loss, deformation, or cracking during pyrolysis, while higher crosslink density generally improves ceramic yield and reduces shrinkage [8], [10], [11].

Following crosslinking, the material undergoes pyrolysis in an inert or reactive atmosphere such as argon, nitrogen, or ammonia to convert the organic polymer into an inorganic ceramic. During pyrolysis, organic groups are eliminated as gaseous species such as hydrogen, methane, ammonia, and hydrocarbons, while the remaining silicon, carbon, nitrogen, boron, or oxygen atoms rearrange to form ceramic bonds such as Si–C, Si–N, B–N, and C–C. The polymer-to-ceramic conversion process typically occurs in several temperature-dependent stages, including crosslinking, polymer decomposition, amorphous ceramic formation, and high-temperature structural rearrangement and crystallization [8],[13].

One of the major challenges in polymer-to-ceramic conversion is the large mass loss and volumetric shrinkage that occur during pyrolysis due to the removal of organic groups and evolution of gaseous species. Shrinkage typically ranges from approximately 20% to 40%, depending on precursor chemistry and processing conditions, and can lead to cracking, porosity, and residual stresses if not carefully controlled. The fraction of mass remaining after pyrolysis is referred to as the ceramic yield, which is a critical parameter in PDC processing. Ceramic yield depends primarily on precursor molecular structure, crosslinking density, and pyrolysis conditions, and precursors with higher crosslink density and fewer volatile groups generally produce higher ceramic yields and lower shrinkage [8], [10], [11].

During polymer-to-ceramic conversion, the material transitions from an organic polymer to an amorphous ceramic and eventually to a nanocrystalline ceramic at higher temperatures. Many PDCs such as SiCN and SiBCN remain amorphous to very high temperatures due to their multi-element composition and structural disorder, which contributes to their excellent creep resistance and thermal stability. Structural evolution during pyrolysis generally includes crosslinking and curing, polymer decomposition and gas evolution, formation of an amorphous ceramic network, densification and phase separation, and crystallization at higher temperatures. These microstructural changes strongly influence mechanical properties, creep resistance, oxidation behavior, and thermal stability of PDCs [9], [13], [11].

Overall, the polymer-to-ceramic conversion process involves crosslinking, pyrolysis, gas evolution, shrinkage, densification, and structural rearrangement, resulting in amorphous or nanocrystalline ceramic materials. Control of crosslinking, pyrolysis temperature, heating rate, and atmosphere is critical for achieving high ceramic yield, minimizing shrinkage and cracking, and tailoring the final ceramic microstructure and properties. The ability to control ceramic

composition and structure through precursor chemistry and pyrolysis conditions is one of the major advantages of the PDC processing route [8]–[13].

1.2.3 Polymer-Derived Ceramic Structure

The structure of PDCs differs significantly from that of traditional monolithic ceramics due to the polymer-to-ceramic conversion process. Instead of forming fully crystalline ceramics, most PDCs initially form amorphous or nanocomposite ceramic structures consisting of mixed bonding environments and multiple phases at the nanoscale. This unique structure is responsible for many of the desirable properties of PDCs, including high-temperature stability, creep resistance, oxidation resistance, and thermal shock resistance [8]–[11].

PDCs such as SiC, SiCN, SiOC, and SiBCN are typically composed of an amorphous ceramic matrix containing nanocrystalline domains and free carbon, resulting in a nanocomposite microstructure rather than a single-phase crystalline ceramic. The nanostructure formed during polymer pyrolysis strongly depends on precursor chemistry, pyrolysis temperature, and atmosphere, which influence phase separation, carbon segregation, and crystallization behavior [9], [13], [11].

1.2.3.1 Amorphous Ceramic Structure

Following pyrolysis at temperatures typically between 800 °C and 1200 °C, PDCs form an amorphous network composed of silicon, carbon, nitrogen, oxygen, and boron depending on precursor chemistry. The bonding environment in these materials consists of a mixture of bonds such as Si–C, Si–N, Si–O, B–N, and C–C, forming a highly disordered atomic structure [9], [13].

This amorphous structure is one of the key reasons PDCs exhibit excellent high-temperature creep resistance, since creep mechanisms such as grain boundary sliding are minimized in amorphous

materials due to the absence of grain boundaries. Additionally, the disordered structure delays crystallization and grain growth, allowing some PDC systems such as SiBCN to remain amorphous at temperatures exceeding 1500 °C. The presence of multiple elements and mixed bonding environments increases structural disorder and reduces atomic diffusion, which contributes to improved thermal stability and creep resistance [9], [10], [13].

Amorphous PDCs are often described as consisting of silicon-centered tetrahedral units bonded to carbon, nitrogen, or oxygen atoms, forming a three-dimensional amorphous network. The exact bonding environment depends on precursor chemistry and processing conditions [9], [13], [11].

1.2.3.2 Nanocomposite Structure and Free Carbon Phase

Many PDCs form nanocomposite structures consisting of an amorphous ceramic matrix with embedded nanocrystalline phases and free carbon. During pyrolysis, excess carbon from the polymer precursor may segregate into a separate amorphous carbon phase, often referred to as free carbon. This free carbon phase can significantly influence mechanical and thermal properties of the material [11], [13].

The nanocomposite structure typically consists of:

- Amorphous Si–C–N or Si–O–C matrix
- Nanocrystalline SiC or Si_3N_4 particles
- Free carbon phase
- Possible BN or other secondary phases in multi-element systems

The presence of free carbon can improve fracture toughness and thermal shock resistance by acting as a crack deflection phase and reducing crack propagation. However, excessive free carbon may

reduce oxidation resistance and high-temperature strength because carbon can oxidize or degrade at high temperatures in oxidizing environments [11], [13].

Nanostructure studies of SiCN and SiOC ceramics have shown that these materials often consist of nanoscale domains rather than homogeneous amorphous structures. The nanoscale heterogeneity and distribution of carbon phases strongly influence crystallization behavior, mechanical properties, and thermal stability of PDCs [9], [11].

1.2.3.3 Phase Separation and Crystallization

At higher temperatures, typically above 1200-1500°C, PDCs undergo phase separation and crystallization. The amorphous ceramic begins to decompose into thermodynamically stable crystalline phases such as SiC, Si_3N_4, BN, and graphite depending on composition and processing conditions [8], [10], [13].

For example:

- SiCN ceramics may separate into SiC + Si_3N_4 + C
- SiOC ceramics may separate into SiC + SiO_2 + C
- SiBCN ceramics may form SiC + BN + C

The addition of elements such as boron or aluminum can delay crystallization and maintain the amorphous structure to higher temperatures, which improves creep resistance and high-temperature mechanical stability. Boron-containing systems such as SiBCN are known to exhibit improved thermal stability because boron can inhibit grain growth and crystallization at high temperatures [9], [10], [13].

Phase separation and crystallization behavior strongly influence mechanical properties, oxidation resistance, and thermal stability of PDCs, and therefore controlling crystallization through precursor chemistry is an important aspect of PDC materials design [9], [13].

1.2.3.4 Structure- Property Relationships

The unique amorphous and nanocomposite structure of PDCs directly influences their mechanical and thermal properties. The absence of large grains and grain boundaries improves creep resistance and thermal shock resistance, while the presence of free carbon and nanocrystalline phases can improve fracture toughness and damage tolerance. Multi-element systems such as SiBCN and SiAlCN exhibit improved high-temperature stability due to their ability to maintain an amorphous structure to higher temperatures compared to binary systems such as SiC [9], [10], [13].

The structure of PDCs can therefore be tailored through precursor chemistry and pyrolysis conditions to achieve specific mechanical, thermal, and oxidation-resistant properties. This ability to tailor ceramic structure and properties through polymer chemistry is one of the major advantages of PDC processing compared to traditional ceramic processing methods [8]-13].

PDCs are characterized by amorphous or nanocomposite microstructures consisting of mixed bonding environments, nanocrystalline phases, and free carbon. The amorphous structure provides excellent creep resistance and thermal stability, while the nanocomposite structure improves toughness and thermal shock resistance. At higher temperatures, phase separation and crystallization occur, forming stable ceramic phases such as SiC, Si_3N_4, BN, and graphite. The ability to control ceramic structure through precursor chemistry and pyrolysis conditions allows PDCs to be tailored for high-temperature structural applications [8]-13].

1.3 Manufacturing Methods

Ceramic matrix composites (CMCs) are typically manufactured using infiltration-based processing techniques in which a porous fiber preform is densified through the introduction of a matrix precursor in liquid, vapor, or molten form. The precursor is subsequently converted into a ceramic matrix through pyrolysis, chemical reaction, or solidification. Multiple infiltration cycles are often required to reduce porosity and achieve the desired mechanical properties and structural integrity. The most common manufacturing methods for CMCs include polymer infiltration and pyrolysis (PIP), chemical vapor infiltration (CVI), and melt infiltration (MI), also known as reactive melt infiltration (RMI) or liquid silicon infiltration (LSI) [18].

These manufacturing techniques differ significantly in processing temperature, densification rate, cost, and resulting microstructure. Polymer infiltration and pyrolysis typically operates at relatively low temperatures but requires many processing cycles. Chemical vapor infiltration produces high purity matrices with controlled fiber interfaces but is time-consuming and expensive. Melt infiltration provides rapid densification and low porosity but may introduce residual metal phases in the matrix. The selection of a manufacturing method depends on the desired material properties, operating temperature, and application requirements.

1.3.1 Polymer Infiltration and Pyrolysis (PIP)

Polymer infiltration and pyrolysis (PIP) is a widely used manufacturing technique for CMCs, particularly for silicon carbide matrix composites. In this process, a porous fiber preform is infiltrated with a liquid polymer precursor that is converted into a ceramic matrix through pyrolysis at elevated temperatures in an inert environment [19]. PIP processing is visualized in Figure 1-5.

During the PIP process, the polymer precursor infiltrates the pore structure of the fiber preform in liquid form or as a solution. The infiltrated preform is then heated to temperatures typically above 1000 °C, where the polymer undergoes pyrolysis and transforms into a ceramic material such as silicon carbide. This polymer-to-ceramic conversion results in significant shrinkage and the formation of porosity within the matrix, which necessitates multiple infiltration and pyrolysis cycles to achieve sufficient densification [19], [20].

The densification behavior of PDCs is strongly dependent on the number of infiltration cycles. Increasing the number of PIP cycles reduces porosity and improves mechanical properties such as Young's modulus and bending strength. However, densification becomes less effective after several cycles due to the formation of closed pores and reduced permeability, which limits further infiltration of the polymer precursor [20].

To reduce shrinkage and improve densification efficiency, filler materials are often added to the polymer precursor. Active fillers may react during pyrolysis to form additional ceramic phases, while inert fillers reduce shrinkage and improve dimensional stability. These filler-enhanced PIP processes improve densification and mechanical performance of CMCs [19].

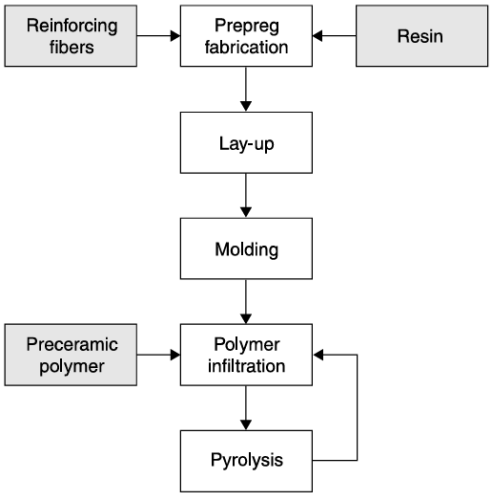

Figure 1-5: Polymer Infiltration and Pyrolysis Process Diagram

1.3.2 Chemical Vapor Infiltration (CVI)

Chemical vapor infiltration (CVI) is a gas-phase processing technique used to manufacture CMCs by depositing ceramic material from gaseous precursors within a porous fiber preform. CVI is commonly used for carbon/carbon and silicon carbide CMCs used in high-temperature aerospace applications [21]. CVI processing is visualized in Figure 1-6.

In the CVI process, a porous fiber preform is placed in a reactor where reactive gases are introduced at elevated temperature and controlled pressure. These gases diffuse through the pore structure of the preform and undergo chemical reactions on the fiber surfaces and pore walls, depositing a solid ceramic matrix such as silicon carbide or pyrolytic carbon. The process relies on gas diffusion through the preform followed by chemical reaction and deposition of the ceramic material [21].

One of the primary limitations of conventional CVI processing is that deposition typically occurs first near the outer surface of the preform, where temperature and gas concentration are highest. This leads to the formation of a dense outer layer that blocks further gas infiltration into the interior, resulting in long processing times and residual porosity. Conventional CVI processing can require hundreds of hours to achieve full densification due to slow gas diffusion and deposition rates [21].

To improve densification and reduce processing time, modified CVI techniques have been developed, including forced-flow CVI, pressure-gradient CVI, and radiofrequency assisted CVI. These techniques create temperature or pressure gradients within the preform that promote more uniform deposition and reduce surface pore closure, allowing densification to occur from the interior outward [21].

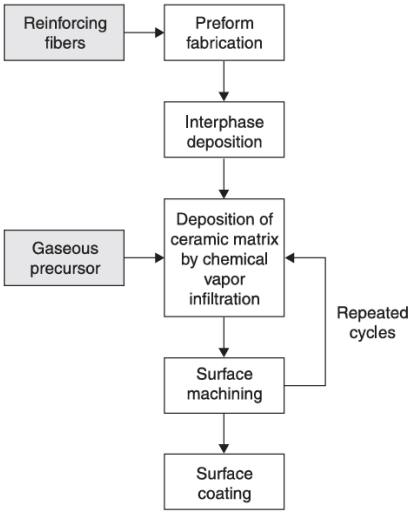

Figure 1-6: Chemical Vapor Infiltration Process Diagram

1.3.3 Melt Infiltration (MI)

Melt infiltration is a manufacturing method in which a molten metal or alloy infiltrates a porous preform and reacts with the preform constituents to form a ceramic matrix. This process is commonly used for silicon carbide-based CMCs and ultra-high temperature CMCs [22]. MI processing is visualized in Figure 1-7.

In melt infiltration processing, a porous fiber preform containing fibers and ceramic or carbon powders is first fabricated. The preform is then infiltrated with molten silicon or other reactive metal alloys. During infiltration, the molten metal reacts with carbon or other constituents in the preform to form ceramic phases such as silicon carbide while simultaneously filling the remaining porosity. This results in relatively low porosity and high thermal conductivity compared to other CMC manufacturing methods [22].

Si(Liquid) + C(solid) -> SiC(solid)

The fabrication of melt infiltrated CMCs typically involves three major steps: application of fiber coatings, fabrication of a porous fiber preform, and final densification through molten silicon

infiltration. During infiltration, molten silicon reacts with free carbon present in the preform to form a continuous silicon carbide matrix phase, while some residual silicon may remain in the composite matrix [22].

Reactive melt infiltration processes can also be used to fabricate ultra-high temperature CMCs, where molten metals react with boron, carbon, or silicon carbide to form ceramic matrices such as zirconium diboride or zirconium carbide during infiltration. These processes rely on capillary forces to infiltrate molten metal into porous preforms and chemical reactions that occur during infiltration to form ceramic phases [23].

Melt infiltration offers several advantages compared to polymer infiltration and pyrolysis and chemical vapor infiltration, including faster densification, lower residual porosity, and lower manufacturing cost. However, the process may result in residual metal phases in the matrix and can cause fiber degradation if processing conditions are not properly controlled.

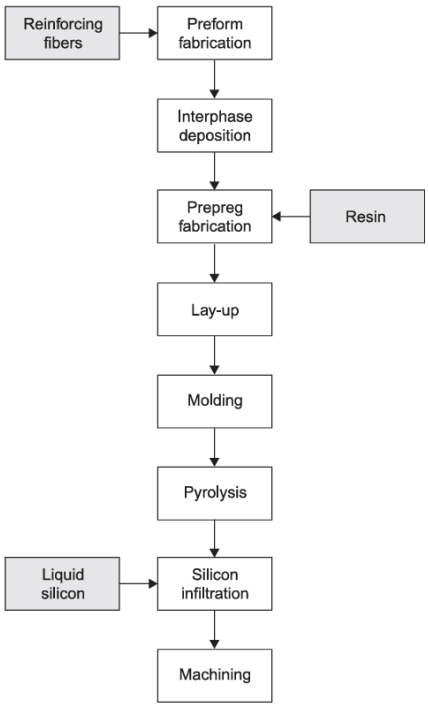

Figure 1-7: Melt Infiltration Process Diagram

1.4 Engineering Applications

Ceramic matrix composites (CMCs) and polymer-derived ceramics (PDCs) are used in engineering applications that involve high temperatures, corrosive environments, thermal shock, wear, and strict mass limitations. Compared with conventional metallic alloys, CMCs offer lower density, improved high-temperature strength retention, oxidation resistance, corrosion resistance, and improved thermal stability. These properties make them attractive for aerospace propulsion systems, thermal protection systems, energy generation systems, automotive components, nuclear systems, and high-temperature industrial processes.

The primary motivation for using CMCs in engineering systems is their ability to operate at temperatures beyond the limits of nickel-based superalloys while maintaining structural integrity and reducing system weight. In many high-temperature systems, increasing operating temperature improves efficiency, particularly in gas turbine engines, propulsion systems, and power generation systems. As a result, CMCs have become important candidate materials for turbine hot-section components and other high-temperature structural components [5], [2], [1]. Figure 1-8 highlights the various industries that benefit from the development of advanced ceramic systems.

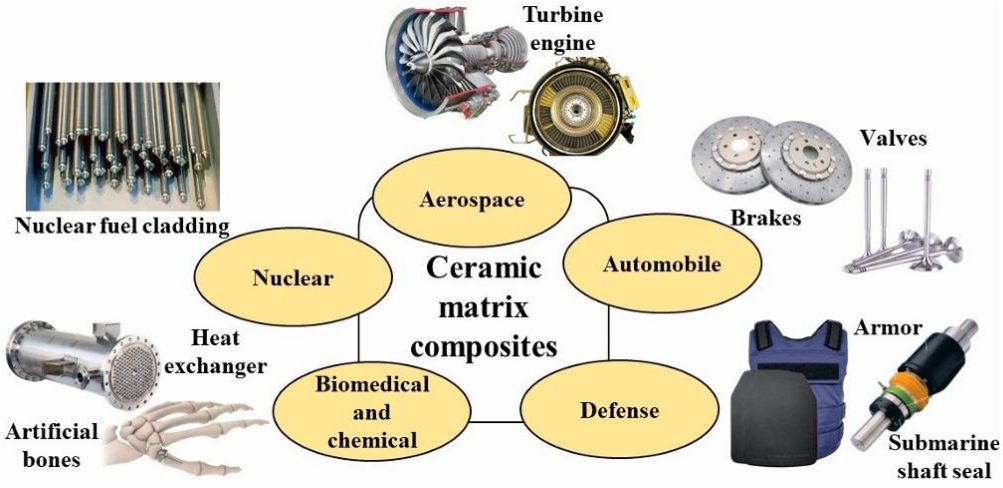

Figure 1-8: Representative Engineering Application Domains of CMCs and PDC-Based Materials [25]

1.4.1 Aerospace Propulsion and Gas Turbine Systems

One of the most important engineering applications of CMCs is in aerospace propulsion and gas turbine engines. Silicon carbide fiber reinforced silicon carbide matrix (SiC/SiC) composites are widely used or studied for combustor liners, turbine shrouds, turbine nozzles, turbine blades, exhaust components, and other hot-section components (Figure 1-9). These materials are attractive because they combine low density, high strength, oxidation resistance, and the ability to operate at temperatures higher than metallic superalloys [2], [1], [25].

The use of CMC components in turbine engines allows higher operating temperatures while reducing cooling requirements. Conventional metallic turbine components require significant cooling air, which reduces engine efficiency. Because CMCs can tolerate higher temperatures, less cooling air is required, resulting in improved engine efficiency, reduced fuel consumption, and lower emissions. Additionally, the lower density of CMCs reduces rotating mass and mechanical stress on engine components, improving overall engine performance [2], [1], [25].

CMCs are also used in industrial gas turbines for power generation. In these systems, CMC combustor liners and turbine components can increase operating temperature, improve thermal efficiency, and reduce maintenance due to improved oxidation resistance and longer component lifetimes. These advantages make CMCs attractive for both aerospace propulsion systems and stationary power generation turbines [1], [25].

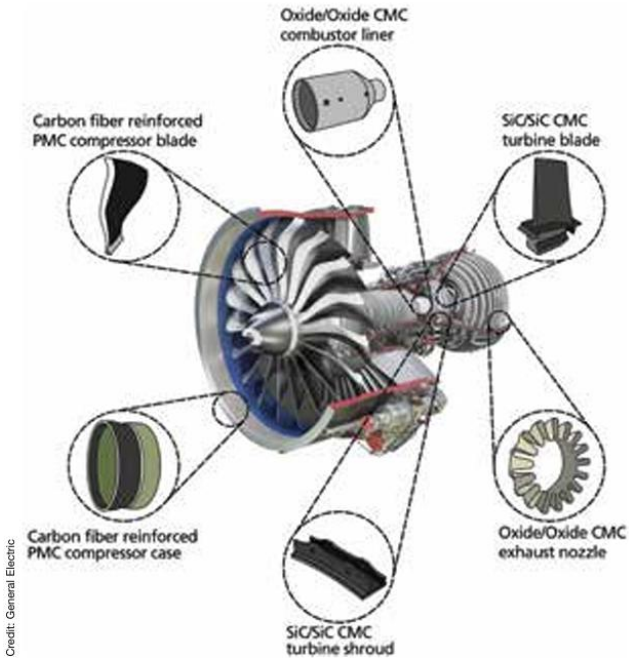

Figure 1-9: CMC Components in a Gas Turbine Engine, adapted from GE Aviation [14]

1.4.2 Space Vehicles, Reentry Systems, and Thermal Protection

CMCs and polymer-derived ceramics are also widely studied for space vehicles and hypersonic applications. Spacecraft reentry vehicles and hypersonic flight vehicles experience extremely high surface temperatures due to aerodynamic heating, requiring materials that can withstand high temperatures, thermal shock, oxidation, and mechanical loads simultaneously. CMCs such as C/SiC, SiC/SiC, and C/C-SiC are commonly used or proposed for thermal protection systems, leading edges, nose cones, rocket nozzles, combustion chambers, and hot structural components [12], [10], [24].

Carbon fiber reinforced silicon carbide composites are especially important for thermal protection systems because they combine high temperature capability with good thermal shock resistance and oxidation resistance. These materials have been used in rocket motor components, nozzle extensions (Figure 1-10), and reentry vehicle structures where temperatures can exceed 2000 °C.

One modern example is the European Space Agency's intermediate experimental vehicle (IXV) using C/SiC in exterior components for reentry, shown in Figure 1-11 [10]. In these applications, the ceramic matrix protects the carbon fibers from oxidation while the fibers provide toughness and resistance to brittle failure [12], [10].

PDCs play an important role in space applications such as matrix precursors, oxidation-resistant coatings, ceramic adhesives, environmental barrier coatings, and lightweight thermal protection materials. Because preceramic polymers can be processed as liquids and then converted to ceramics through pyrolysis, they enable near-net-shape manufacturing and coating of complex geometries. PDC-based coatings are also used for oxidation protection, environmental barrier coatings, and atomic oxygen resistant coatings for spacecraft operating in low Earth orbit [12], [10]. Development of C/SiC composites for satellite thrusters due to their ability to produce higher impulses compared to traditional configurations is a significant application of these materials (Figure 1-12).

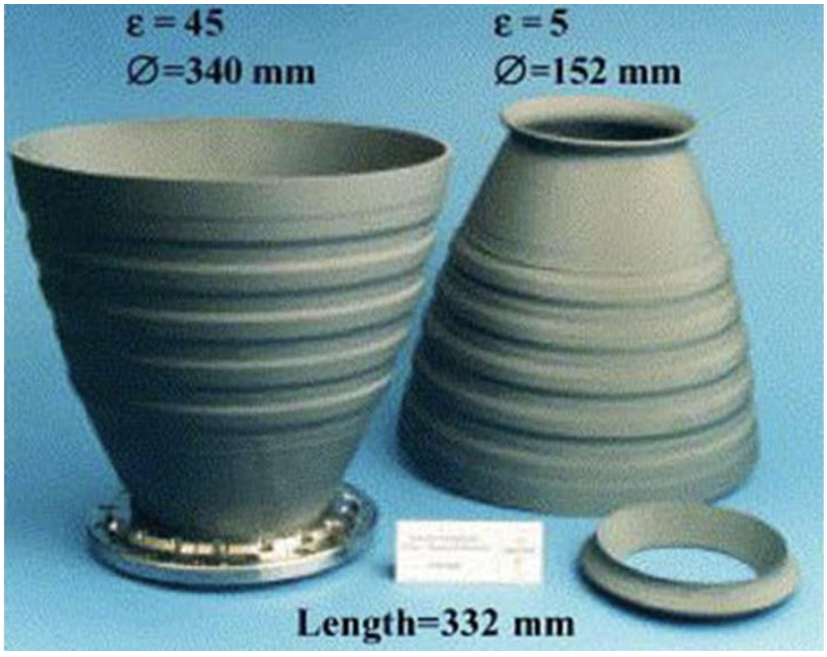

Figure 1-10: C/SiC Nozzle Extensions developed for ULA's Vulcan Cryogenic Engine [10]

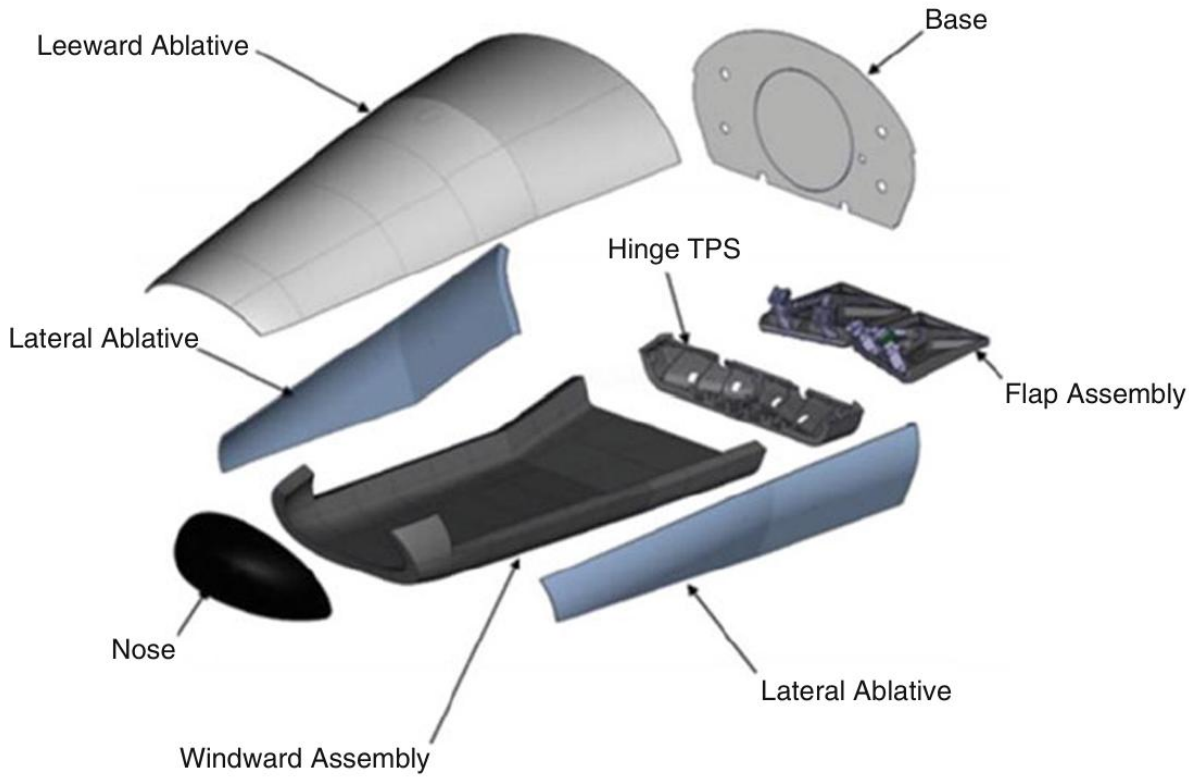

Figure 1-11: C/SiC Components for ESA's IXV, a.) Nose Assembly, b.) Shingles, Based Windward Assembly, and c.) Flap Assembly [10]

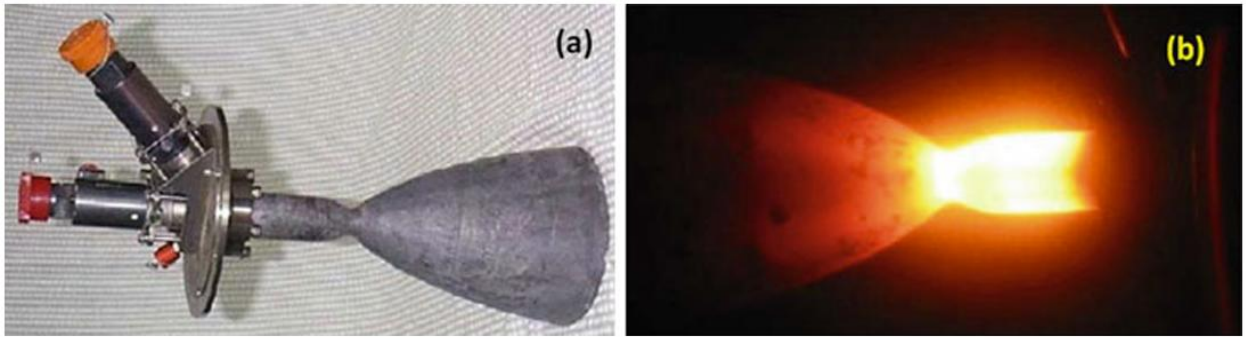

Figure 1-12: a.) 150N Bipropellant C/SiC rocket nozzle, b.) Hotfire of 150 Bipropellant C/SiC Rocket Nozzle [10]

1.4.3 Automotive and Friction Applications

In the automotive industry, CMCs are primarily used in high-performance and high-temperature components rather than large structural components due to cost considerations. One of the most common applications is carbon-ceramic brake systems, where CMC brake rotors provide excellent thermal stability, low thermal expansion, high wear resistance, and reduced mass compared with cast iron brake rotors. These systems are widely used in high-performance vehicles and motorsports [5], [24].

Other automotive applications include turbocharger components, exhaust systems, engine components, catalytic converter substrates, and wear-resistant parts such as seals and bearings. In these applications, the benefits of CMCs include high-temperature stability, corrosion resistance, reduced weight, and improved durability under thermal cycling conditions [5], [24].

1.4.4 Energy, Nuclear, and High-Temperature Process Systems

CMCs are also used in energy generation, nuclear reactors, and high-temperature industrial processes. In energy systems such as gas turbines, heat exchangers, furnaces, and power generation systems, CMCs can operate at higher temperatures than metals, improving system efficiency and

reducing energy consumption. Their oxidation resistance and thermal stability make them suitable for long-term exposure to high-temperature oxidizing environments [1], [25].

In nuclear applications, silicon carbide-based CMCs are considered for fuel cladding, reactor core components, and structural materials due to their high-temperature strength, corrosion resistance, low neutron activation, and good radiation resistance. These materials are being studied for advanced nuclear reactors and fusion reactor components where materials must operate under high temperature, radiation, and corrosive environments simultaneously [5], [1].

CMC materials are also used in high-temperature industrial equipment such as heat exchangers, reformers, chemical processing equipment, refractory components, and furnace hardware. Their resistance to oxidation, corrosion, and thermal shock allows them to operate in harsh industrial environments where metallic components would degrade quickly [5], [1], [25].

1.4.5 Other Engineering Applications

Additional engineering applications of CMCs include defense systems, biomedical devices, electronics, and chemical processing equipment. In defense applications, CMCs are used for lightweight armor, missile components, propulsion systems, and high-temperature structural components. Their high specific strength and thermal resistance make them suitable for high-speed and high-temperature environments [5].

In biomedical applications, ceramics and ceramic composites are used for implants, dental materials, joint replacements, and bone repair materials due to their biocompatibility, wear resistance, and corrosion resistance. PDCs are also being investigated for biomedical coatings, sensors, microelectronics, and MEMS devices due to their ability to be processed into complex shapes and micro-scale structures [12], [10].

1.4.6 Summary of Application Trends

Overall, the engineering applications of CMCs and PDCs are concentrated in environments where materials must withstand high temperatures, corrosive environments, wear, radiation, or mechanical loading while maintaining low weight and long service life. The most important application areas include aerospace propulsion, thermal protection systems, gas turbines, automotive braking systems, nuclear reactors, and high-temperature industrial equipment. As manufacturing methods improve and costs decrease, the use of CMCs and PDC-derived materials is expected to expand into additional structural, multifunctional, and extreme-environment engineering applications.

1.5 References

[1] Krenkel, Walter, ed. Ceramic matrix composites: fiber reinforced ceramics and their applications. John Wiley & Sons, 2008.

[2] Naslain, Roger. "Design, preparation and properties of non-oxide CMCs for application in engines and nuclear reactors: an overview." Composites Science and Technology 64.2 (2004): 155-170.

[3] Chawla, Krishan K. Ceramic matrix composites. Springer Science & Business Media, 2013.

[4] Dever, Joyce A., Michael V. Nathal, and James A. DiCarlo. "Research on high-temperature aerospace materials at NASA Glenn Research Center." Journal of Aerospace Engineering 26.2 (2013): 500-514.

[5] Shrivastava, Shriya, et al. "Ceramic matrix composites: classifications, manufacturing, properties, and applications." Ceramics 7.2 (2024): 652-679.

[6] Colombo, Paolo, et al. "Polymer-derived ceramics: 40 years of research and innovation in advanced ceramics." Journal of the American Ceramic Society 93.7 (2010): 1805-1837.

[7] Ren, Zhongkan, Shakir Bin Mujib, and Gurpreet Singh. "High-temperature properties and applications of Si-based polymer-derived ceramics: a review." Materials 14.3 (2021): 614.

[8] Riedel, Ralf, et al. "Silicon-based polymer-derived ceramics: synthesis properties and applications-a review dedicated to Prof. Dr. Fritz Aldinger on the occasion of his 65th birthday." Journal of the Ceramic Society of Japan 114.1330 (2006): 425-444.

[9] Greil, Peter. "Polymer derived engineering ceramics." Advanced engineering materials 2.6 (2000): 339-348.

[10] Packirisamy, S., et al. "Polymer-derived ceramics and their space applications." Handbook of Advanced Ceramics and Composites: Defense, Security, Aerospace and Energy Applications. Cham: Springer International Publishing, 2020. 975-1080.

[11] Gao, Yan, et al. "Processing route dramatically influencing the nanostructure of carbon-rich SiCN and SiBCN polymer-derived ceramics. Part I: Low temperature thermal transformation." Journal of the European Ceramic Society 32.9 (2012): 1857-1866.

[12] Wen, Qingbo, Zhaoju Yu, and Ralf Riedel. "The fate and role of in situ formed carbon in polymer-derived ceramics." Progress in Materials Science 109 (2020): 100623.

[13] Wang, Jian, et al. "Recent advances in preceramic polysilazane precursors in additive manufacturing." Additive Manufacturing Frontiers 3.1 (2024): 200119.

[14] Ren, Zhongkan, and Gurpreet Singh. "Nonoxide polymer-derived CMCs for “super” turbines." *American Ceramic Society bulletin* 98.3 (2019).

[15] Zimmermann, A., et al. "High-temperature deformation of amorphous Si–C–N and Si–B–C–N ceramics derived from polymers." Acta materialia 50.5 (2002): 1187-1196.

[16] Wang, Zhen, et al. "Microstructure observation and analysis of 3D carbon fiber reinforced SiC-based composites fabricated through filler enhanced polymer infiltration and pyrolysis." Ceramics International 38.1 (2012): 535-540.

[17] Namazu, Takahiro, Tomohiro Ishikawa, and Yoshio Hasegawa. "Influence of polymer infiltration and pyrolysis process on mechanical strength of polycarbosilane-derived silicon carbide ceramics." Journal of materials science 46.9 (2011): 3046-3051.

[18] Santhosh, Unni, et al. "A polymer infiltration and pyrolysis (PIP) process model for ceramic matrix composites (CMCs)." Journal of the American Ceramic Society 104.12 (2021): 6108-6130.

[19] Venkatachalam, Vinothini, Burkard Esser, and Jon Binner. "Processing and performance of ultra high temperature ceramic matrix composite (UHTCMCs) using radio frequency assisted chemical vapour infiltration (RF-CVI)." Composites Part A: Applied Science and Manufacturing 185 (2024): 108358.

[20] Corman, G. S., and K. L. Luthra. "Silicon melt infiltrated ceramic composites (HiPerComp™)." Handbook of ceramic composites. Boston, MA: Springer US, 2005. 99-115.

[21] Kütemeyer, Marius, et al. "Fabrication of ultra high temperature ceramic matrix composites using a reactive melt infiltration process." Journal of the European Ceramic Society 36.15 (2016): 3647-3655.

[22] Fellet, Melissae, and Wolfgang Rossner. "Ceramic-matrix composites take the heat." MRS Bulletin 40.11 (2015): 916-918.

[23] Zok, Frank W., and Carlos G. Levi. "Mechanical properties of porous-matrix ceramic composites." Advanced Engineering Materials 3.1-2 (2001): 15-23.

[24] Boakye, Emmanuel E., et al. "Evaluation of SiC/SiC minicomposites with yttrium disilicate fiber coating." Journal of the American Ceramic Society 101.1 (2018): 91-102.

[25] Shrivastava, Shriya, et al. "Ceramic matrix composites: classifications, manufacturing, properties, and applications." Ceramics 7.2 (2024): 652-679.

[26] Tülümen, Hasan Metin, et al. "Investigation of feedstock preparation for injection molding of oxide–oxide ceramic composites." Journal of Manufacturing and Materials Processing 3.1 (2019): 9.

[27] Kim, Jeongguk. "Tensile fracture behavior and characterization of ceramic matrix composites." Materials 12.18 (2019): 2997.

I would like to acknowledge the use of Microsoft Copilot for polishing the language and improving the clarity of certain sections of this thesis. All AI-suggested edits were manually reviewed and refined, and I remain solely responsible for the original research, analysis, and final text.

CHAPTER 2: MULTI-CYCLE SiCN-CF AND SiBCN-CF STUDY, METHOD 1

This chapter investigates the traditional polymer infiltration and pyrolysis (PIP) process used to fabricate silicon carbon nitride (SiCN) and silicon boron carbon nitride (SiBCN) ceramic matrix composites (CMCs) reinforced with carbon fiber bundles. In the conventional PIP process, multiple infiltration and pyrolysis cycles are performed to increase ceramic yield and matrix density within the fiber bundles. While this method is effective at improving ceramic content and mechanical performance, it requires repeated high-temperature furnace cycles, which increases processing time and manufacturing complexity.

In this study, a recipe for a conventional PIP process is used to baseline the single cycle samples and compare the performance of the multi-cycle samples [7]. Boron-modified and unmodified polysilazane liquid precursors were used to infiltrate carbon fiber bundles in an oxygen-free environment. Following infiltration, the polymer was crosslinked and pyrolyzed to convert the polymer into a ceramic matrix. This infiltration, crosslinking, and pyrolysis process was repeated for multiple cycles to increase ceramic yield and composite density. The resulting SiCN-CF and SiBCN-CF mini-composites were evaluated using mass analysis, Fourier transfer infrared spectroscopy (FTIR), scanning electron microscopy (SEM), and oxidation testing to evaluate chemical, structural and mechanical evolution of the samples.

2.1 Materials

A commercial carbon fiber cloth (6K, 2×2 twill weave, 0.017 in thickness, 10.9 oz/yd² areal weight) obtained from Fibre Glast Developments Corporation was used as the reinforcement material in this study. The preceramic polymer precursor used for SiCN fabrication was

polysilazane (Ceraset PSZ 20, Clariant Corporation). Isopropanol (≥99.9%, MW 60.096 g/mol, Fisher Scientific) was used as a solvent to reduce precursor viscosity for infiltration.

For SiBCN samples, trimethyl borate (TMB, ≥98%, MW 103.91 g/mol, Sigma-Aldrich) was added to the polysilazane precursor to introduce boron into the ceramic network. All precursor preparation and infiltration processes were performed in an oxygen-free glovebox environment to prevent premature oxidation and to improve ceramic yield.

2.2 Preparation of Preceramic Precursor

2.2.1 SiCN – Preceramic Polymer

To achieve an acceptable viscosity for infiltration into the carbon fiber bundles, the polysilazane (PSZ) precursor is diluted at a 4:3 weight ratio with the isopropanol (IPA) in an oxygen-free glovebox. This solution is stirred at 300rpm overnight to ensure complete mixing and uniform viscosity.

2.2.2 SiBCN – Preceramic Polymer

Boron-modified polysilazane was prepared following procedures described in the literature [1]. In an oxygen-free glovebox, trimethyl borate (TMB) reagent was slowly added to the PSZ at a rate of approximately 1 mL/min. The ideal concentration of TMB to PSZ is around a 1:1 weight ratio. The mixture is then stirred at 300rpm overnight to ensure homogeneous boron incorporation to the polymer network.

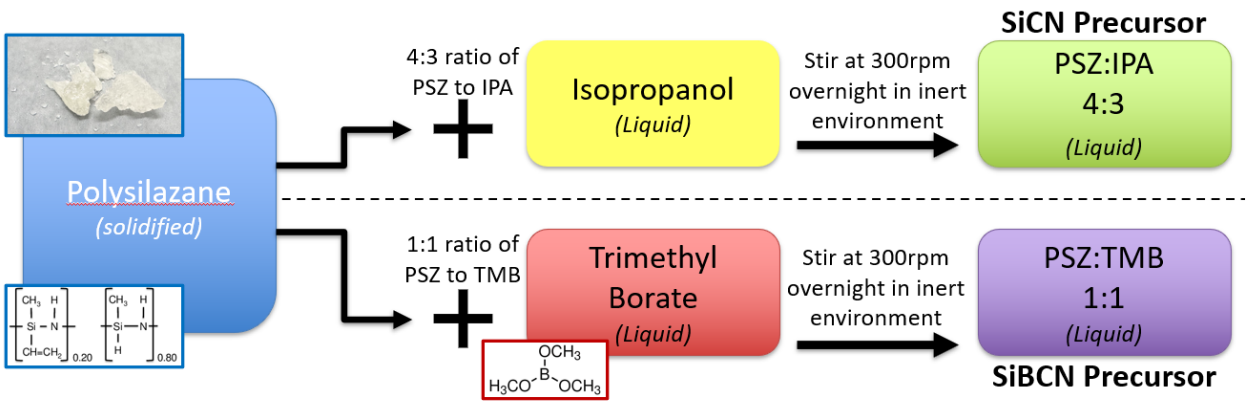

Figure 2-1: Liquid Preceramic Polymer Fabrication

2.3 Preparation of PDC/CF Mini-Composites (Method 1)

Carbon fiber bundles were cut from the carbon fiber cloth into 5 cm long samples with an approximate mass of 10 mg. Preceramic polymer precursor was infiltrated into each carbon fiber bundle at a ratio of 1µL:1mg using a precision micropipette to achieve a consistent polymer-to-fiber ratio.

After infiltration, the samples were crosslinked at 180°C for 1 hour to stabilize the polymer network prior to pyrolysis. All infiltration and crosslinking processes were performed in an oxygen-sealed glovebox to prevent oxidation and improve ceramic yield.

Following crosslinking, the samples were pyrolyzed in a nitrogen atmosphere furnace at 800°C for 30 minutes to convert the polymer into a ceramic matrix. The entire pyrolysis program takes 8 hours. The pyrolysis temperature program is shown in Figure 2-2. This process completed one full polymer infiltration and pyrolysis (PIP) cycle.

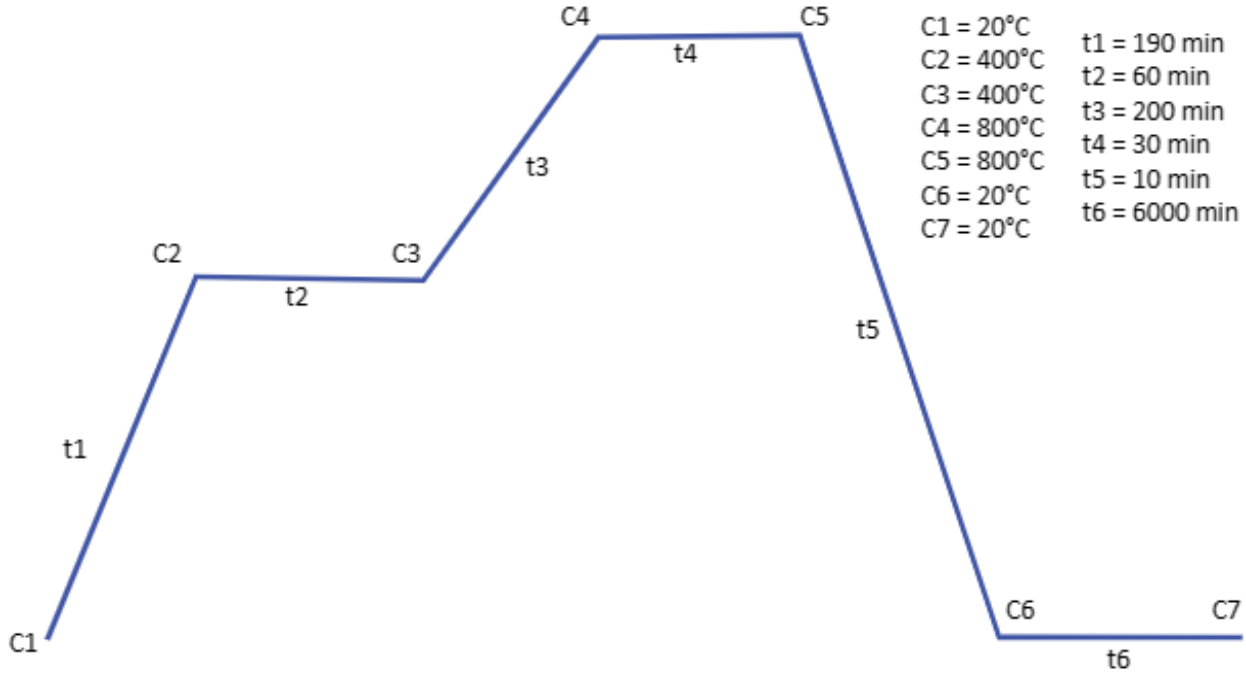

Figure 2-2: Pyrolysis Program Diagram

For Method 1 processing, the infiltration, crosslinking, and pyrolysis steps were repeated for multiple cycles. After each pyrolysis cycle, the samples were re-infiltrated with 10 μL of precursor, crosslinked, and pyrolyzed again at 800°C. This multi-cycle PIP process increased ceramic matrix content within the fiber bundles. The schematic of the fabrication process is shown in Figure 2-3.

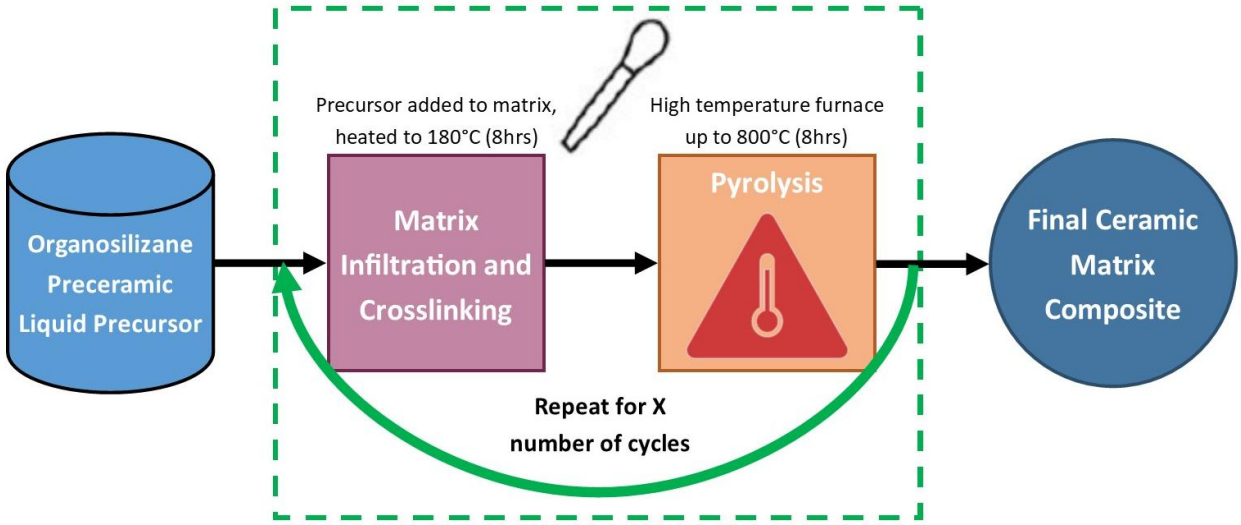

Figure 2-3: Method 1 Process

2.4 Characterization and Testing

This study utilized several characterization techniques to analyze the relation between cycle number and sample quality, oxidation resistance, and composition.

Masses after each major processing step were recorded and used to analyze sample composition and ceramic yield. The presence and evolution of various chemical functional groups of the silazane precursors in the composites were investigated using a Perkin Elmer Spectrum 400 FTIR spectrometer in the range of 500-2500 cm^{-1}. The surface morphology of the samples was studied using SEM on a Carl Zeiss EVO MA10 system with an incident voltage of 5 kV. To understand the oxidation stability of the CMCs, the samples were heated to 800°C in stagnant air in a SentroTech box furnace with a heating rate of 5 °C per minute. Oxidation testing simulates extreme environments that are applicable to aerospace components such as rocket nozzles and aircraft engines. The intense heat and presence of oxygen decomposes the integrity of the materials bonds, so it is a viable test to how the samples would perform in an aerospace environment.

2.4.1 Mass Analysis

Mass measurements were recorded at each stage of the fabrication process to evaluate mass changes throughout processing, polymer infiltration effectiveness, and overall ceramic yield for the multi-cycle PIP process. Each sample was weighed in the neat carbon fiber condition, after crosslinking, and after each pyrolysis cycle. Tracking mass at these stages enables evaluation of polymer uptake, mass retention during pyrolysis, and progressive matrix formation. From these measurements, several key metrics were calculated to characterize composite evolution.

Variable Definitions:

$$m_0 = \textit{initial neat carbon fiber mass}$$

$$m_{XL,i} = \textit{mass after infiltration and crosslinking for cycle } i$$

$$m_{P,i} = \textit{mass after pyrolysis for cycle } i$$

$$N = \textit{total number of cycles}$$

Derived Quantities and Metrics

Crosslink (XL) Mass Change: mass increase from infiltration and crosslinking

Equation 2-1: Crosslink Mass Change Per Cycle (Method 1)

$$\Delta m_{XL,i} = m_{XL,i} - m_{P,i-1}$$

$$(for\ i = 1, m_{P,0} = m_0)$$

Pyrolysis (PYRL) Mass Change: mass loss during pyrolysis

Equation 2-2: Pyrolysis Mass Change Per Cycle (Method 1)

$$\Delta m_{P,i} = m_{P,i} - m_{XL,i}$$

Ceramic Yield Per Cycle: fraction of polymer retained as a ceramic after pyrolysis in cycle *i*

Equation 2-3: Ceramic Yield Per Cycle (Method 1)

$$Ceramic\ Yield\ (\%)_i = \left(1 - \frac{m_{P,i}}{m_{XL,i}}\right) * 100$$

Preceramic Polymer Mass Added: Total mass of polymer introduced through all infiltration cycles

Equation 2-4: Preceramic Polymer Mass Added (Method 1)

$$\Delta m_{poly,total} = \Sigma_{i=1}^{N} \Delta m_{XL,i}$$

Total Mass Change: net mass increase relative to the initial neat fiber condition

Equation 2-5: Total Mass Change (Method 1)

$$\Delta m_{total} = m_{P,N} - m_0 = \Sigma_{i=1}^{N} \Delta m_{XL,i} + \Sigma_{i=1}^{N} \Delta m_{P,i}$$

Total Ceramic Yield (%): mass retained after all pyrolysis steps relative to total crosslinked mass

Equation 2-6: Total Ceramic Yield (Method 1)

$$Total\ Ceramic\ Yield\ (\%) = \left(1 - \frac{\Sigma_{i=1}^{N} \Delta m_{P,i}}{\Sigma_{i=1}^{N} \Delta m_{XL,i}}\right) * 100$$

Carbon Fiber Ratio (%): fraction of the final composite mass attributed to the original fiber

Equation 2-7: Carbon Fiber Ratio (Method 1)

$$Carbon\ Fiber\ Ratio(\%) = \left(\frac{m_0}{m_{P,N}}\right) * 100$$

Ceramic Ratio (%): fraction of the final composite mass attributed to the converted ceramic matrix

Equation 2-8: Ceramic Ratio (Method 1)

$$Ceramic\ Ratio(\%) = \left(\frac{m_{P,N} - m_0}{m_{P,N}}\right) * 100 = 100 - Carbon\ Fiber\ Ratio(\%)$$

The masses and calculated mass changes after each processing step using Equation 2-1 and Equation 2-2 for SiCN-CF and SiBCN-CF samples processed using Method 1 are summarized in Table 2-1. The derived ceramic yields for each cycle using Equation 2-3, as well as total preceramic polymer mass added (Equation 2-4), total mass change (Equation 2-5), final ceramic yield (Equation 2-6), carbon fiber ratio (Equation 2-7), and ceramic ratio (Equation 2-8) for each sample type is summarized and Table 2-2.

Table 2-1: Recorded Masses and Mass Changes during Method 1 PIP Processing

Type	Total Number of Cycles	Neat CF Mass	1st Cycle				2nd Cycle				3rd Cycle			
			XL Mass	PYRL Mass	XL Mass Change	PRYL Mass Change	XL Mass	PYRL Mass	XL Mass Change	PRYL Mass Change	XL Mass	PYRL Mass	XL Mass Change	PRYL Mass Change
SiCN-CF	1x	10.3	18.7	16.1	8.4	2.6								
	2x	9.8	19.5	16.4	9.7	3.1	23.4	21.2	7	2.2				
	3x	9.8	24.3	19.8	14.5	4.5	29.3	25.8	9.5	3.5	32.1	29.9	6.3	2.2
SiBCN-CF	1x	10.2	12.8	12.4	2.6	0.4								
	2x	9.8	12.6	12.2	2.8	0.4	15.3	14.3	3.1	1				
	3x	9.8	13.2	12.6	3.4	0.6	15.9	15	3.3	0.9	17	16.3	2	0.7

* *All masses reported in mg*

Table 2-2: Derived Yield Metrics and Final Composition for Method 1 Samples

Type	Total Number of Cycles	1st Cycle Ceramic Yield (%)	2nd Cycle Ceramic Yield (%)	3rd Cycle Ceramic Yield (%)	Final Mass	Total Preceramic Polymer Mass Added	Total Mass Change	Final Ceramic Yield (%)	Carbon Fiber Ratio (%)	Ceramic Ratio (%)
SiCN-CF	1x	69.05%			16.1	8.4	5.8	69.05%	63.98%	36.02%
	2x	68.04%	68.57%		21.2	16.7	11.4	68.26%	46.23%	53.77%
	3x	68.97%	63.16%	65.08%	29.9	30.3	20.1	66.34%	32.78%	67.22%
SiBCN-CF	1x	84.62%			12.4	2.6	2.2	84.62%	82.26%	17.74%
	2x	85.71%	32.26%		14.3	5.9	4.5	76.27%	68.53%	31.47%
	3x	82.35%	27.27%	65.00%	16.3	8.7	6.5	74.71%	60.12%	39.88%

* *All masses reported in mg*

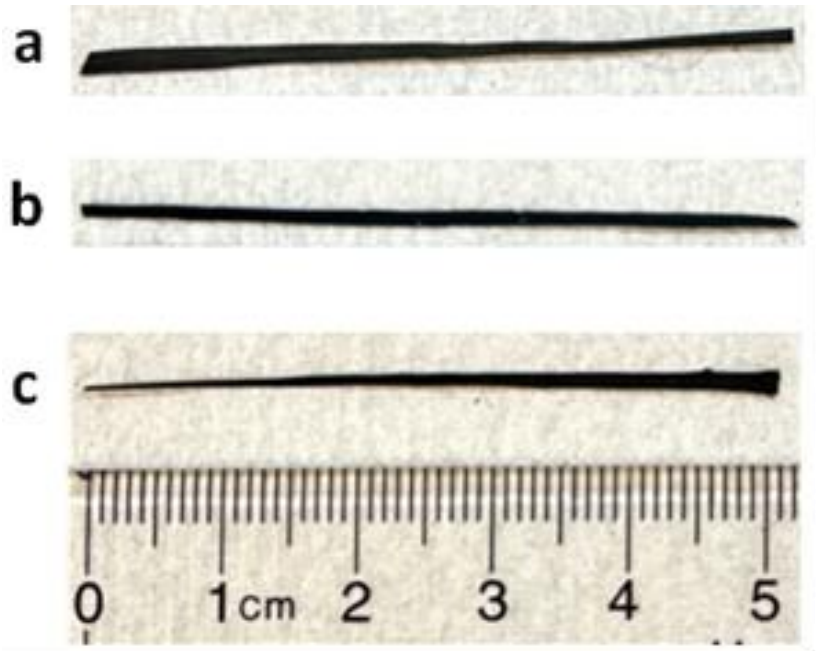

Figure 2-4: a.) Neat Carbon Fiber, b.) Crosslinked Sample, c.) Pyrolyzed Sample

2.4.2 Fourier-Transform Infrared Spectroscopy

Fourier Transform Infrared Spectroscopy (FTIR) is commonly used in polymer-derived ceramic research to identify functional groups present in polysilazane-based precursors and to monitor the conversion from polymer to ceramic through the disappearance of organic bonds and formation of ceramic bonding structures (Si–C, Si–N, Si–O) [5]. FTIR spectra were collected for the precursor, crosslinked samples, and pyrolyzed samples for both SiCN and SiBCN materials. Spectra from multiple cycles were compared, and minimal differences were observed between cycles, which was expected since the chemical composition of the ceramic matrix should not significantly change with additional infiltration cycles. Therefore, only Cycle 1 SiCN and SiBCN FTIR spectra are presented in Figure 2-5 and Figure 2-6.

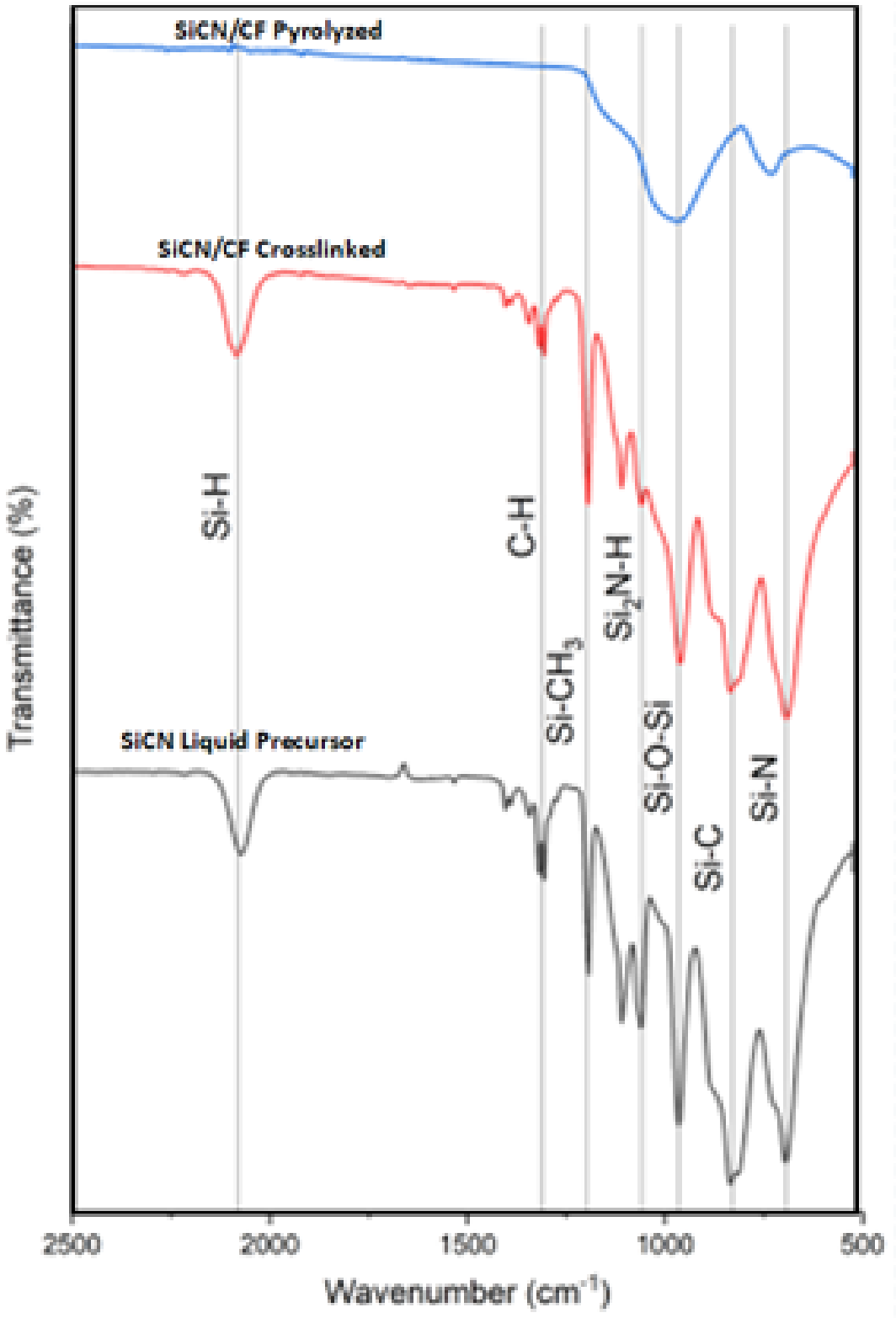

Figure 2-5: FTIR Spectra of PSZ precursor, crosslinked SiCN-CF, and pyrolyzed SiCN-CF

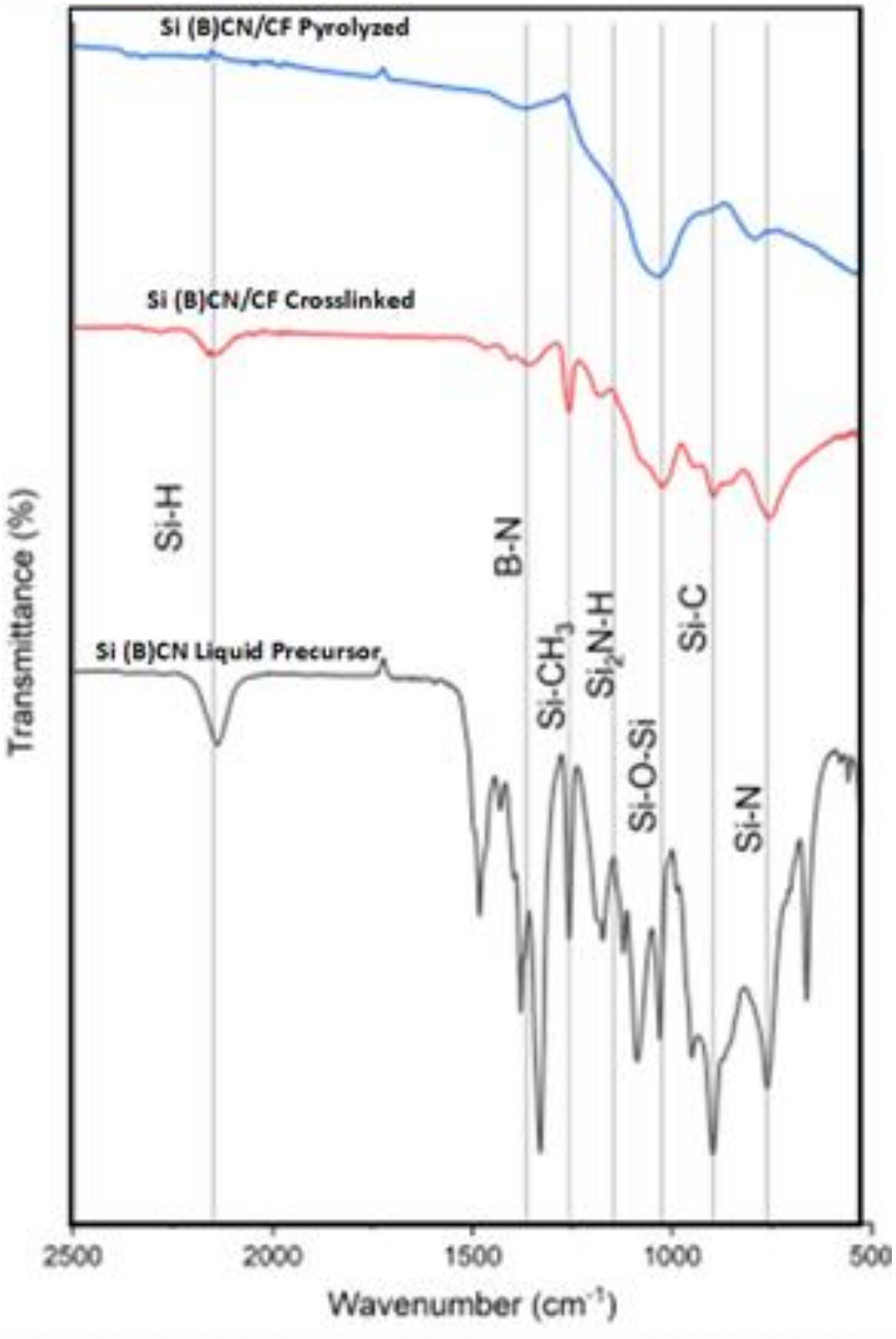

Figure 2-6: FTIR Spectra of PSZ-TMB precursor, crosslinked SiBCN-CF, and pyrolyzed SiBCN-CF

2.4.3 Scanning Electron Microscopy

Scanning electron microscopy (SEM) was used to examine the surface morphology and ceramic coating coverage of the SiCN-CF and SiBCN-CF samples produced using the Method 1 PIP processing. SEM images were taken at magnifications of 1500× (Figure 2-7) and 800× (Figure 2-8) for each sample type. These images were used to observe the fiber coverage, coating thickness, and surface quality and defects of the samples.

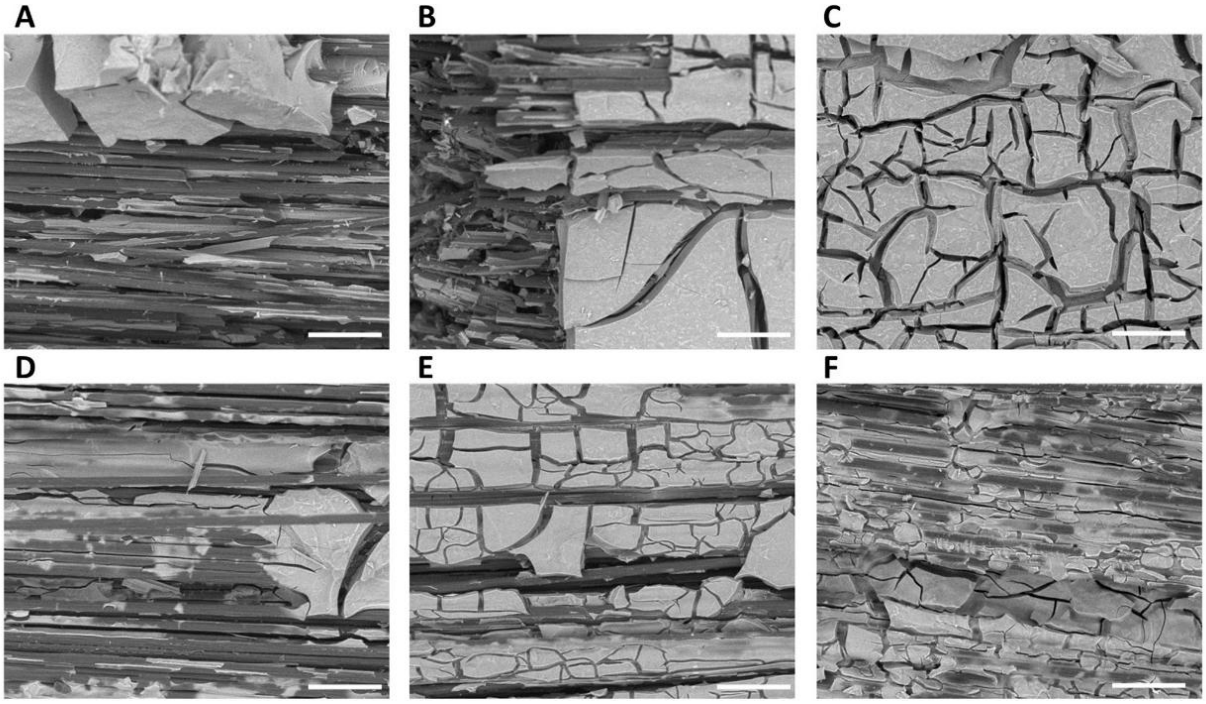

Figure 2-7: Method 1 SEM Images, 1500x magnification, scale bar has a length of 50 µm. a.) SiCN-CF Cycle 1, b.) SiCN-CF Cycle 2, c.) SiCN-CF Cycle 3, d.) SiBCN-CF Cycle 1, e.) SiBCN-CF Cycle 2, f.) SiBCN-CF Cycle 3.

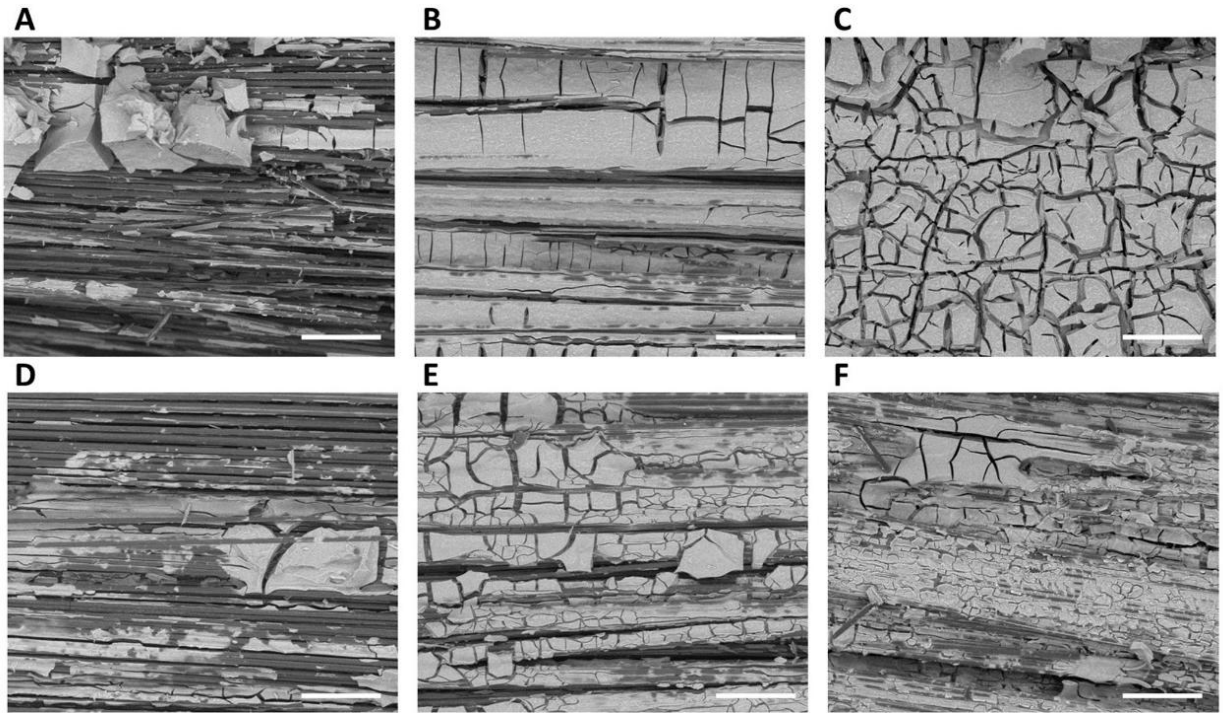

Figure 2-8: Method 1 SEM Images, 800x magnification, scale bar has a length of 100 µm. a.) SiCN-CF Cycle 1, b.) SiCN-CF Cycle 2, c.) SiCN-CF Cycle 3, d.) SiBCN-CF Cycle 1, e.) SiBCN-CF Cycle 2, f.) SiBCN-CF Cycle 3

2.4.4 Oxidation Testing

Oxidation testing was performed to evaluate the high-temperature oxidation resistance of SiCN-CF and SiBCN-CF composite samples fabricated using Method 1 processing. An uncoated carbon fiber sample was included as a control.

Following the final pyrolysis cycle, all samples were weighed to obtain their post-pyrolysis mass. The samples were then placed in a furnace in ambient air. The furnace temperature increased at a heating rate of approximately 5°C per minute until reaching 800°C, then held for 30 minutes. After the oxidation exposure, the samples were removed from the furnace, allowed to cool to room temperature, and weighed again to obtain the post-oxidation mass. From these measurements, several key metrics were calculated to evaluate high-temperature oxidation performance as a function of cycle number and material system.

Variable Definitions:

$$m_{CF} = \textit{initial neat carbon fiber mass}$$

$$m_{final} = \textit{mass after final pyrolysis cycle}$$

$$m_{ox} = \textit{mass after oxidation testing}$$

Derived Quantities and Metrics

Ceramic Mass: mass increase from carbon fiber to post-pyrolysis due to ceramic formation

Equation 2-9: Ceramic Mass

$$m_{ceramic} = m_{final} - m_{CF}$$

Oxidation Mass Loss: mass loss during high-temperature oxidation exposure

Equation 2-10: Oxidation Mass Loss

$$\Delta m_{ox} = m_{final} - m_{ox}$$

Oxidation Mass Retention: fraction of post-pyrolysis mass remaining after oxidation

Equation 2-11: Oxidation Mass Retention

$$Mass\ Retention(\%) = \left(\frac{m_{ox}}{m_{final}}\right) * 100$$

Oxidation Mass Retention Efficiency: fraction of ceramic mass remaining after oxidation

Equation 2-12: Oxidation Mass Retention Efficiency

$$Mass\ Retention\ Efficiency(\%) = \left(\frac{m_{ox}}{m_{ceramic}}\right) * 100$$

The mass changes and derived metrics are summarized in Table 2-3, and visual results following oxidation exposure are shown in Figure 2-9.

Table 2-3: Oxidation Mass Results and Derived Metrics for Method 1

Type	Number of Cycles	Neat CF Mass	Final Mass	Ceramic Mass	Post Oxidation Mass	Mass Loss from Oxidation	Mass Retention (%)	Mass Retention Efficiency (%)
SiCN-CF	1x	10.3	16.1	5.8	4.4	11.7	27.33%	75.86%
	2x	9.8	21.2	11.4	10.2	11.0	48.11%	89.47%
	3x	9.8	29.9	20.1	20.8	9.1	69.57%	103.48%
SiBCN-CF	1x	10.2	12.4	2.2	2.4	10.0	19.35%	109.09%
	2x	9.8	14.3	4.5	4.2	10.1	29.37%	93.33%
	3x	9.8	16.3	6.5	5.9	10.4	36.20%	90.77%

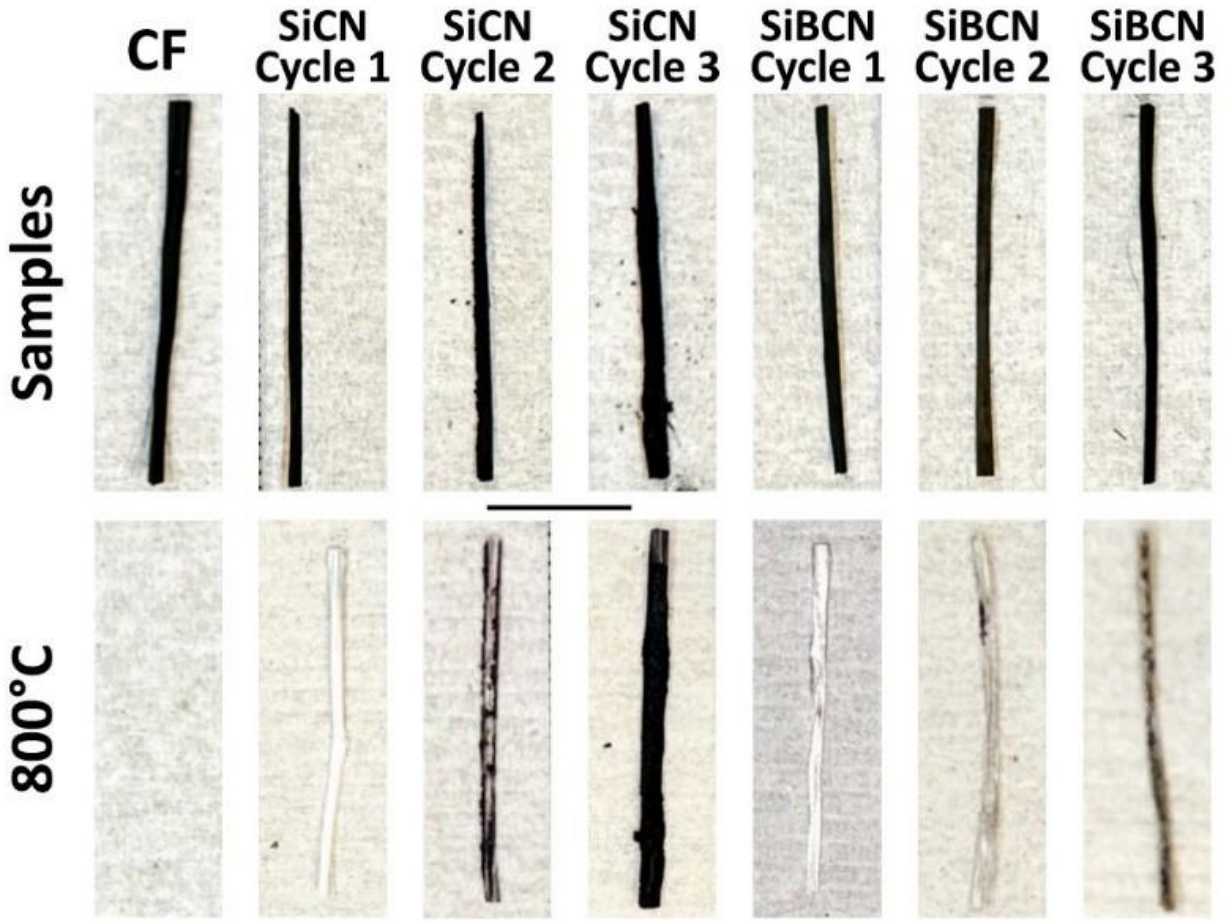

Figure 2-9: Oxidation Test Visual Results, scale bar is 2cm

2.5 Discussion

2.5.1 Mass Analysis

Mass analysis revealed clear trends in polymer uptake, densification behavior, and matrix development across multiple PIP cycles. Mass gain during infiltration and crosslinking decreased with increasing cycle number for both SiCN-CF and SiBCN-CF systems. The first cycle resulted in the largest increase in mass, corresponding to initial pore filling within the fiber preform. Additional cycles exhibited progressively smaller mass increases, indicating reduced available porosity as the composite densified. This trend suggests that the material approaches a saturation condition, where additional infiltration contributes less to overall ceramic matrix formation. A corresponding decrease in mass change during pyrolysis was observed in later cycles. This behavior is consistent with reduced preceramic polymer uptake, resulting in smaller amounts of material undergoing conversion during pyrolysis.

Comparison between material systems showed that SiCN-CF samples consistently exhibited greater total polymer uptake than SiBCN-CF samples across all cycles, resulting in significantly higher overall mass gain and increased ceramic content in the final composite. In contrast, SiBCN-CF samples demonstrated more limited infiltration, leading to lower total matrix formation.

Ceramic yield remained relatively consistent for SiCN-CF samples across cycles, showing stable polymer-to-ceramic conversion behavior. SiBCN-CF samples had more variability in ceramic yield, suggesting less uniform conversion and reduced matrix development.

Analysis of final mass ratio further highlights the distinction between the two systems. SiCN-CF composites transitioned toward a ceramic-dominated structure with increasing cycles, while SiBCN-CF composites remained fiber-dominated, even after multiple infiltration steps. This

difference is primarily attributed to variations in polymer uptake rather than inherent differences in conversion efficiency.

These results indicate that polymer infiltration effectiveness is the dominant factor governing final composite composition and densification, while ceramic yield alone does not fully capture matrix development. Although repeated PIP cycles increase overall ceramic content, the diminishing mass uptake observed in later cycles demonstrates that additional processing yields progressively smaller gains in densification.

A potential explanation for the observed differences in polymer uptake between the SiCN-CF and SiBCN-CF systems is the variation in precursor viscosity resulting from their respective compositions. The SiBCN precursor, formed by mixing polysilazane with trimethyl borate (TMB) at a 1:1 ratio, exhibited significantly lower viscosity compared to the neat polysilazane used for the SiCN-CF system. This reduced viscosity likely enhanced flowability but limited the ability of the precursor to remain within the fiber preform during infiltration and crosslinking. As a result, a portion of the SiBCN precursor may have drained from the structure prior to crosslinking, leading to reduced overall polymer retention. In contrast, the higher viscosity of the SiCN precursor likely improved retention within the fiber bundles, promoting greater polymer uptake and ultimately resulting in higher ceramic content after pyrolysis. This suggests that precursor rheology plays a critical role in infiltration efficiency and should be carefully considered when optimizing polymer-derived ceramic processing routes.

This behavior represents a key limitation of the traditional multi-cycle PIP process, motivating the investigation of alternative processing approaches that can achieve comparable matrix formation with reduced processing time.

2.5.2 Fourier Transform Infrared Spectroscopy Analysis

FTIR analysis was performed to confirm the chemical conversion of the polysilazane precursor into SiCN and SiBCN ceramic materials after crosslinking and pyrolysis. The FTIR spectra showed characteristic peaks corresponding to Si–CH_3 (~1260 cm^{-1}) and Si–O–Si (~1060 cm^{-1}), indicating the presence of silicon-containing polymer structures in the precursor and crosslinked samples. An absorption band near 1175 cm^{-1} corresponded to Si_2N–H bonding, which is commonly observed in polysilazane-derived ceramic precursors [5]. In both SiCN and SiBCN samples, peaks associated with Si–H (~2100 cm^{-1}) were present in the precursor spectra and decreased after crosslinking, indicating polymer crosslinking reactions and network formation prior to pyrolysis [2], [3], [5]. For SiBCN samples, a broad peak associated with B–N bonding was observed and became more prominent after pyrolysis, indicating incorporation of boron into the ceramic network structure [4]. After pyrolysis, strong peaks corresponding to Si–O–Si (~1060 cm^{-1}) and Si–C (~800 cm^{-1}) were observed in both SiCN and SiBCN samples, indicating the formation of ceramic phases and an amorphous Si–C–N or Si–B–C–N network [2]–[4]. Additionally, peaks associated with hydrogen-containing functional groups such as Si–CH_3, C–H, and Si–H were significantly reduced after pyrolysis, indicating decomposition of organic groups and conversion to an inorganic ceramic structure during polymer-to-ceramic transformation [5]. These FTIR results confirmed successful decomposition of organic groups and conversion of the polymer precursor into inorganic ceramic materials and are consistent with previously reported polysilazane-derived ceramic systems [2]–[6]. FTIR spectra showed minimal differences between cycles, which was expected since additional PIP cycles primarily increase ceramic matrix quantity rather than significantly changing the ceramic chemistry.

2.5.3 Microstructure Analysis

Scanning electron microscopy revealed clear trends in ceramic coating development and surface morphology as a function of PIP cycle number.

Lower cycle samples (Cycle 1) exhibited thin, discontinuous ceramic coatings with visible regions of exposed carbon fiber, indicating incomplete infiltration and matrix formation. As the number of cycles increased, the ceramic coatings became progressively thicker and more continuous, resulting in improved fiber coverage and matrix connectivity in Cycle 2 and Cycle 3 samples. It is also noted that higher cycle numbers of SiCN-CF show more ceramic buildup on the surface, where higher cycle SiBCN-CF have better fiber definition. This shows that the SiBCN precursor showed better distribution and wetting throughout the samples, which is a likely effect of the SiBCN precursor rheology, discussed in Section 2.5.1.

Despite this improvement in coating continuity, non-uniform coating thickness was observed across fiber bundles in all samples. Additionally, higher cycle samples showed increased surface roughness and the formation of microcracks within the ceramic matrix. In several cases, these cracks formed interconnected networks, particularly in the SiCN samples.

The presence of microcracking is attributed to shrinkage stresses generated during pyrolysis. Repeated pyrolysis cycles lead to cumulative volumetric contraction of the polymer-derived ceramic, which introduces internal stresses that exceed the fracture resistance of the matrix, resulting in crack formation.

These results indicate a trade-off inherent to the multi-cycle PIP process: increasing cycle number improves fiber wetting and matrix continuity but also promotes defect accumulation due to shrinkage-induced stresses. This behavior is consistent with the trends observed in mass analysis

and oxidation testing, where increased ceramic content was accompanied by diminishing structural efficiency at higher cycle counts.

2.5.4 Oxidation Testing

The oxidation testing results demonstrate that the incorporation of a polymer-derived ceramic matrix significantly improves the high-temperature oxidation resistance of carbon fiber composites. All ceramic-coated samples remained structurally intact following exposure to 800°C in air, while the uncoated carbon fiber control sample completely disintegrated, confirming the successful creation of a protective ceramic barrier to resist complete mass loss during high-temperature oxidation.

Mass retention increased with increasing PIP cycle number for both SiCN-CF and SiBCN-CF systems, indicating that additional infiltration and pyrolysis cycles enhance oxidation resistance. This trend corresponds directly to increased ceramic mass within the composite, which improves matrix densification, reduces porosity, and promotes more continuous coating of the carbon fibers. These effects collectively reduce oxygen diffusion pathways and limit oxidative degradation.

Differences in oxidation behavior between the two material systems were also observed. SiCN-CF samples exhibited higher mass retention at higher cycle numbers, indicating superior oxidation resistance at elevated ceramic loading. In contrast, SiBCN-CF samples demonstrated more consistent mass retention efficiency across cycles and comparatively better performance at lower ceramic loading levels. This suggests that while SiCN benefits more strongly from increased matrix content, SiBCN provides more efficient oxidation protection when ceramic content is limited.

These results show that oxidation performance is determined by both ceramic loading and material composition. Increasing ceramic content enhances the formation of protective oxide layers and improves resistance to oxygen diffusion, while compositional differences influence the efficiency of oxidation protection mechanisms. Overall, the results confirm that multi-cycle PIP processing improves oxidation resistance, with performance dependent on both the number of processing cycles and the ceramic system employed.

2.5.5 Limitations of the Multi-Cycle PIP Process

While the multi-cycle PIP process successfully increased ceramic matrix content and improved oxidation resistance with increasing cycle number, the process requires multiple high-temperature pyrolysis cycles. Each pyrolysis cycle requires long furnace processing times under controlled atmosphere conditions, making the process time-consuming and difficult to scale for large-scale manufacturing of CMC components.

In addition, repeated pyrolysis cycles introduce shrinkage and can lead to microcracking within the ceramic matrix, which may negatively affect mechanical properties and long-term durability. The decreasing effectiveness of additional infiltration cycles and the increasing processing time associated with multiple pyrolysis cycles represent significant limitations of the traditional PIP process.

These limitations motivated the development of the modified processing method described in Chapter 3, which utilizes multiple infiltration and crosslinking cycles followed by a single pyrolysis cycle in order to reduce processing time and improve scalability while maintaining ceramic matrix formation.

CHAPTER 3: MULTI-CYCLE SiCN-CF AND SiBCN-CF STUDY, METHOD 2

This chapter investigates a modified polymer infiltration and pyrolysis (PIP) process designed to reduce processing time and improve the scalability of polymer-derived ceramic matrix composites (CMC)s. One of the primary limitations of the traditional PIP process described in Chapter 2 is the large number of high-temperature pyrolysis cycles required to achieve sufficient ceramic matrix content. Each pyrolysis cycle requires long furnace processing times under controlled atmosphere conditions, making the process time-consuming and difficult to scale for large-scale manufacturing of CMCs. In addition, repeated pyrolysis cycles introduce shrinkage and can lead to microcracking within the ceramic matrix.

The objective of Method 2 was to increase ceramic yield and matrix densification by incorporating multiple infiltration and crosslinking cycles followed by a single pyrolysis cycle. Boron-modified and unmodified polysilazane liquid precursors were used to infiltrate carbon fiber bundles in an oxygen-free environment. Unlike the fabrication method described in Chapter 2, which utilizes multiple infiltration and pyrolysis cycles, this method delays pyrolysis until after several infiltration cycles have been completed. This approach allows increased polymer infiltration prior to ceramic conversion and is expected to improve ceramic matrix formation while significantly reducing processing time. Weight analysis, X-ray diffraction (XRD), oxidation testing, scanning electron microscopy (SEM), and tensile testing were used to evaluate the properties and microstructure of the resulting SiCN-CF and SiBCN-CF mini-composites.

3.1 Materials

The materials used in Method 2 processing were identical to those described in Section 2.1. Carbon fiber cloth was used as the reinforcement material, and polysilazane (Ceraset PSZ 20) was used as

the preceramic polymer precursor. Isopropanol was used to adjust precursor viscosity for infiltration, and trimethyl borate was added to the polysilazane precursor for SiBCN fabrication.

All infiltration and crosslinking procedures were performed in an oxygen-free glovebox environment, and pyrolysis was conducted in a nitrogen atmosphere furnace. Detailed material specifications are provided in Section 2.1.

3.2 Preparation of Preceramic Precursors

The preparation of the SiCN and SiBCN preceramic polymer precursors used in Method 2 processing followed the same procedures described in Section 2.2. The polysilazane precursor was diluted with isopropanol to achieve appropriate infiltration viscosity, and trimethyl borate was added to the polysilazane precursor for SiBCN samples. No modifications were made to the precursor preparation procedure for Method 2 processing.

3.3 Preparation of PDC/CF Mini-Composites (Method 2)

Carbon fiber bundles were prepared using the same procedure described in Section 2.3. However, the infiltration process used in Method 2 differed from the multi-cycle PIP process described in Chapter 2. Instead of performing pyrolysis after each infiltration cycle, multiple infiltration and crosslinking cycles were performed prior to a single final pyrolysis step.

Carbon fiber bundles were infiltrated with preceramic polymer precursor using a micropipette to ensure uniform distribution throughout the fiber bundle. Each infiltration used 10 μL of precursor to maintain the same polymer-to-fiber ratio used in Method 1. After infiltration, the samples were crosslinked at 180°C for 1 hour in a nitrogen environment to stabilize the polymer network.

Following crosslinking, the samples were re-infiltrated with precursor and crosslinked again. This infiltration and crosslinking process was repeated for multiple cycles to increase polymer content within the fiber bundles prior to ceramic conversion. All infiltration and crosslinking operations were performed in an oxygen-sealed glovebox, and the samples were not removed until the final crosslinking cycle was completed.

After the desired number of infiltration and crosslinking cycles were completed, the samples were pyrolyzed in a nitrogen atmosphere at 800°C for 30 minutes to convert the polymer into a ceramic matrix. This process resulted in the formation of SiCN or SiBCN ceramic matrices surrounding the carbon fiber reinforcement. A schematic of the repeated infiltration and crosslinking followed by a single pyrolysis process is shown in Figure 3-1.

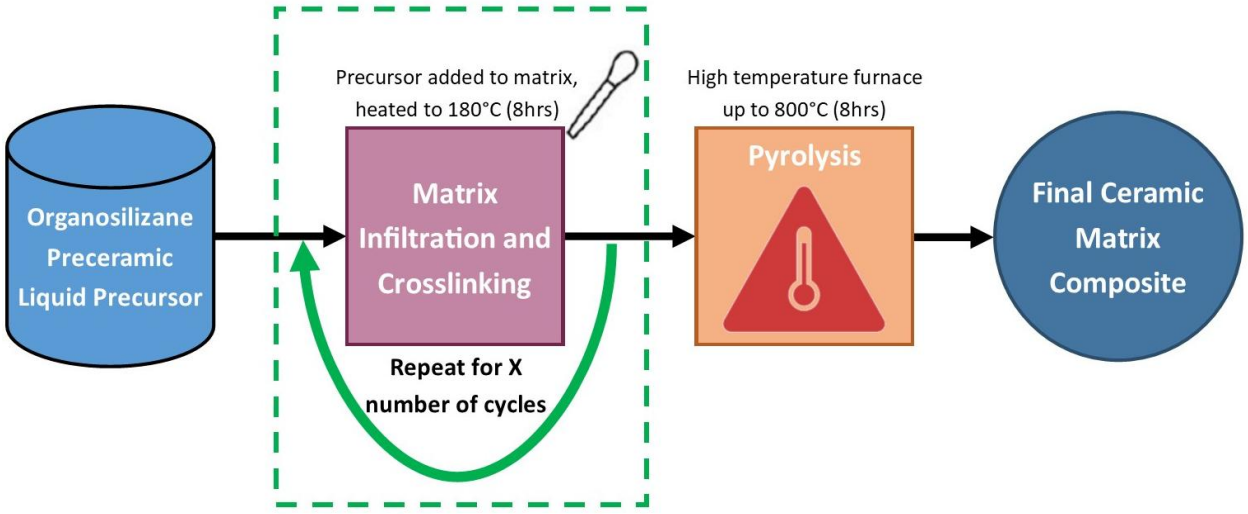

Figure 3-1: Method 2 Process

3.4 Characterization and Testing

This study utilized several characterization techniques to analyze sample composition, quality, oxidation resistance, and mechanical performance. Masses after each major processing step were recorded and used to analyze sample composition and ceramic yield. The elemental composition of pyrolyzed composite samples was analyzed using X-Ray Fluorescence analysis with a Hitachi SU8010 system equipped with IXRF analysis capabilities. The surface morphology of the samples was studied using SEM on a Carl Zeiss EVO MA10 system with an incident voltage of 5 kV. High-temperature oxidation performance was tested at 800°C in stagnant air in a SentroTech box furnace with a heating rate of 5 °C per minute. Mechanical properties of the composite samples were evaluated via tensile testing using a Shimadzu Universal Testing machine.

3.4.1 Mass Analysis

Mass measurements were recorded throughout the fabrication process to evaluate polymer infiltration effectiveness and final ceramic accumulation for the modified polymer infiltration and pyrolysis (PIP) processing route (Method 2). Each sample was weighed in the neat carbon fiber condition, after each infiltration and crosslinking cycle, and after the single pyrolysis. Unlike the multi-cycle PIP process described in Chapter 2, Method 2 utilizes multiple infiltration and crosslinking steps followed by a single pyrolysis step. As a result, intermediate pyrolysis measurements were not obtained, and the analysis focuses on cumulative polymer uptake and final mass retention, rather than cycle-by-cycle conversion behavior.

Tracking mass at these stages enables evaluation of total polymer incorporation prior to pyrolysis, mass loss during ceramic conversion, and final composite composition. From these measurements, several key metrics were calculated to characterize the composite evolution.

Variable Definitions:

$$m_0 = initial\ neat\ carbon\ fiber\ mass$$

$$m_{XL,i} = mass\ after\ infiltration\ and\ crosslinking\ for\ cycle\ i$$

$$m_P = mass\ after\ pyrolysis$$

$$N = total\ number\ of\ cycles$$

Derived Quantities and Metrics

Crosslink (XL) Mass Change: mass increase from infiltration and crosslinking

Equation 3-1: Crosslink Mass Change Per Cycle (Method 2)

$$\Delta m_{XL,i} = m_{XL,i} - m_{XL,i-1}$$

$$(for\ i = 1, m_{XL,0} = m_0)$$

Pyrolysis (PYRL) Mass Change: mass loss during pyrolysis

Equation 3-2: Pyrolysis Mass Change (Method 2)

$$\Delta m_P = m_P - m_{XL,3}$$

Preceramic Polymer Mass Added: total mass of polymer introduced through all infiltration cycles

Equation 3-3: Preceramic Polymer Mass Added (Method 2)

$$\Delta m_{poly,total} = \Sigma_{i=1}^{N} \Delta m_{XL,i}$$

Pre-Pyrolysis Polymer Ratio (%): fraction of pre-pyrolysis sample attributed to preceramic polymer

Equation 3-4: Pre-Pyrolysis Polymer Ratio (Method 2)

$$Polymer\ Ratio(\%) = \left(\frac{\Sigma_{i=1}^{N} \Delta m_{XL,i}}{m_0}\right) * 100$$

Total Mass Change: net mass increase relative to the initial neat fiber condition

Equation 3-5: Total Mass Change (Method 2)

$$\Delta m_{total} = m_P - m_0 = \Sigma_{i=1}^{N} \Delta m_{XL,i} + \Delta m_P$$

Ceramic Yield (%): mass retained after all pyrolysis steps relative to the total crosslinked mass

Equation 3-6: Ceramic Yield (Method 2)

$$Ceramic\ Yield\ (\%) = \left(1 - \frac{\Delta m_P}{\Sigma_{i=1}^{N} \Delta m_{XL,i}}\right) * 100$$

Carbon Fiber Ratio (%): fraction of the final composite mass attributed to the original fiber

Equation 3-7: Carbon Fiber Ratio (Method 2)

$$Carbon\ Fiber\ Ratio(\%) = \left(\frac{m_0}{m_P}\right) * 100$$

Ceramic Ratio (%): fraction of the final composite mass attributed to the converted ceramic matrix

Equation 3-8: Ceramic Ratio (Method 2)

$$Ceramic\ Ratio(\%) = \left(\frac{m_P - m_0}{m_P}\right) * 100 = 100 - Carbon\ Fiber\ Ratio(\%)$$

The summarized masses and calculated mass changes after each processing step using Equation 3-1 and Equation 3-2 for SiCN-CF and SiBCN-CF samples processed using Method 2 are summarized in Table 3-1. Derived metrics, including total polymer uptake (Equation 3-3), pre-pyrolysis polymer ratio (Equation 3-4), total mass change (Equation 3-5), ceramic yield (Equation 3-6), carbon fiber ratio (Equation 3-7), and ceramic ratio (Equation 3-8), are summarized in Table 3-2.

Table 3-1: Recorded Masses and Mass Changes during Method 2 PIP Processing

Sample	Neat CF Mass	Cycle 1		Cycle 2		Cycle 3		Pyrolysis	
		XL Mass	XL Mass Change	XL Mass	XL Mass Change	XL Mass	XL Mass Change	PYRL Mass	PYRL Mass Change
SiCN-CF	10.2	18.9	8.7	26.1	7.2	31.9	5.8	25.7	6.2
	9.9	17.7	7.8	24.5	6.8	30.4	5.9	25.5	4.9
	9.7	16.3	6.6	21.4	5.1	25.8	4.4	22.3	3.5
	9.6	18.4	8.8	25.9	7.5	31.4	5.5	24.3	7.1
	10	18.1	8.1	24.2	6.1	28.7	4.5	23.2	5.5
SiBCN-CF	9.7	13.5	3.8	16.2	2.7	17	0.8	12.3	4.7
	10	14.4	4.4	16.7	2.3	18.2	1.5	13.2	5
	9.8	14.2	4.4	16.9	2.7	18	1.1	12.5	5.5
	9.8	14.3	4.5	16.8	2.5	18.3	1.5	13.5	4.8
	10.1	14.7	4.6	16.4	1.7	17.6	1.2	14.3	3.3

** All masses reported in mg*

Table 3-2: Derived Yield Metrics and Final Composition for Method 2 Samples

Sample	Final Mass	Total Preceramic Polymer Mass Added	Pre-PYRL Polymer Ratio (%)	Total Mass Change	Ceramic Yield (%)	Carbon Fiber Ratio (%)	Ceramic Ratio (%)
SiCN-CF	25.7	21.7	212.75%	15.5	71.43%	39.69%	60.31%
	25.5	20.5	207.07%	15.6	76.10%	38.82%	61.18%
	22.3	16.1	165.98%	12.6	78.26%	43.50%	56.50%
	24.3	21.8	227.08%	14.7	67.43%	39.51%	60.49%
	23.2	18.7	187.00%	13.2	70.59%	43.10%	56.90%
SiBCN-CF	12.3	7.3	75.26%	2.6	35.62%	78.86%	21.14%
	13.2	8.2	82.00%	3.2	39.02%	75.76%	24.24%
	12.5	8.2	83.67%	2.7	32.93%	78.40%	21.60%
	13.5	8.5	86.73%	3.7	43.53%	72.59%	27.41%
	14.3	7.5	74.26%	4.2	56.00%	70.63%	29.37%

** All masses reported in mg*

3.4.2 X-Ray Fluorescence

X-Ray fluorescence (XRF) was used to determine the elemental composition of the pyrolyzed composite samples. The technique enables the identification of key elements present in the ceramic matrix and carbon fiber reinforcement. Pyrolyzed samples were irradiated with primary X-rays, causing excitation of inner-shell electrons. The resulting secondary (fluorescent) X-rays emitted from the sample were detected and analyzed to determine elemental composition. The results for a neat carbon fiber sample, SiCN-CF and SiBCN-CF are shown in Figure 3-2.

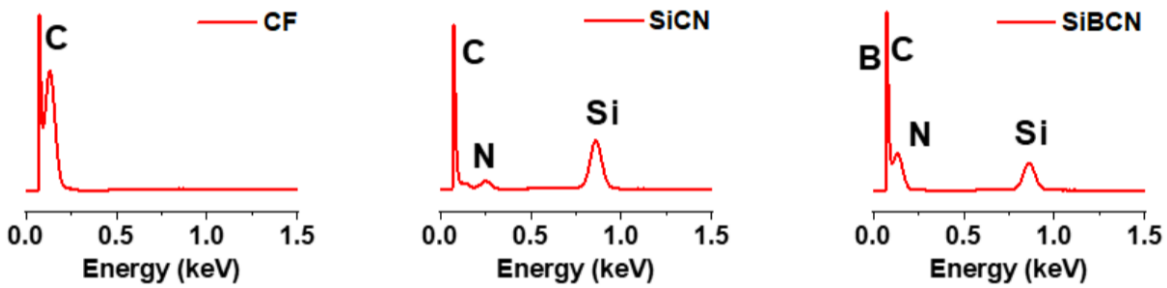

Figure 3-2: XRF Results - Neat Carbon Fiber and Method 2 SiCN-CF and SiBCN-CF Samples. Data collection and visualization provided by Arijit Roy.

3.4.3 Oxidation Testing

Oxidation testing was performed to evaluate the high-temperature oxidation resistance of the SiCN-CF and SiBCN-CF mini-composites produced using the Method 2 multi-infiltration single-pyrolysis process. An uncoated carbon fiber sample was also tested as a control.

Following the single pyrolysis cycle, all samples were weighed to obtain their post-pyrolysis mass. The samples were then placed in a furnace in ambient air. The furnace temperature increased at a heating rate of approximately 5°C per minute until reaching 800°C, then held for 30 minutes. After the oxidation exposure, the samples were removed from the furnace, allowed to cool to room temperature, and weighed again to obtain the post-oxidation mass. From these measurements,

several key metrics were calculated to evaluate high-temperature oxidation performance using equations defined in Section 2.4.2.

The mass changes and derived metrics are summarized in Table 3-3, the visual results following oxidation exposure are shown in Figure 3-3.

Table 3-3: Oxidation Mass Results and Derived Metrics for Method 2

Type	Neat CF Mass	Final Mass	Ceramic Mass	Post Oxidation Mass	Mass Loss from Oxidation	Mass Retention (%)	Mass Retention Efficiency (%)
SiCN-CF	10	23.2	13.2	8.4	4.8	36.21%	63.64%
SiBCN-CF	10.1	14.3	4.2	3.2	1	22.38%	76.19%

**all masses reported in mg*

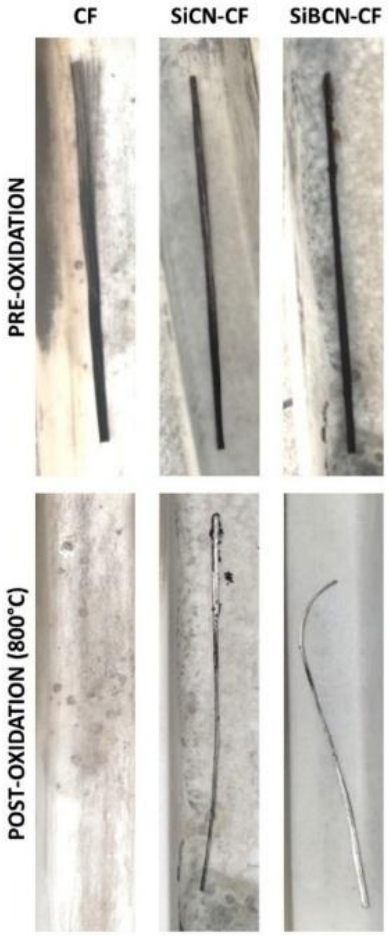

Figure 3-3: Oxidation Test Visual Results for Method 2

3.4.4 Scanning Electron Microscopy

Scanning electron microscopy (SEM) was used to examine the surface morphology, ceramic coating coverage, fracture surfaces, and oxidation damage of the SiCN-CF and SiBCN-CF mini-composites fabricated using the Method 2 processing method.

Images were obtained for neat carbon fiber samples, pyrolyzed composite samples, and oxidized samples. The SEM images were used to evaluate ceramic coating thickness, matrix distribution, fiber–matrix bonding, fracture behavior, and oxidation damage. SEM images of neat carbon fiber, pyrolyzed SiCN-CF, oxidized SiCN-CF, pyrolyzed SiBCN-CF, and oxidized SiBCN-CF composites are shown in Figure 3-4, Figure 3-5, Figure 3-6, Figure 3-7, and Figure 3-8, respectively.

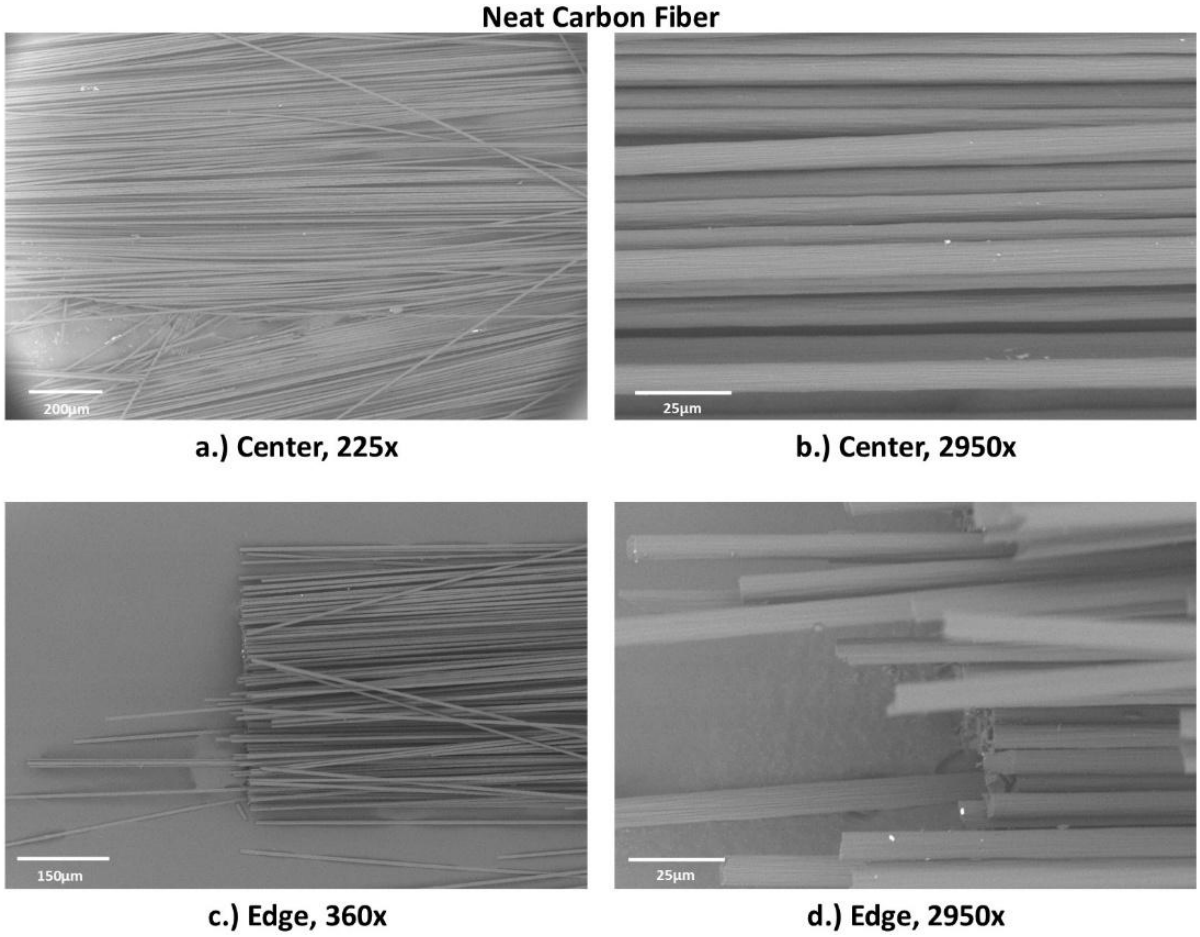

Figure 3-4: Carbon Fiber SEM Images

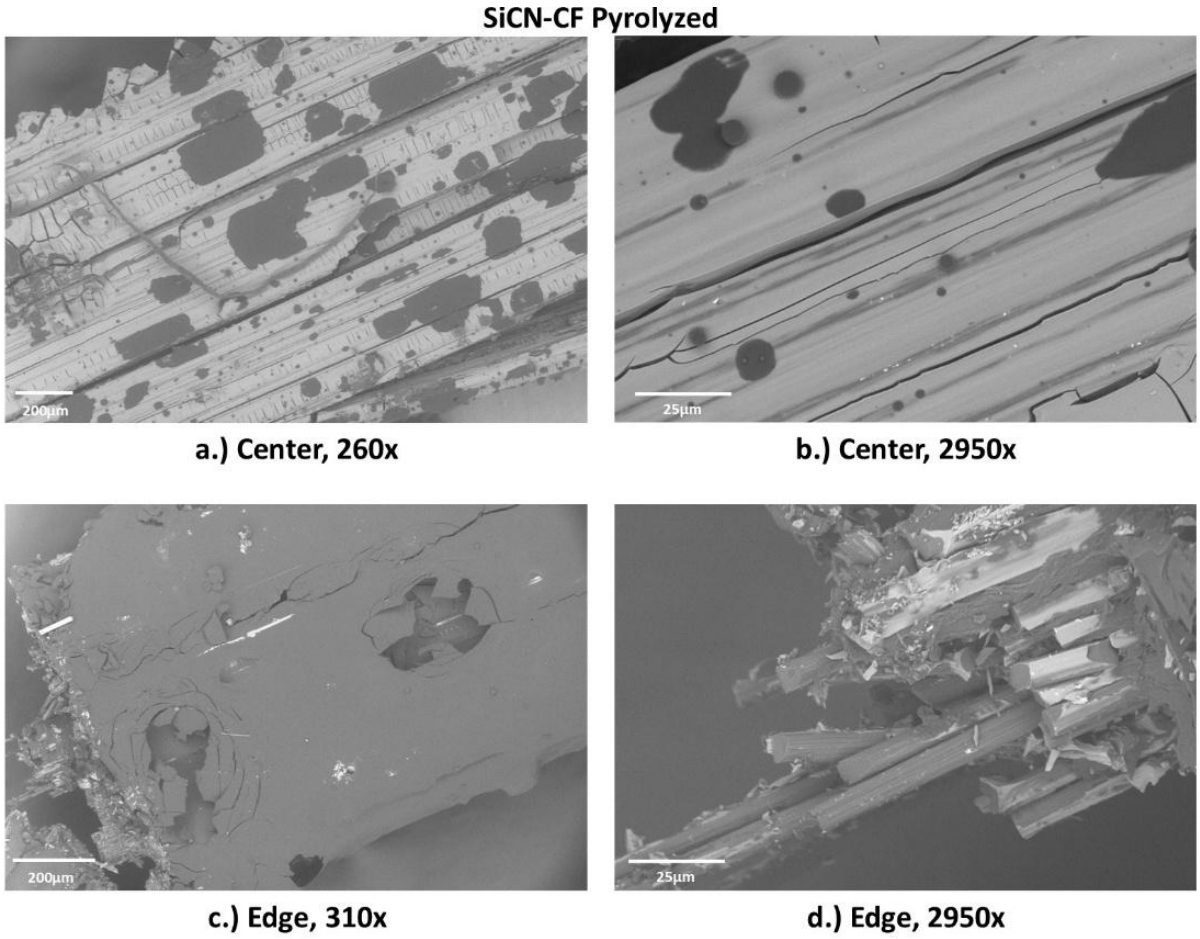

Figure 3-5: Pyrolyzed Method 2 SiCN-CF SEM Images

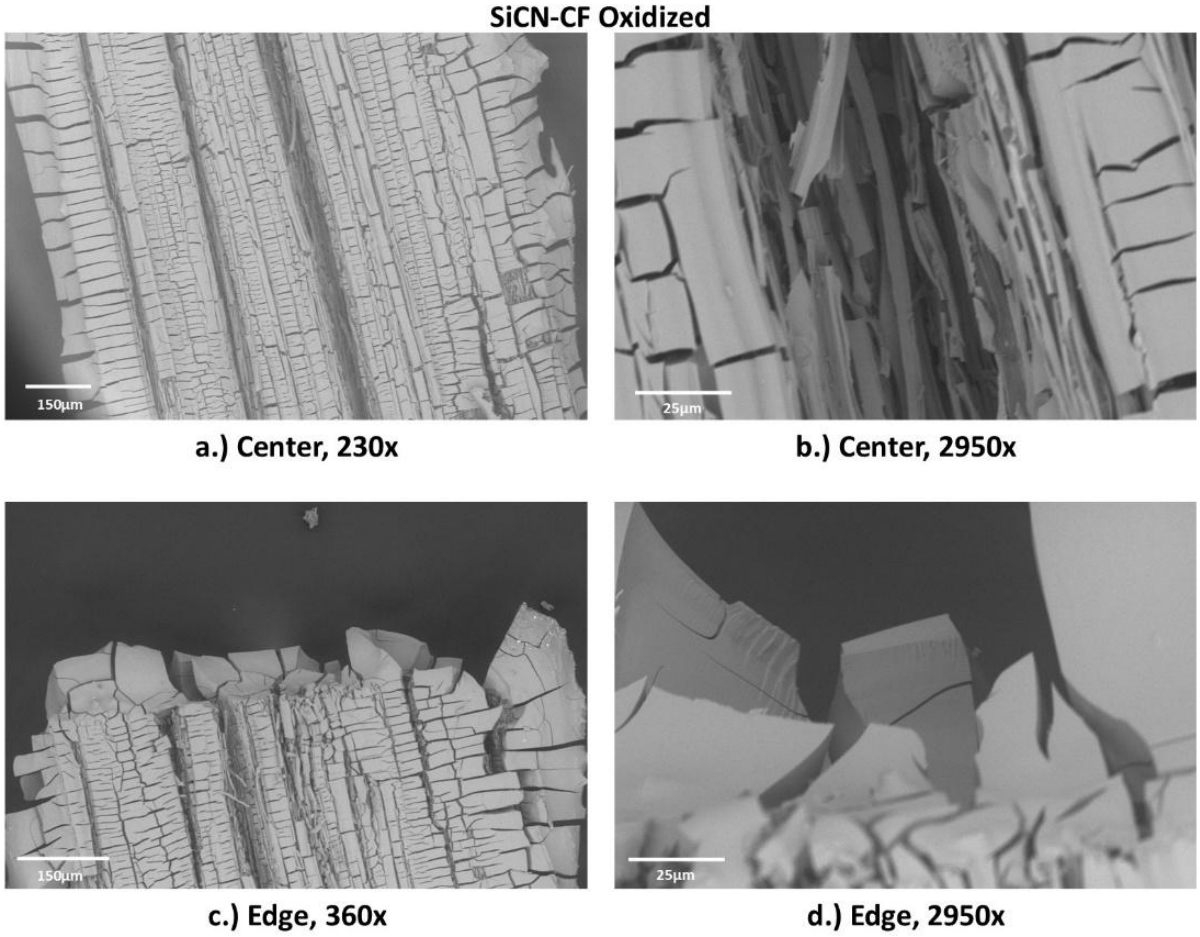

Figure 3-6: Oxidized Method 2 SiCN-CF SEM Images

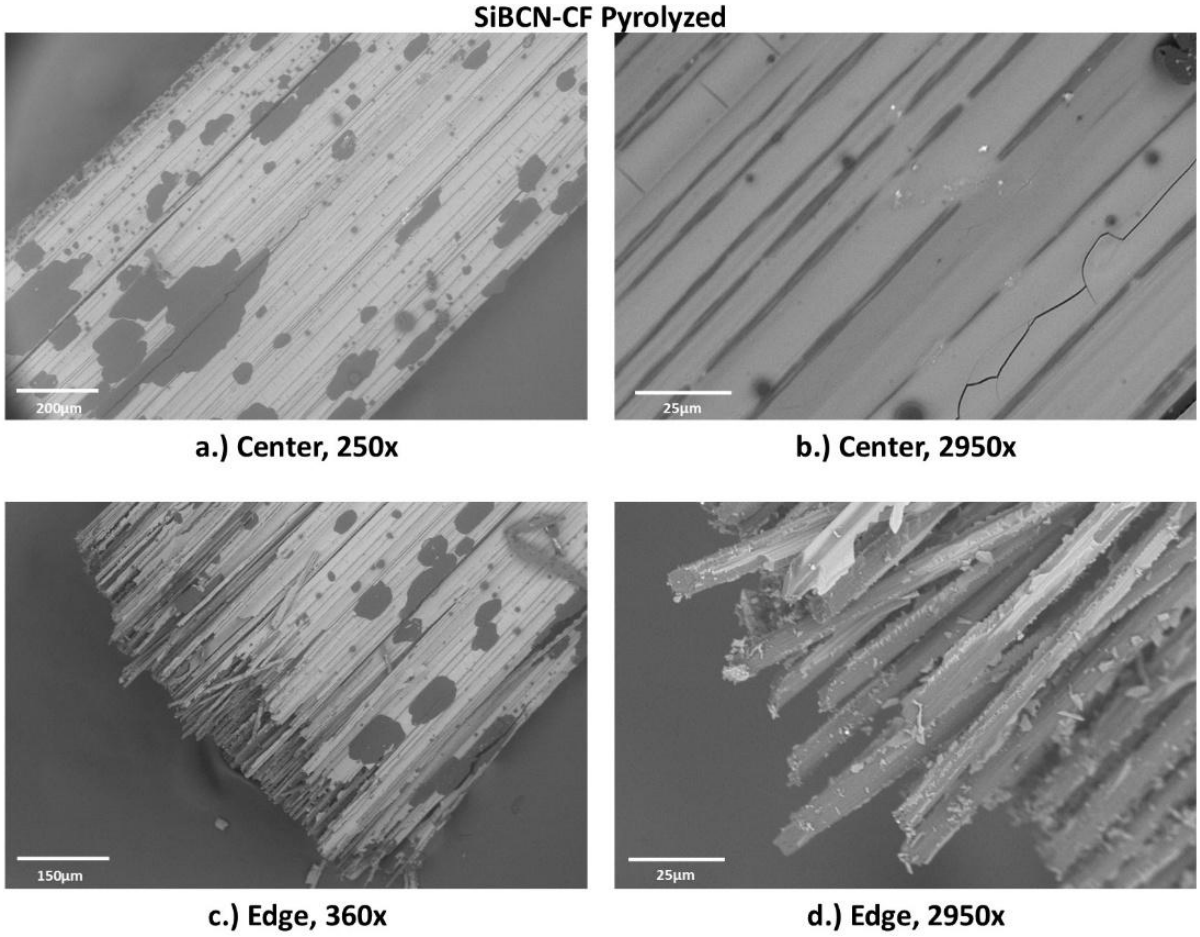

Figure 3-7: Pyrolyzed Method 2 SiBCN-CF SEM Images

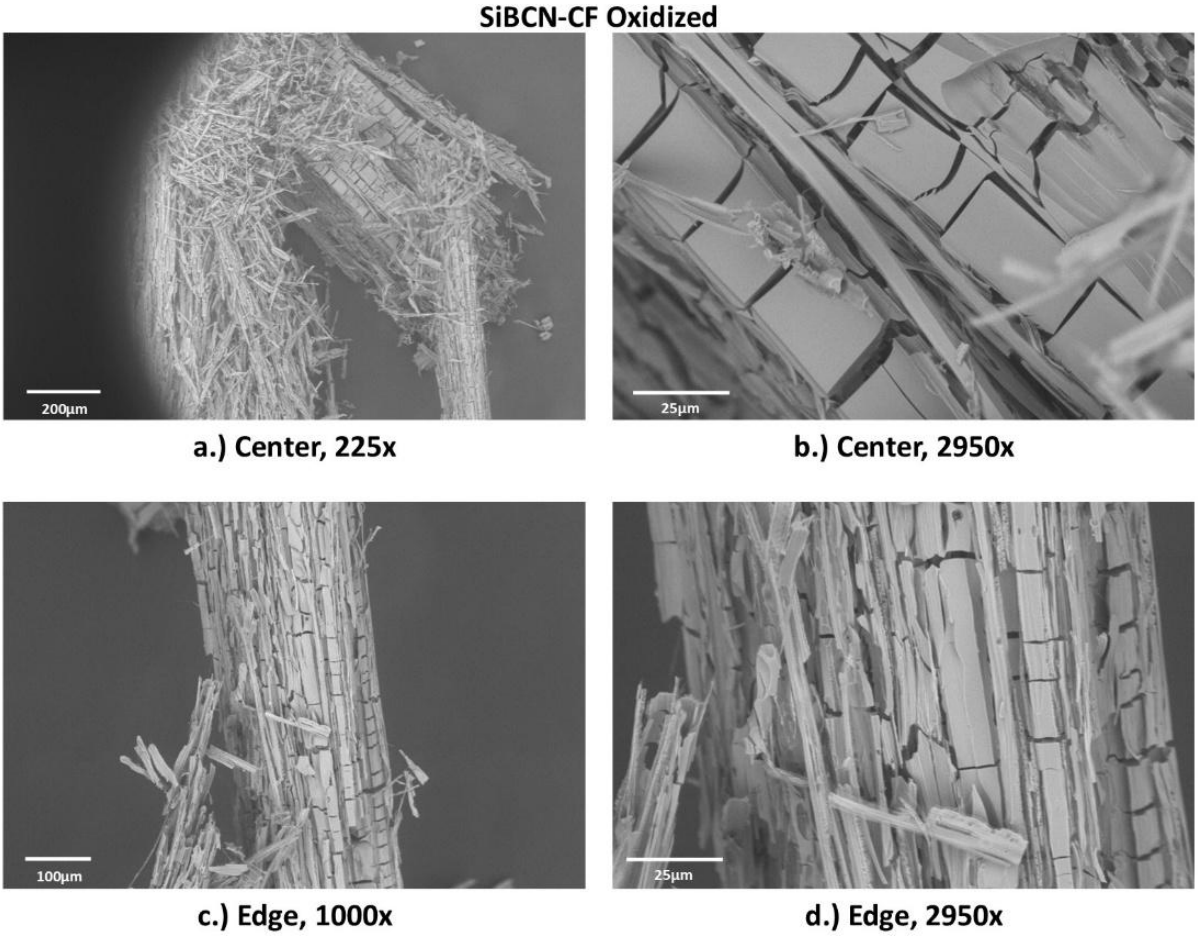

Figure 3-8: Oxidized Method 2 SiBCN-CF SEM Images

3.4.5 Tensile Testing

Tensile testing was performed to evaluate the mechanical properties of the SiCN-CF and SiBCN-CF mini-composites fabricated using the Method 2 multi-infiltration single-pyrolysis processing method. Tensile testing provides important information regarding composite strength, stiffness, and failure behavior, which are critical for structural applications of CMCs.

Mini-composite specimens were prepared from carbon fiber bundles infiltrated with the preceramic polymer and pyrolyzed to form CMCs. The composite bundles were mounted onto cardstock tabs using glue, following methods reported in previous fiber bundle testing studies. To reduce slippage, painters tape was added over the sample contact with the mount to create friction with the load cell clamps. Each cardstock tab contained a slot corresponding to a gauge length of approximately 30 mm, as shown in Figure 3-9. After the specimens were mounted in the testing machine grips, the sides of the cardstock tabs were cut to allow load transfer directly to the specimen.

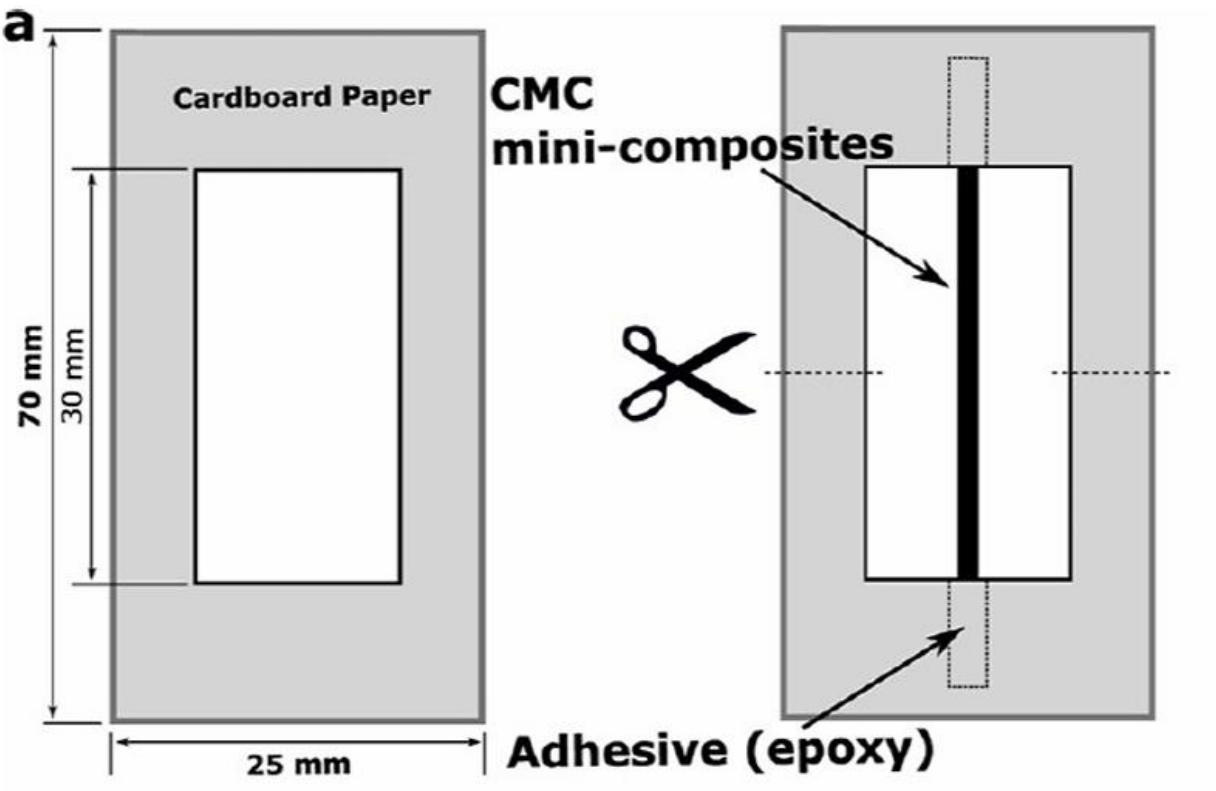

Figure 3-9: Tensile Testing Setup [7]

Figure 3-10: Tensile Test Samples with Applied Glue to Mounts

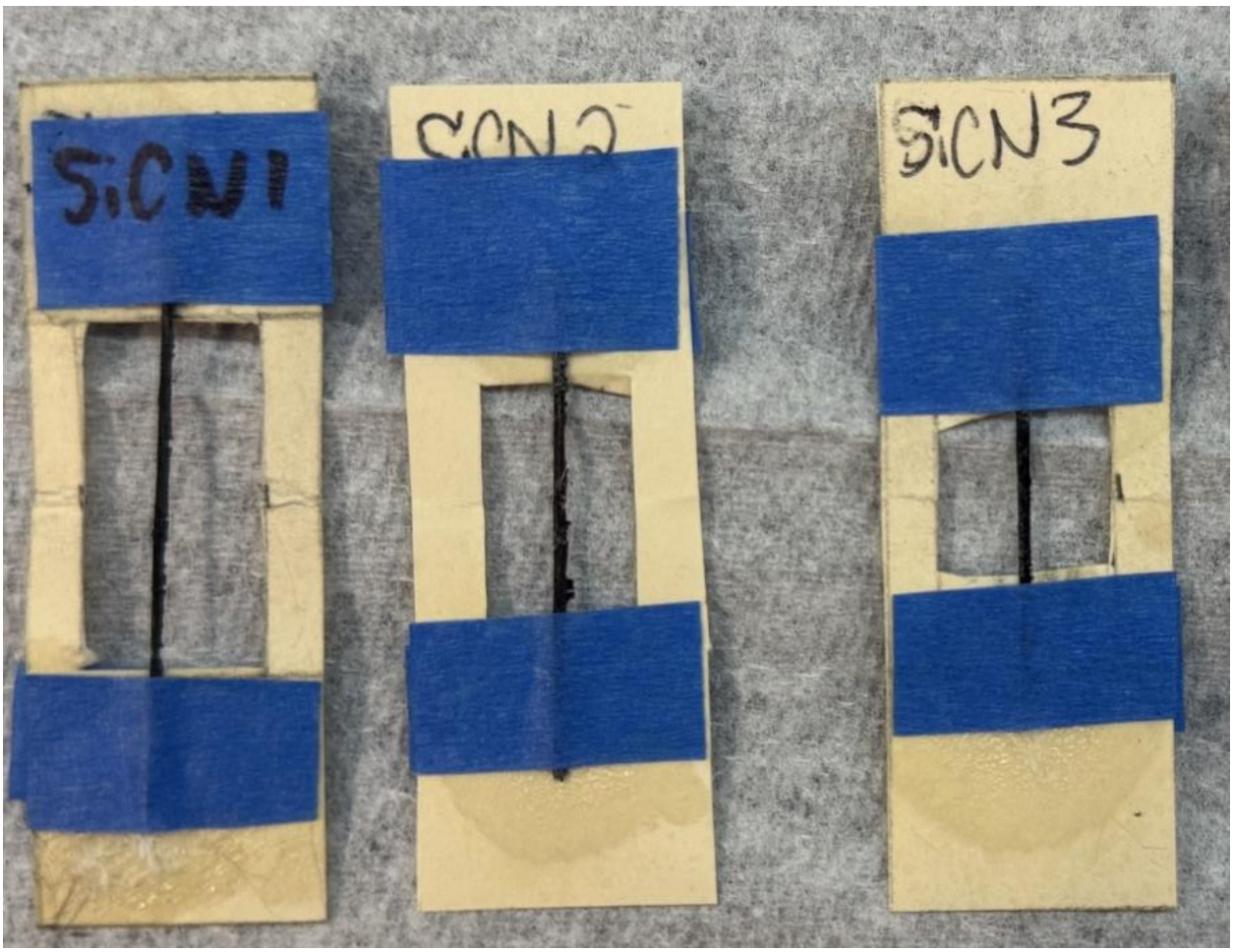

Figure 3-11: Tensile Test Samples with Tape for Added Grip

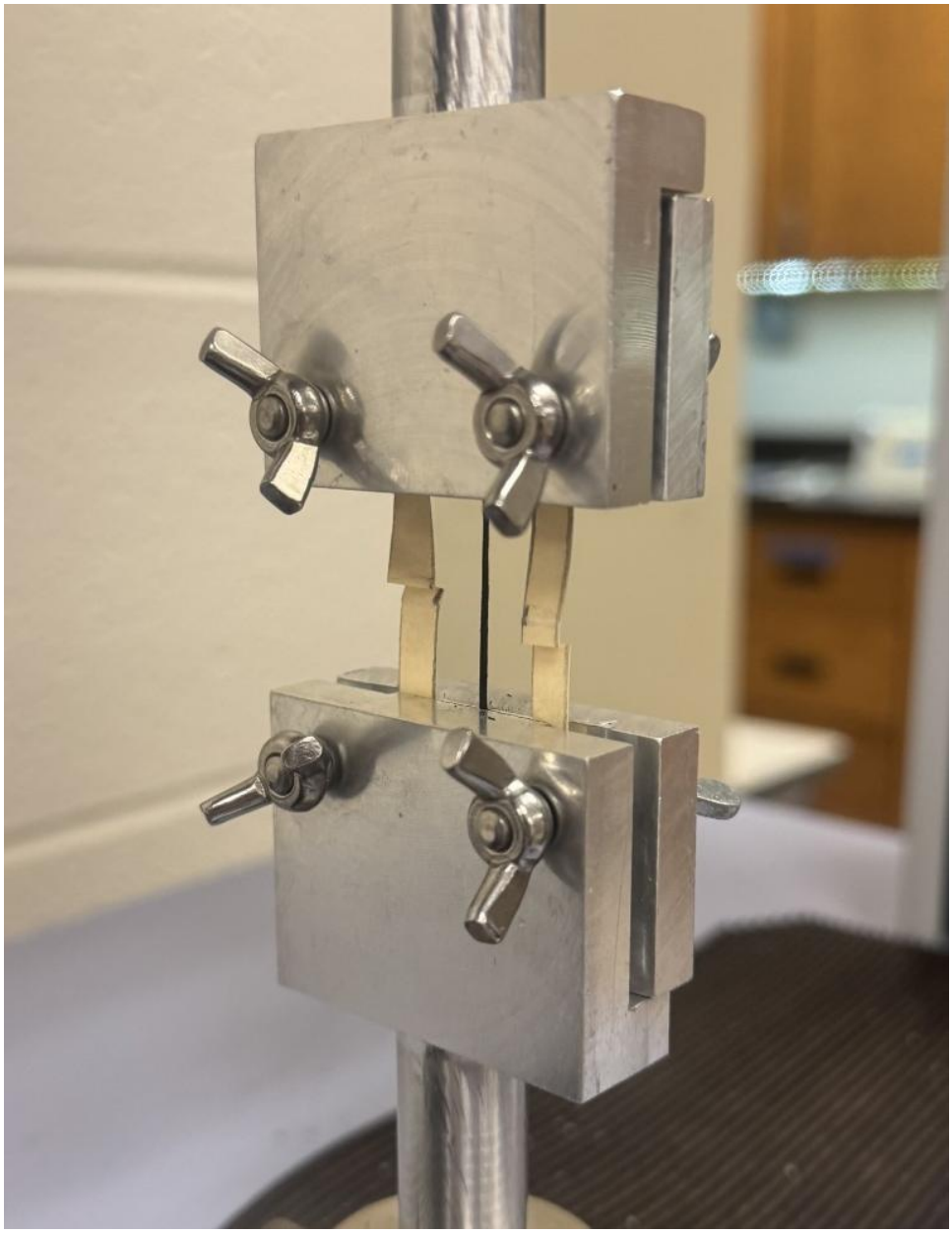

Figure 3-12: Tensile Test Sample Mounted to Load Cell

Tensile tests were performed under displacement-controlled loading using a 5 kN load cell at a crosshead speed of 0.2 mm/min to maintain quasi-static loading conditions. Load and displacement data were recorded throughout the test until specimen failure. Specimen dimensions were measured prior to testing in order to calculate engineering stress and engineering strain.

Engineering stress was calculated using Equation 3-9:

Equation 3-9: Engineering Stress Equation

$$\sigma = F / A$$

where

σ = *engineering stress*

F = *applied load*

A = *initial cross-sectional area of the specimen*

Engineering strain was calculated using Equation 3-10:

Equation 3-10: Engineering Strain Equation

$$\varepsilon = \Delta L / L_0$$

where

ε = *engineering strain*

ΔL = *change in gauge length*

L_0 = *original gauge length*

Mechanical toughness was calculated using Equation 3-11:

Equation 3-11: Mechanical Toughness Equation

$$U_T = \int_0^{\varepsilon_f} \sigma \, d\varepsilon$$

where

U_T = *mechanical toughness (energy per unit volume, MJ/m^3)*

σ = *stress*

ε = *strain*

ε_f = *strain at failure*

Young's modulus was determined from the slope of the linear elastic region of the stress-strain curve, and ultimate tensile strength was defined as the maximum stress reached before failure.

Multiple specimens were tested for each material type to ensure repeatability. Some test results were excluded from analysis due to specimen slippage in the grips or fracture occurring at the grip locations rather than within the gauge length. Only specimens that failed within the gauge section were used for calculation of average mechanical properties. The results of all samples for neat carbon fiber, Method 2 SiCN-CF, and Method 2 SiBCN-CF are shown in Figure 3-13, Figure 3-14, and Figure 3-15, respectively. The best performing sample of each sample type was compared in Figure 3-16. The average mechanical properties are reported in Table 3-4.

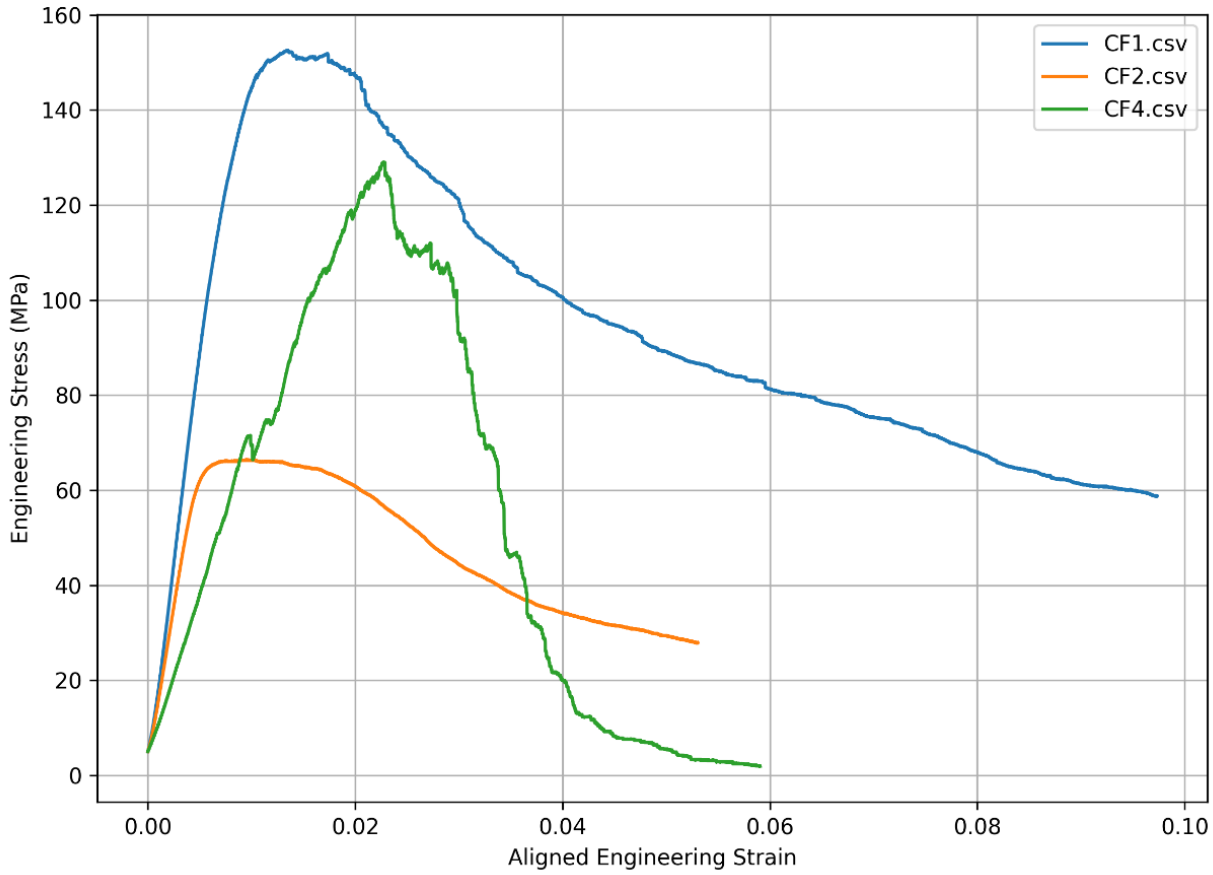

Figure 3-13: Neat Carbon Fiber Stress-Strain Plot

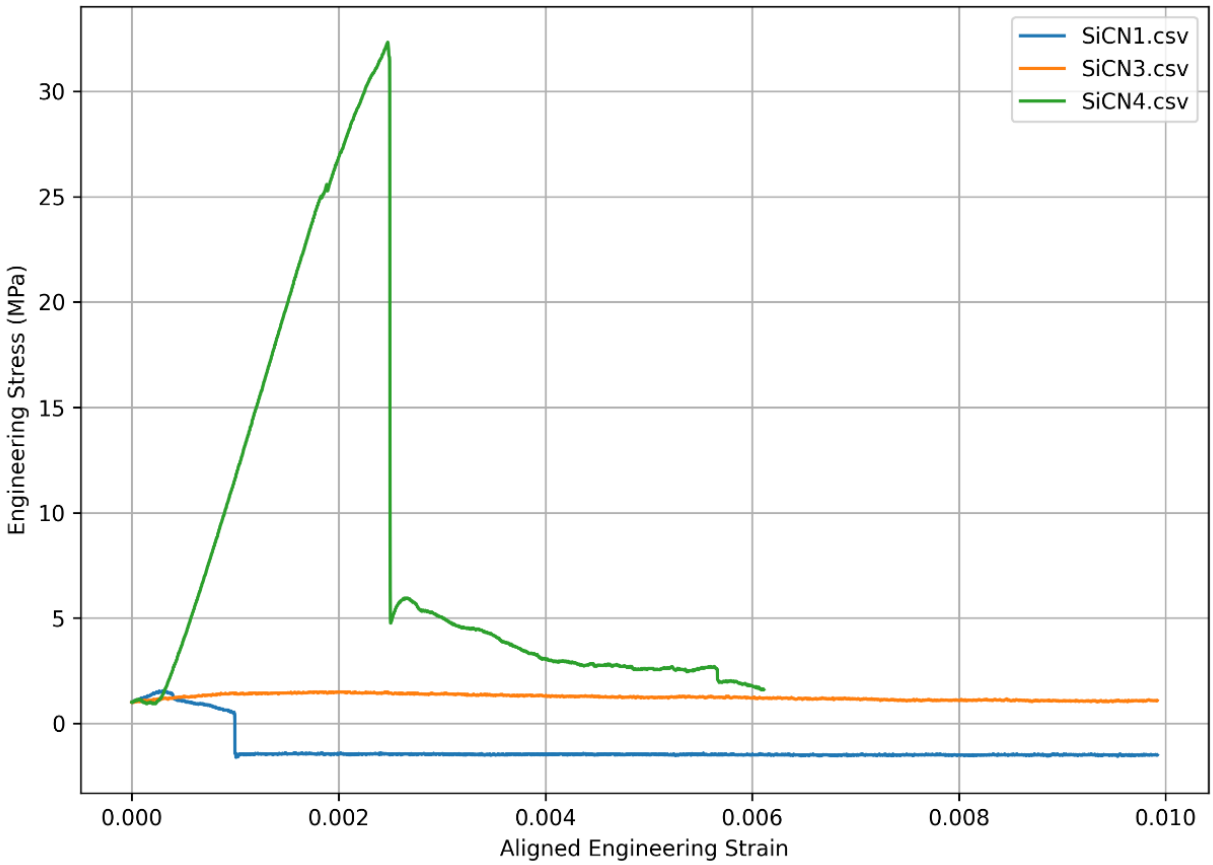

Figure 3-14: Method 2 SiCN-CF Stress-Strain Plot

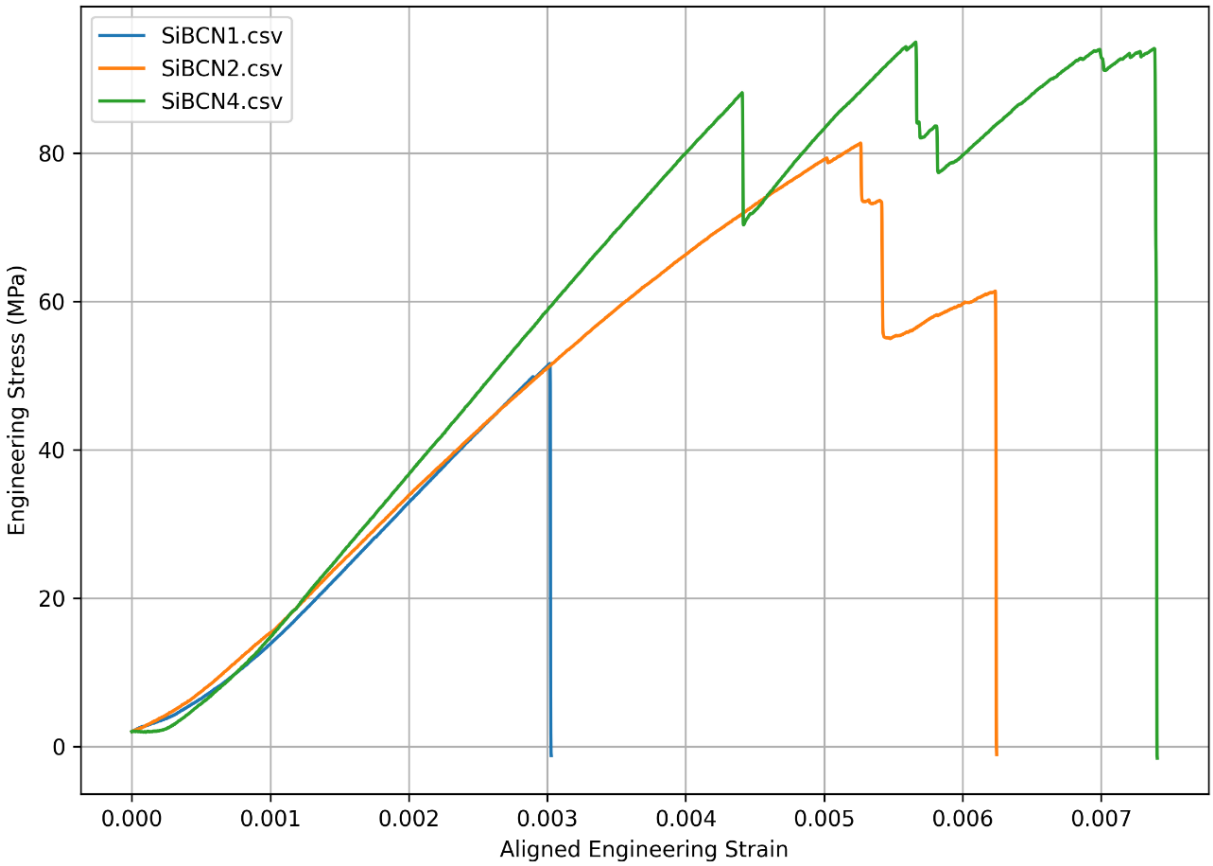

Figure 3-15: Method 2 SiBCN-CF Stress-Strain Plot

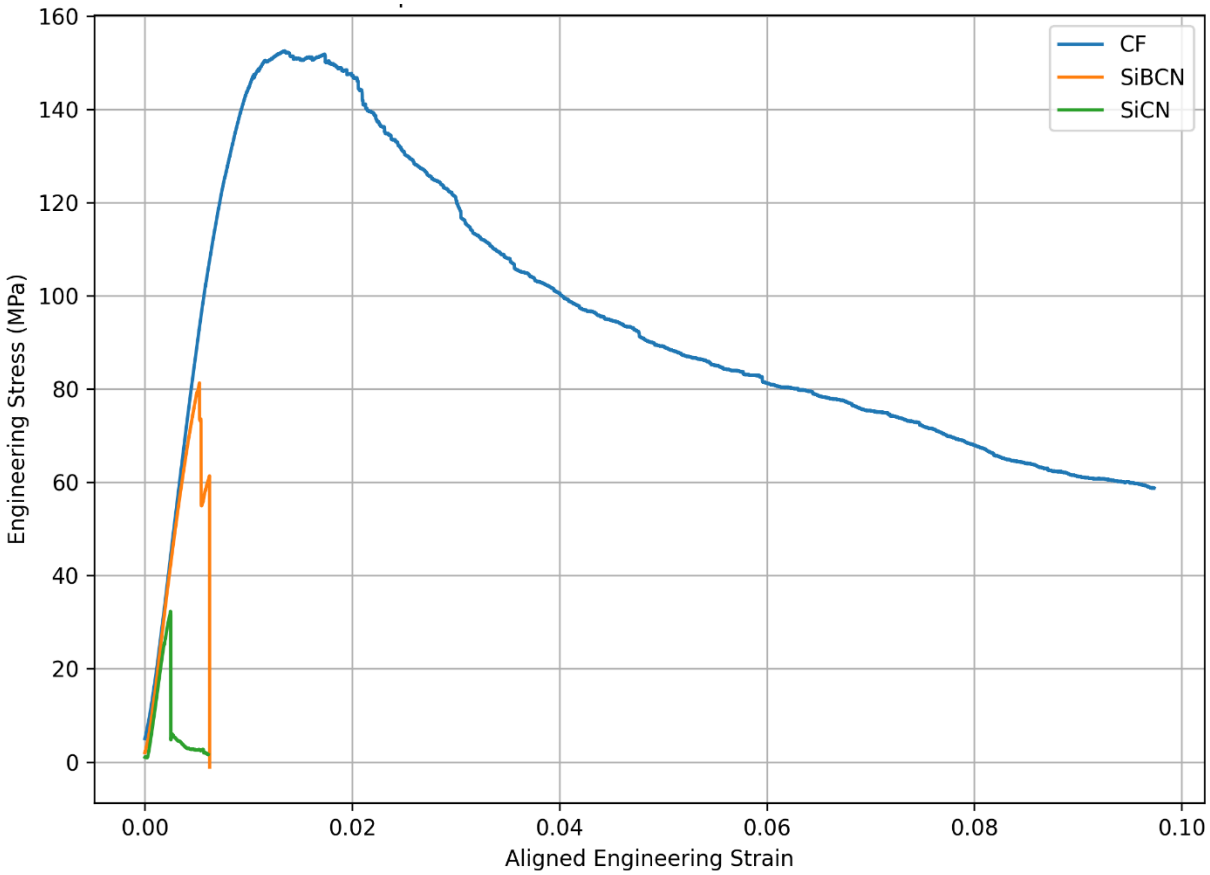

Figure 3-16: Neat Carbon Fiber, Method 2 SiCN-CF, and Method 2 SiBCN-CF Stress-Strain Plot Comparison

Table 3-4: Neat Carbon fiber, Method 2 SiCN-CF, and Method 2 SiBCN-CF Mechanical Properties Comparison

Material	Elastic Modulus (GPa)	UTS (MPa)	Failure Strain	Toughness (MJ/m^3)
Neat CF	14.133	116.023	0.015	4.903
SiCN-CF	17.063	32.333	0.002	0.051
SiBCN-CF	18.558	75.971	0.005	0.267

3.5 Discussion

3.5.1 Mass Analysis

Mass analysis of Method 2 reveals clear trends in polymer uptake, ceramic accumulation, and final composite composition. SiCN-CF samples exhibited significantly greater polymer uptake than SiBCN-CF samples, with total preceramic polymer mass additions ranging from 16.1 to 21.8 mg compared to 7.3 to 8.5 mg for SiBCN-CF. This corresponds to pre-pyrolysis polymer ratios of approximately 166-227% for SiCN-CF and 74-87% for SiBCN-CF, indicating substantially greater precursor incorporation in the SiCN system.

Following pyrolysis, this difference in polymer uptake directly translated to final mass and ceramic accumulation. SiCN-CF samples exhibited final masses between 22.3 and 25.7 mg, corresponding to total mass increases of 12.6-15.6 mg. In contrast, SiBCN-CF samples exhibited significantly lower final masses between 12.3 and 14.3 mg, with total mass increases limited to 2.6-4.2 mg. This indicates that SiCN-CF samples achieved approximately 3-4 times greater ceramic accumulation compared to SiBCN-CF.

Although ceramic yield values for SiCN-CF samples (67-78%) were generally higher than those of SiBCN-CF samples (33-56%), the results demonstrate that conversion efficiency alone does not govern final ceramic content. Instead, the dominant factor controlling ceramic accumulation is the total amount of polymer successfully infiltrated prior to pyrolysis.

A similar trend in polymer uptake was observed in Method 2 as in the multi-cycle PIP process described in Section 2.5.1. The reduced polymer uptake in the SiBCN-CF system is attributed to the lower viscosity of the precursor mixture resulting from the addition of trimethyl borate (TMB) to polysilazane. As discussed previously, the lower viscosity improves flowability but reduces

retention within the fiber preform during infiltration and crosslinking, leading to decreased overall polymer incorporation. In contrast, the higher viscosity of the SiCN precursor promotes retention within the fiber bundles, resulting in greater polymer uptake and increased ceramic accumulation after pyrolysis. The consistency of this behavior across both processing methods highlights the critical role of precursor rheology in governing infiltration efficiency and final composite composition.

Analysis of final composition further reinforces this distinction. SiCN-CF composites exhibited ceramic fractions between approximately 56% and 61%, indicating a ceramic-dominated structure. In contrast, SiBCN-CF composites exhibited ceramic fractions between approximately 21% and 29%, remaining strongly fiber-dominated. These results are consistent with the limited polymer uptake observed in the SiBCN system.

3.5.2 X-Ray Fluorescence Analysis

XRF spectra revealed distinct differences between neat carbon fiber and ceramic-coated composites. Neat carbon fiber samples were dominated by a strong carbon peak, with minimal contribution from other elements. In contrast, both SiCN-CF and SiBCN-CF samples exhibited additional peaks corresponding to ceramic-related elements. Silicon and nitrogen peaks were present in both coated samples, indicating successful incorporation of ceramic phases. The persistence of a strong carbon signal across all samples is consistent with the underlying carbon fiber reinforcement.

The SiBCN-CF samples showed a boron signal, distinguishing them from SiCN-CF and confirming that boron was successfully retained through processing and incorporated into the final ceramic network.

It should be noted that the B, C, and N peaks occur in a low-energy region (<0.4 keV) where spectral overlap and detector sensitivity can introduce uncertainty. However, the combined presence and relative intensities of these peaks are consistent with expected elemental compositions for SiCN and SiBCN polymer-derived ceramics.

XRF analysis confirms that Method 2 successfully produces ceramic-coated carbon fiber composites with the intended chemical compositions, including successful incorporation of SiCN and SiBCN ceramic phases.

3.5.3 Oxidation Testing

The oxidation results for Method 2 demonstrate that ceramic matrix incorporation provides significant protection against high-temperature oxidation compared to uncoated carbon fiber. While the uncoated carbon fiber sample completely disintegrated, both SiCN-CF and SiBCN-CF samples remained intact after exposure to 800°C, confirming the effectiveness of the ceramic matrix as an oxygen diffusion barrier.

SiCN-CF samples exhibited higher overall oxidation resistance, as indicated by greater mass retention compared to SiBCN-CF. This behavior is attributed to the higher ceramic loading achieved in the SiCN samples, which results in improved matrix continuity, reduced porosity, and more effective protection of the carbon fibers. In contrast, SiBCN-CF samples demonstrated higher mass retention efficiency, indicating more effective oxidation protection per unit of ceramic material. Despite lower overall ceramic loading, the SiBCN matrix appears to provide comparatively efficient oxidation resistance, likely due to differences in oxide formation and glassy phase behavior that enhance surface sealing and limit oxygen diffusion.

Both material systems exhibited visible curling or warping following oxidation exposure. This suggests the presence of residual thermal stresses, likely caused by thermal expansion mismatches between the carbon fiber reinforcement and the ceramic matrix during heating and cooling cycles.

The oxidation performance of Method 2 samples is governed by a trade-off between total ceramic loading and material efficiency. SiCN provides higher absolute oxidation resistance due to greater ceramic content, while SiBCN offers more efficient protection at lower ceramic loading levels. These results highlight the importance of both processing strategy and material composition in determining oxidation performance.

3.5.4 Microstructure Analysis

Scanning electron microscopy was used to evaluate ceramic coating formation, matrix distribution, fracture characteristics, and oxidation-induced damage in SiCN-CF and SiBCN-CF composites fabricated using the Method 2 processing method.

SEM images of the pyrolyzed samples confirmed successful ceramic coating formation on carbon fiber surfaces for both material systems. The coatings were generally continuous and well distributed along individual fibers, indicating that repeated infiltration cycles prior to a single pyrolysis step enabled effective precursor penetration and matrix development. However, localized non-uniformities were observed. In particular, SiCN-CF samples exhibited regions of ceramic accumulation, attributed to polymer-rich pooling prior to pyrolysis, which resulted in concentrated ceramic regions after conversion shown by the dark regions in Figure 3-5. SiBCN-CF samples, in contrast, showed more uniform coating distribution and clearer fiber definition, suggesting improved precursor wetting and infiltration behavior.

Microcracking was observed in both material systems in the pyrolyzed state. These cracks are attributed to shrinkage stresses generated during polymer-to-ceramic conversion, which induce internal stresses within the matrix as the material densifies. Cracking was slightly more pronounced in SiCN-CF samples, consistent with the observed regions of matrix accumulation and non-uniform shrinkage.

SEM images of oxidized samples revealed the formation of a continuous but segmented oxide scale on the composite surfaces. The oxide layer for both samples exhibited characteristic cracking patterns consistent with thermal expansion mismatch between the oxide scale, underlying ceramic matrix, and carbon fibers during high-temperature exposure and cooling. Despite the presence of cracking, the oxide scale remained largely continuous, and the underlying fiber bundles remained structurally intact. This indicates that the ceramic coating provided effective shielding of the carbon fibers, limiting direct oxidation and preserving overall composite morphology. The cracks observed in the oxide layer did not appear to fully penetrate to the fiber surfaces, suggesting partial retention of protective capability.

SiBCN-CF samples showed greater fiber exposure and localized fragmentation following oxidation. While ceramic coatings were still present, the oxide layer appeared less continuous, indicating slightly reduced oxidation resistance relative to SiCN-CF. This behavior may be explained by the reduced amount of ceramic material produced for the SiBCN-CF sample, discussed in Section 0.

Overall, the SEM results demonstrate that Method 2 produces continuous ceramic coatings with improved distribution compared to single-cycle processing while avoiding the extensive crack networks associated with repeated pyrolysis cycles. Additionally, the oxidized SEM analysis

provides direct evidence that ceramic coatings contribute to oxidation resistance through oxide scale formation, with SiCN-CF exhibiting more effective surface protection and SiBCN-CF showing improved initial coating uniformity but slightly reduced oxidation performance.

3.5.5 Tensile Testing

Tensile testing was performed to evaluate the mechanical properties of the SiCN-CF and SiBCN-CF mini-composites fabricated using the Method 2 processing method. Tensile testing provided information regarding composite stiffness, strength, and failure behavior.

The stress–strain curves showed linear elastic behavior followed by brittle failure, which is characteristic of CMC and fiber bundle composites. Young's modulus was determined from the slope of the linear elastic region, and ultimate tensile strength was determined from the maximum stress prior to failure.

Some tensile test data were excluded from analysis due to specimen slippage in the grips or fracture occurring at the grip locations rather than within the gauge length. Only specimens that failed within the gauge section were used to calculate mechanical properties. This ensured that the reported results represent the mechanical behavior of the composite material rather than gripping effects.

The mechanical properties obtained for the multi-infiltration single-pyrolysis composites were compared to single-cycle SiCN and SiBCN composite data in order to evaluate the effect of increased infiltration cycles on mechanical performance. These comparisons are discussed further in the following section.

CHAPTER 4: COMPARING PROCESSING METHODS

This chapter compares the traditional multi-cycle polymer infiltration and pyrolysis (PIP) process described in Chapter 2 with the modified multi-infiltration single-pyrolysis process described in Chapter 3.

The traditional PIP process requires multiple infiltration and pyrolysis cycles to gradually increase ceramic matrix content within the fiber bundles. While this method is effective at producing CMCs with improved oxidation resistance and ceramic matrix formation, the repeated high-temperature pyrolysis cycles significantly increase processing time and manufacturing complexity. Each pyrolysis cycle requires controlled atmosphere furnace processing and introduces thermal shrinkage and potential microcracking in the ceramic matrix.

The modified processing method investigated in this study was designed to reduce the number of pyrolysis cycles by performing multiple infiltration and crosslinking cycles prior to a single final pyrolysis step. This approach allows additional polymer infiltration before ceramic conversion, which may increase ceramic matrix formation while significantly reducing furnace processing time. Reducing the number of pyrolysis cycles is important for improving manufacturing efficiency, reducing energy consumption, and increasing the scalability of CMC fabrication.

This chapter compares the results obtained from both processing methods, including mass analysis and ceramic yield, oxidation resistance, microstructure observed through scanning electron microscopy, and mechanical properties measured through tensile testing. In addition, the processing time and manufacturing implications of each method are discussed to evaluate the potential scalability of each processing approach for larger-scale CMC manufacturing.

4.1 Ceramic Yield Comparison

Comparison of Method 1 and Method 2 reveals consistent trends in polymer uptake, ceramic conversion, and final composite composition, despite differences in processing sequence. While the two methods differ in the number of pyrolysis steps performed, both demonstrate that polymer infiltration effectiveness is the dominant factor governing final ceramic accumulation.

Both methods showed that SiCN-CF samples achieved significantly greater polymer uptake than SiBCN-CF samples. In Method 1, this was observed through progressively increasing mass with each infiltration cycle, while in Method 2, cumulative polymer uptake prior to pyrolysis resulted in pre-pyrolysis polymer ratios exceeding 200% for SiCN-CF samples, compared to less than 90% for SiBCN-CF samples. In both processing routes, polymer uptake decreased with successive infiltration cycles, indicating progressive densification and reduced available porosity within the fiber preform. This behavior suggests that the composite approaches a saturation limit, where additional infiltration contributes to diminishing increases in matrix content.

To directly compare the effects of polymer uptake, ceramic conversion, and processing efficiency between the two methods, a summary of key mass and yield metrics is presented in Table 4-1.

Table 4-1: Comparison of Polymer Uptake, Ceramic Conversion, and Final Composition for Cycle 3 Method 1 Samples and Method 2 Samples

Method	Material	Preceramic Polymer Added (mg)	Ceramic Material Added (mg)	Ceramic Yield (%)	Ceramic Ratio (%)	Processing Time
Method 1 (3rd Cycle)	SiCN-CF	30.3	20.1	66.3	67.2	High
	SiBCN-CF	8.7	6.5	74.7	39.9	High
Method 2 (Averaged)	SiCN-CF	19.8	14.3	73.8	59.1	Low
	SiBCN-CF	7.9	3.3	41.4	24.8	Low

As shown in Table 4-1, Method 1 and Method 2 exhibit consistent relationships between polymer uptake and final ceramic content. For both methods, SiCN-CF samples demonstrate significantly higher preceramic polymer addition compared to SiBCN-CF samples, resulting in greater ceramic material accumulation and higher ceramic fractions in the final composite. While ceramic yield values vary between materials and processing methods, the differences in yield are smaller than the corresponding differences in polymer uptake and ceramic content. This shows that conversion efficiency during pyrolysis is not the limiting factor, and that similar yield values can produce significantly different final compositions depending on the amount of polymer initially infiltrated. Final mass and composition trends were also consistent across both methods. SiCN-CF samples exhibited significantly greater final mass and ceramic content compared to SiBCN-CF samples, reflecting their higher polymer uptake. In both methods, SiCN-CF composites transitioned toward ceramic-dominated structures, with ceramic fractions exceeding approximately 55–65%. In contrast, SiBCN-CF composites remained fiber-dominated, with ceramic fractions generally below 40%. These results further reinforce that increasing polymer uptake directly increases final ceramic accumulation, regardless of processing route.

Although both methods produced similar relationships between polymer uptake and final ceramic content, Method 2 achieved these outcomes using a simplified and more efficient processing route. Given that each pyrolysis cycle requires substantially more processing time and energy than infiltration and crosslinking steps, Method 2 offers a significant advantage in terms of processing efficiency and scalability. While Method 1 provides greater insight into cycle-by-cycle densification and conversion behavior, Method 2 demonstrates that comparable levels of ceramic accumulation can be achieved with fewer thermal processing steps.

4.2 Oxidation Resistance Comparison

The oxidation testing results for Method 1 and Method 2 reveal that high-temperature oxidation performance is strongly governed by ceramic loading, while material composition and processing method influence the efficiency of oxidation protection.

Across both processing methods, a clear relationship is observed between ceramic mass and oxidation resistance. Samples with higher ceramic loading consistently exhibited greater mass retention after oxidation, indicating improved resistance to oxygen diffusion and reduced material degradation. This trend is evident in both SiCN-CF and SiBCN-CF systems and confirms that ceramic matrix content is the dominant factor controlling absolute oxidation performance. The relationship between ceramic loading and oxidation performance is shown in Figure 4-1, which shows a direct correlation between ceramic mass and mass retention across both methods.

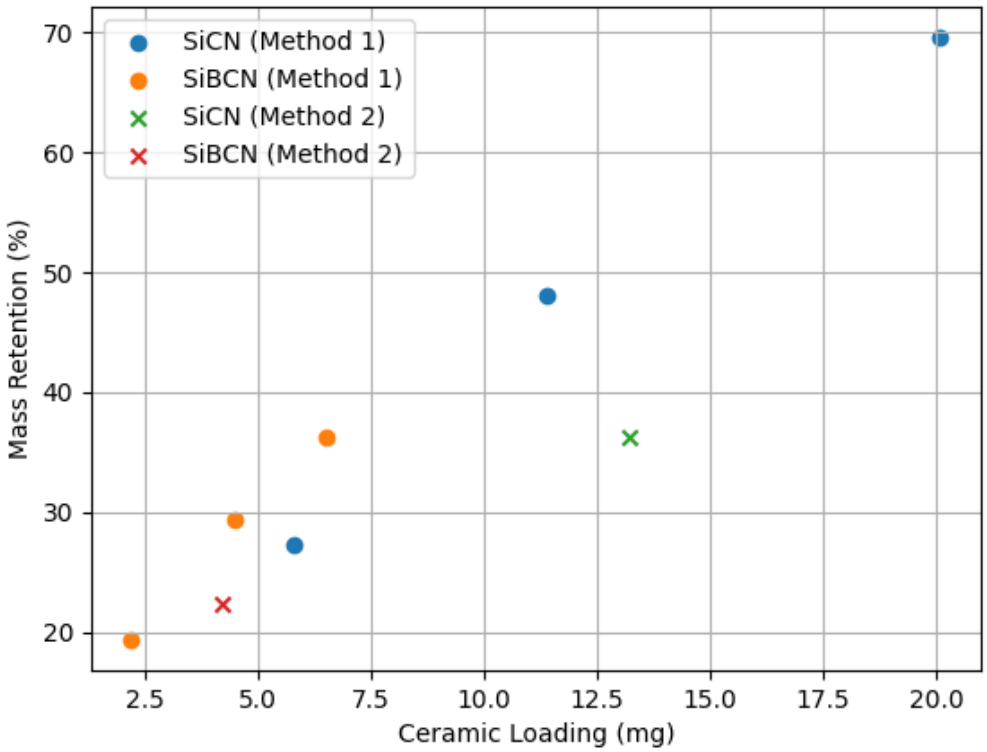

Figure 4-1: Ceramic Loading vs. Oxidation Mass Retention

SiCN-CF samples consistently achieved higher ceramic loading than SiBCN-CF samples for both processing methods, resulting in superior overall oxidation resistance. For example, in Method 1, SiCN-CF samples reached mass retention values as high as 69.57% at the highest cycle number, compared to 36.20% for SiBCN-CF. Similarly, in Method 2, SiCN-CF exhibited higher mass retention (36.21%) than SiBCN-CF (22.38%). These results demonstrate that increased ceramic content in the SiCN system leads to improved matrix continuity and more effective protection of the carbon fiber reinforcement.

In contrast, SiBCN-CF samples demonstrated higher mass retention efficiency across both methods, indicating more effective oxidation protection per unit of ceramic material. This behavior is particularly evident at lower ceramic loading levels, where SiBCN achieves comparable oxidation resistance despite significantly lower total ceramic mass. This suggests that the SiBCN matrix provides more efficient oxidation protection, which is consistent with previous literature [7].

Overall, the comparison demonstrates a trade-off between absolute oxidation resistance and material efficiency. Method 1 achieves higher oxidation resistance through increased ceramic loading and matrix densification, while Method 2 highlights the efficiency of each material system. SiCN provides superior protection at high ceramic loading, whereas SiBCN offers more efficient oxidation resistance at lower ceramic content. These results emphasize the importance of both processing strategy and material selection in optimizing oxidation performance for polymer-derived CMCs.

4.3 Microstructure Comparison

Scanning electron microscopy (SEM) was used to examine ceramic coating formation, matrix distribution, fiber-matrix bonding, and microstructural damage in composites fabricated using both Method 1 and Method 2 processing methods. SEM images provided direct comparison of coating morphology and matrix development resulting from the different processing routes.

For Method 1 samples, SEM images showed that ceramic coating thickness and coverage increased with increasing number of infiltration and pyrolysis cycles. Lower cycle samples exhibited thin, discontinuous coatings with regions of exposed carbon fiber, indicating incomplete matrix formation. With additional cycles, coatings became thicker and more continuous. However, this was accompanied by the development of significant surface cracking and matrix fragmentation. High-magnification images revealed extensive, interconnected crack networks within the ceramic matrix, particularly in higher cycle samples. These features are attributed to cumulative shrinkage and thermal stresses introduced during repeated polymer-to-ceramic conversion and multiple high-temperature pyrolysis cycles. The result is a non-uniform, segmented matrix that, while thicker, contains a high density of defects.

In contrast, Method 2 samples exhibited a markedly different microstructure. SEM images showed smoother, more continuous ceramic coatings along individual fibers, with improved fiber definition and fewer large-scale crack networks. The multi-infiltration single-pyrolysis approach allowed polymer precursors to infiltrate the fiber bundles more effectively prior to ceramic conversion, resulting in more uniform matrix formation. While localized matrix accumulation and microcracking were still observed, these defects were less severe and less interconnected than those seen in Method 1 samples.

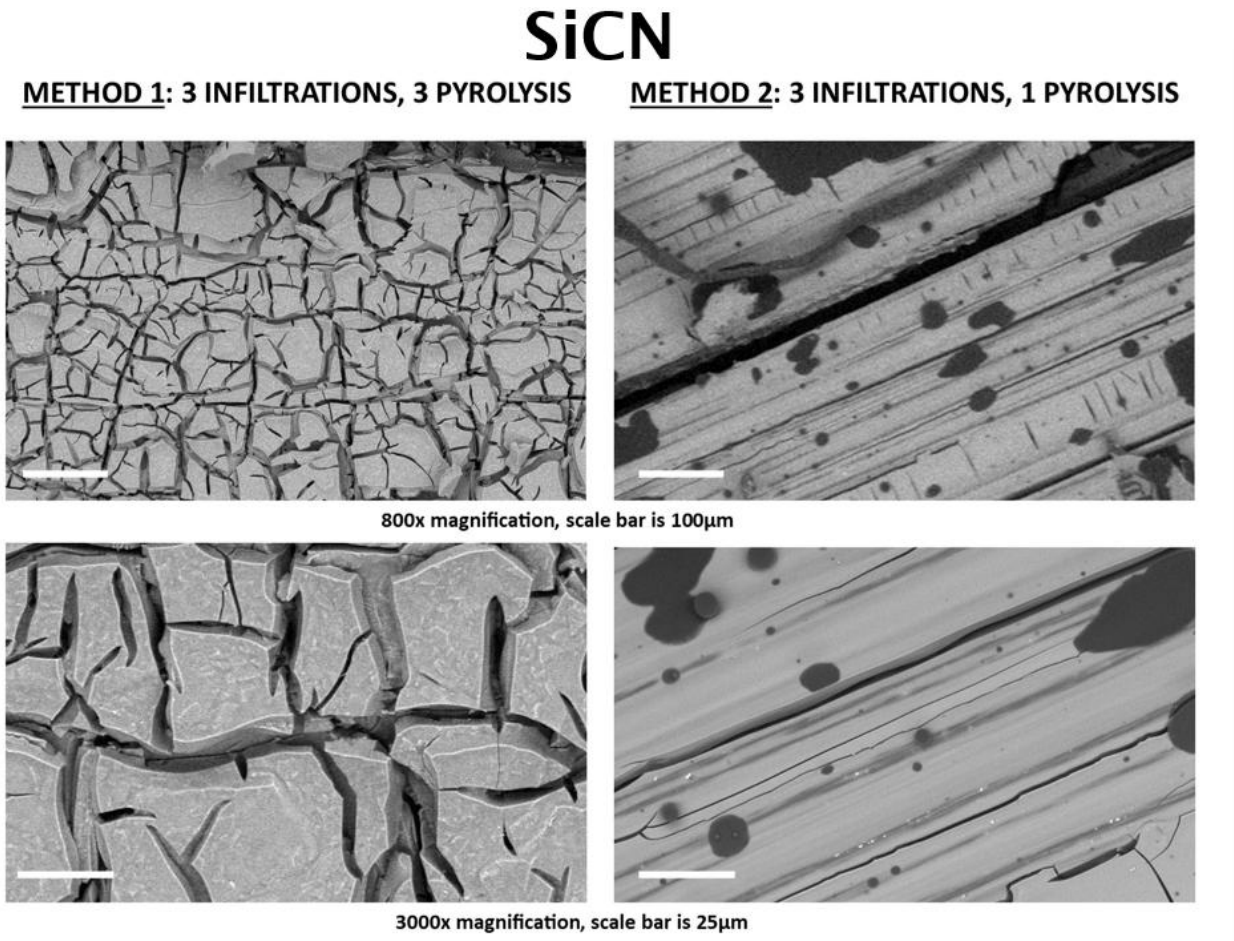

Figure 4-2: Pyrolyzed SiCN-CF Method 1 and Method 2 SEM Image Comparison

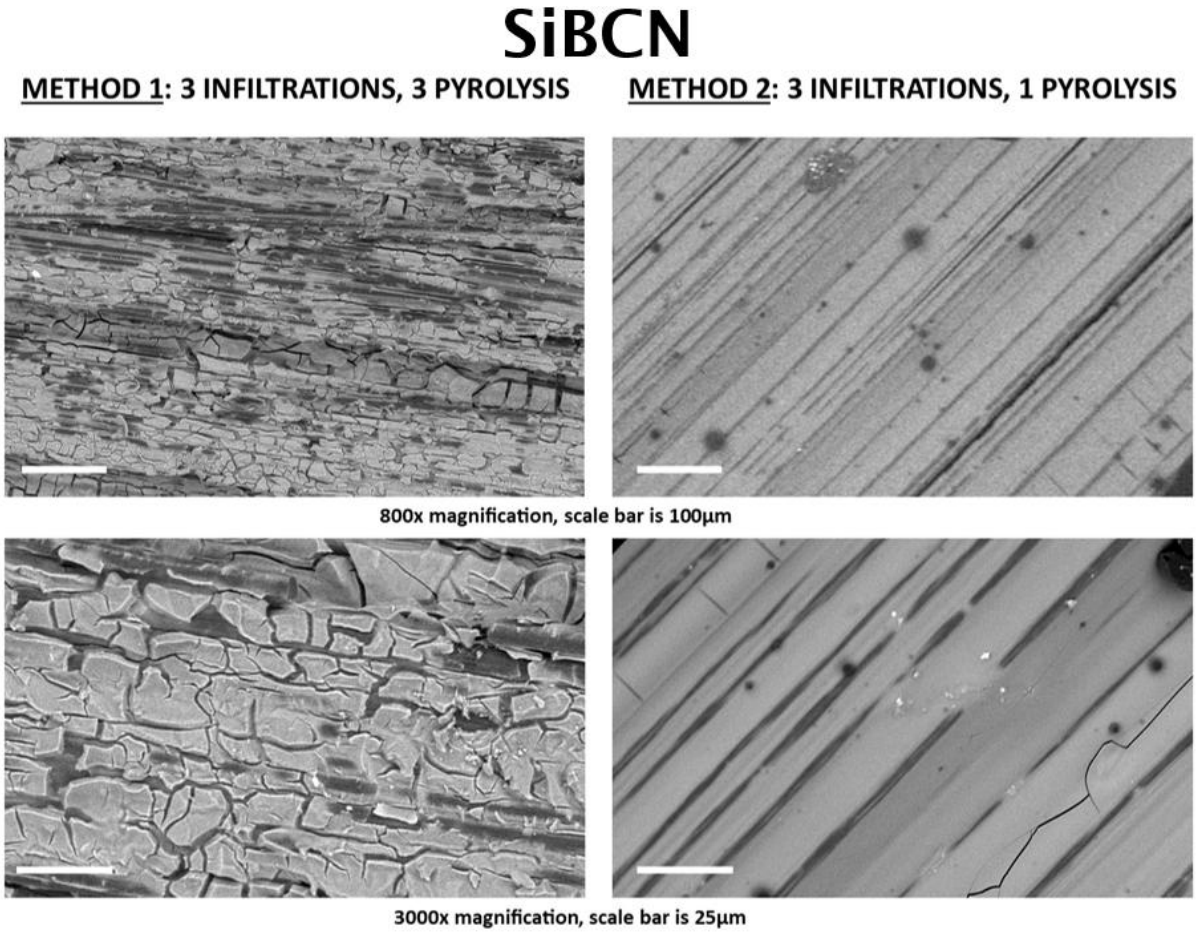

Figure 4-3: Pyrolyzed SiBCN-CF Method 1 and Method 2 SEM Image Comparison

Direct comparison between the two methods in Figure 4-2 and Figure 4-3 highlights a key processing-structure relationship. Method 1 promotes progressive matrix buildup through repeated ceramic formation but introduces cumulative shrinkage damage that leads to extensive cracking and matrix fragmentation. In contrast, Method 2 delays ceramic conversion until after multiple infiltration steps, reducing the number of shrinkage events and thereby limiting crack formation. This results in a more continuous and structurally coherent ceramic matrix.

SEM analysis indicates that while both methods are capable of producing ceramic coatings within carbon fiber bundles, Method 2 achieves comparable or improved matrix continuity with significantly reduced microstructural damage. This supports the conclusion that the multi-

infiltration single-pyrolysis process offers a more efficient pathway to producing high-quality CMCs, with improved microstructural integrity and reduced processing complexity.

4.4 Mechanical Properties Comparison

Mechanical properties of Method 2 mini-composites were compared to single-cycle SiCN-CF and SiBCN-CF composites to evaluate the effect of increased infiltration and the resulting changes in fiber-to-ceramic phase balance. The stress–strain curves for all samples exhibited linear elastic behavior followed by failure. However, the relative contributions of fiber-dominated and ceramic-dominated behavior varied significantly with processing and material system.

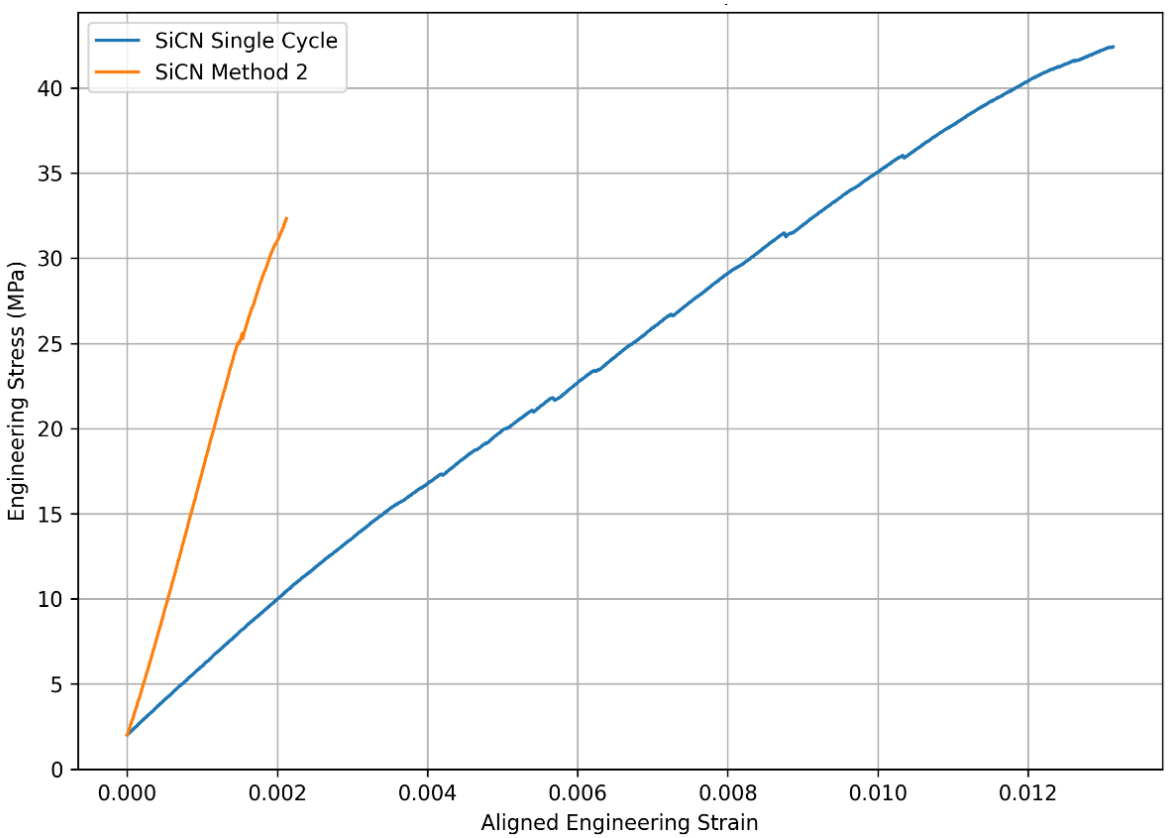

Figure 4-4: Single Cycle vs. Method 2 SiCN-CF Stress-Strain Plot Comparison

For SiCN-CF composites, additional infiltration cycles resulted in a large increase in elastic modulus (3.26 GPa to 16.10 GPa), indicating a substantial increase in ceramic content and matrix

stiffness. However, this increase in ceramic fraction reduced the relative contribution of carbon fibers to load bearing, leading to decreased ultimate tensile strength (42 MPa to 32 MPa) and a significant reduction in toughness (0.317 to 0.038 MJ/m³). The stress-strain response became steeper and more brittle, indicating a transition toward ceramic-dominated failure, where cracks propagate rapidly through the matrix with limited fiber bridging or energy absorption.

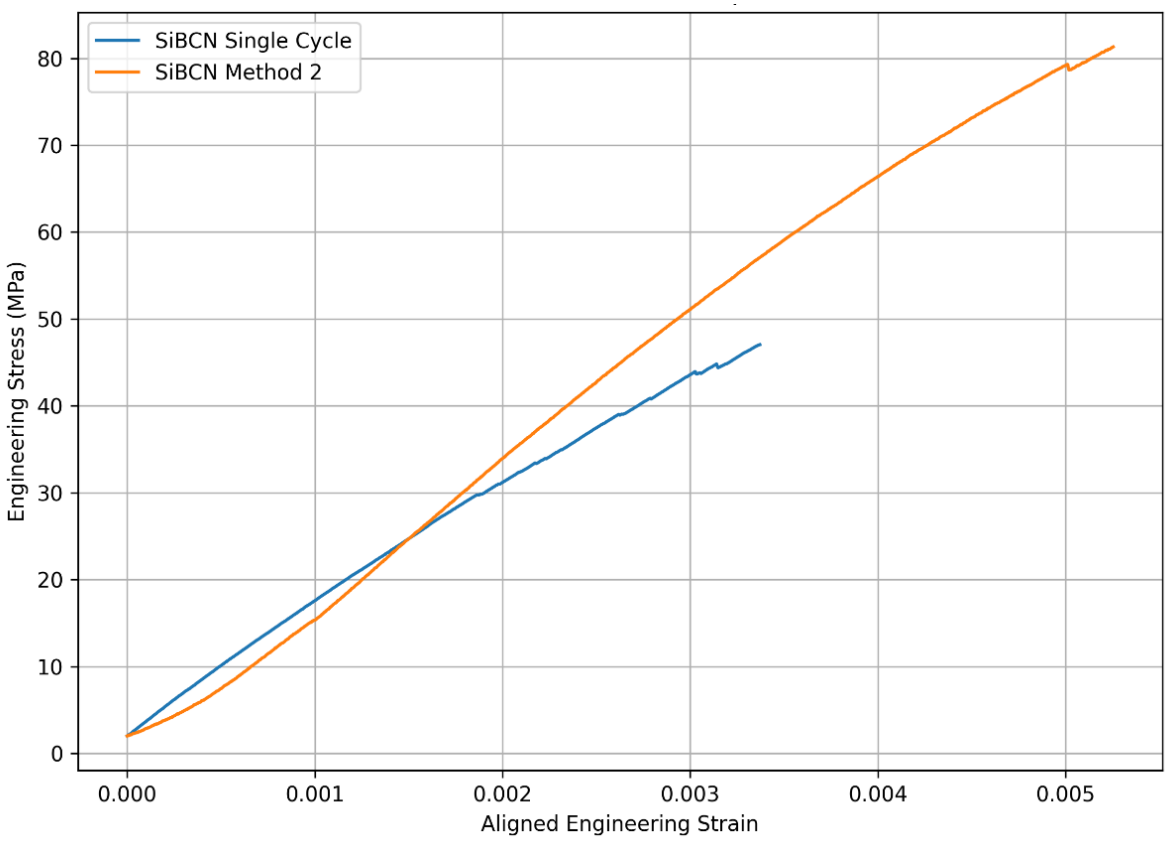

Figure 4-5: Single Cycle vs. Method 2 SiBCN-CF Stress-Strain Plot Comparison

In contrast, SiBCN-CF composites showed improvements in elastic modulus (14.83 GPa to 17.98 GPa), ultimate tensile strength (47 MPa to 81 MPa), and toughness (0.089 to 0.228 MJ/m³) with additional infiltration. These results suggest that the increase in ceramic content did not excessively suppress the contribution of carbon fibers. Instead, the fiber-to-ceramic balance remained favorable for load transfer, allowing fibers to effectively carry load and bridge cracks. The stress-strain curves further support this, showing higher load capacity and more progressive failure behavior.

Table 4-2: Single Cycle vs. Method 2 SiCN-CF and SiBCN-CF Mechanical Property Comparison

Material	Method	Elastic Modulus (GPa)	UTS (MPa)	Toughness (MJ/m^3)
SiCN-CF	Single Cycle	3.263	42.415	0.317
	Method 2	16.100	32.335	0.038
SiBCN-CF	Single Cycle	14.833	47.046	0.089
	Method 2	17.983	81.313	0.228

The differing responses between SiCN and SiBCN systems indicate that the effect of increased ceramic content is strongly dependent on how it alters the relative phase balance. In SiCN-CF composites, higher ceramic content leads to matrix-dominated behavior and brittle failure, whereas in SiBCN-CF composites, the ceramic matrix enhances interfacial bonding and load transfer without eliminating fiber-dominated mechanisms.

These results demonstrate that optimal mechanical performance in polymer-derived CMCs depends not only on increasing ceramic content but on maintaining a balanced fiber-to-ceramic ratio. The Method 2 process successfully increases stiffness in both systems, but only the SiBCN system preserves sufficient fiber contribution to achieve improvements in strength and toughness.

4.5 Processing Time and Manufacturing Scalability

The primary objective of the modified multi-infiltration single-pyrolysis processing method was to reduce overall fabrication time while improving scalability of polymer-derived CMC manufacturing. Comparison of processing timelines between the traditional multi-cycle PIP method and the modified approach demonstrates a substantial reduction in total processing time.

For the traditional method, three full PIP cycles, each consisting of infiltration, crosslinking, and pyrolysis, result in a total processing time of approximately 30 hours. In contrast, the modified method consolidates ceramic conversion into a single pyrolysis step following multiple infiltration and crosslinking cycles, reducing total processing time to approximately 14 hours, representing a ~53% reduction. This reduction is primarily driven by the elimination of repeated high-temperature pyrolysis cycles, which are the most time- and energy-intensive steps in the process. While infiltration and crosslinking steps remain, these occur at lower temperatures and contribute minimally to overall processing time compared to pyrolysis.

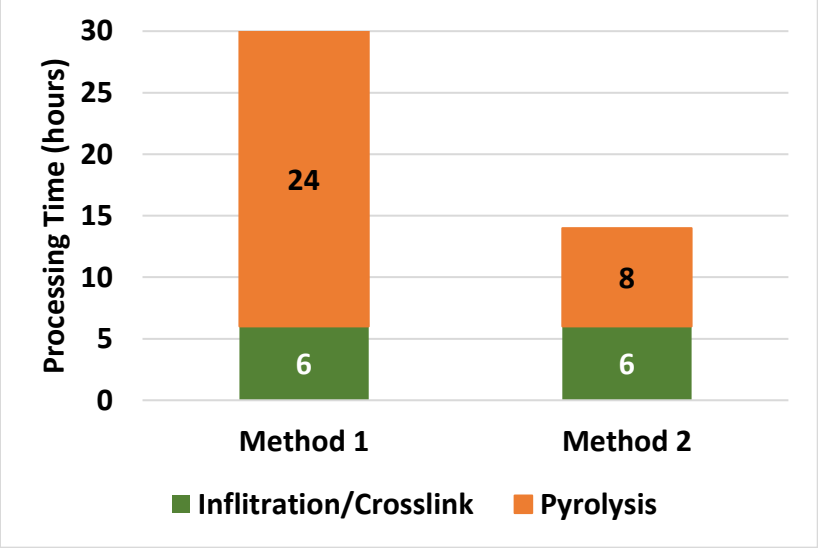

Figure 4-6: Processing Time Comparison for Method 1 and Method 2

Despite the reduced processing time, the modified method achieves comparable performance when accounting for differences in ceramic loading. Additional pyrolysis cycles in the traditional method provide diminishing returns in terms of mechanical and oxidation performance, indicating that repeated ceramic conversion is not the dominant factor in performance improvement. From a manufacturing perspective, this reduction in processing time has significant implications. Shorter processing cycles directly translate to increased production throughput, lower energy consumption, and reduced operational costs. Furthermore, minimizing high-temperature furnace usage alleviates a major bottleneck in large-scale CMC production.

The modified multi-infiltration single-pyrolysis method provides a more time-efficient and scalable manufacturing pathway for polymer-derived CMCs. By maintaining comparable material performance while significantly reducing processing time, this approach offers a practical route toward broader adoption of CMCs in aerospace and high-temperature applications.

4.6 Summary of Processing Method Comparison

The comparison between the traditional multi-cycle PIP method (Method 1) and the modified multi-infiltration single-pyrolysis method (Method 2) demonstrates that composite performance is governed by a balance between ceramic loading and processing efficiency.

Method 1 consistently achieves the highest ceramic loading through repeated infiltration and pyrolysis cycles, resulting in superior absolute oxidation resistance and increased matrix densification. However, this approach introduces significant drawbacks, including cumulative thermal shrinkage, matrix cracking, and diminishing returns with additional cycles. The repeated high-temperature processing also leads to substantially increased fabrication time and greater risk of defect accumulation, limiting scalability for large-scale manufacturing. In contrast, Method 2

achieves comparable performance relative to its reduced ceramic loading by maximizing infiltration efficiency prior to a single pyrolysis step. This processing route produces more uniform and continuous ceramic coatings with fewer microstructural defects, as confirmed through SEM analysis. Although total ceramic content is lower, the resulting composites demonstrate efficient oxidation resistance.

Mechanical property comparisons further emphasize that increasing ceramic content does not universally improve performance. SiCN-CF composites, which become ceramic-dominated, exhibit increased stiffness but reduced strength and toughness due to brittle matrix behavior. Conversely, SiBCN-CF composites maintain a more balanced phase distribution, allowing for simultaneous improvements in stiffness, strength, and toughness. These results highlight the importance of optimizing phase balance rather than maximizing ceramic content alone.

From a manufacturing perspective, the most significant advantage of Method 2 is the substantial reduction in processing time. By eliminating multiple high-temperature pyrolysis cycles, total fabrication time is reduced by approximately 53%, while maintaining comparable material performance. This reduction directly translates to increased throughput, lower energy consumption, and improved feasibility for large-scale production.

Overall, the results demonstrate a clear trade-off between maximum performance and processing efficiency. Method 1 maximizes ceramic loading and absolute oxidation resistance, while Method 2 maximizes efficiency, microstructural quality, and scalability. The findings of this study suggest that the modified multi-infiltration single-pyrolysis approach provides a more practical and scalable pathway for polymer-derived ceramic matrix composite manufacturing, particularly when optimized for material-specific performance objectives.

CHAPTER 5:CONCLUSIONS AND FUTURE WORK

This work demonstrated the successful fabrication of SiCN and SiBCN carbon fiber–reinforced polymer-derived ceramic matrix composites using both traditional multi-cycle PIP and a modified multi-infiltration single-pyrolysis processing approach. The modified method achieved comparable ceramic formation, oxidation resistance, and mechanical behavior while significantly reducing processing time and furnace utilization.

Across all characterization methods, ceramic loading was identified as the primary driver of absolute oxidation resistance, while material efficiency and composition influenced performance per unit ceramic. SiBCN systems exhibited improved efficiency, while SiCN systems showed more ceramic-dominated behavior. Microstructural analysis further revealed that although multiple infiltration cycles improve coating continuity, repeated pyrolysis introduces thermal stresses that can lead to matrix cracking and diminishing returns.

Overall, the modified single-pyrolysis PIP method reduced processing time by approximately 50% while maintaining performance, demonstrating a clear pathway toward scalable and cost-effective manufacturing of polymer-derived CMCs. These results support a shift in processing strategy from maximizing ceramic loading to optimizing ceramic efficiency and processing design.

Future work should focus on expanding both material systems and processing capability to further enhance performance and scalability. Investigation of higher-order polymer-derived ceramic systems, such as SiHfBCN, could enable improved ultra-high temperature behavior. Incorporation of ceramic reinforcement phases, including SiC, should also be explored to enhance mechanical performance.

From a manufacturing perspective, studies on complex geometries and larger-scale components are needed to validate the process for real-world applications. Further optimization of infiltration strategies, cycle number, and pyrolysis conditions will help refine the balance between processing efficiency and material performance.

Additional mechanical characterization, including four-point bending and improved tensile testing methods, is necessary to better capture structural behavior. Continued efforts to reduce pyrolysis time and improve furnace efficiency will be critical for advancing the scalability of polymer-derived ceramic matrix composite manufacturing.

REFERENCES

[1] Singh, Gurpreet, and Romil Bhandavat. "Boron-modified silazanes for synthesis of SiBNC ceramics." U.S. Patent No. 9,453,111. 27 Sep. 2016.

[2] Mujib, Shakir Bin, et al. "Self-supporting carbon-rich SiOC ceramic electrodes for lithium-ion batteries and aqueous supercapacitors." *RSC advances* 11.56 (2021): 35440-35454.

[3] Ren, Zhongkan, Christel Gervais, and Gurpreet Singh. "Fabrication and characterization of silicon oxycarbide fibre-mats via electrospinning for high temperature applications." RSC advances 10.63 (2020): 38446-38455.

[4] Zhang, Qian, et al. "Synthesis and structural evolution of dual-boron-source-modified polysilazane derived SiBCN ceramics." *New Journal of Chemistry* 40.8 (2016): 7034-7042.

[5] Kim, Kiho, Hyun Ju, and Jooheon Kim. "Pyrolysis behavior of polysilazane and polysilazane-coated-boron nitride for high thermal conductive composite." *Composites Science and Technology* 141 (2017): 1-7.

[6] Kim, Kiho, Hyun Ju, and Jooheon Kim. "Pyrolysis behavior of polysilazane and polysilazane-coated-boron nitride for high thermal conductive composite." *Composites Science and Technology* 141 (2017): 1-7.

[7] Mujib, Shakir Bin, Mohammed Rasheed, and Gurpreet Singh. "Evaluating use of boron- and hafnium-modified polysilazanes for ceramic matrix minicomposites." *ACS omega* 7.49 (2022): 45325-45335.

I would like to acknowledge the use of Microsoft Copilot for polishing the language and improving the clarity of certain sections of this thesis. All AI-suggested edits were manually reviewed and refined, and I remain solely responsible for the original research, analysis, and final text.